The role of resuscitation promoting factors in peptidoglycan hydrolysis and reactivation from dormancy in *Mycobacterium smegmatis.*

Germar Matthew Beukes

0604339F

A dissertation submitted to the Faculty of Health Science, University of the Witwatersrand, in fulfillment of the requirements for the degree

of

Master of Science in Medicine

Johannesburg

2013

Declaration

I, Germar Matthew Beukes declare that this dissertation is my own work. It is being submitted for the degree of Master of Science in Medicine at the University of the Witwatersrand, Johannesburg. It has not been submitted before for any degree or examination at this or any other University.

31 May 2013

_____ _____

(Germar Matthew Beukes) Date

Dedications

My Mother, Marinda Beukes, a single parent that worked three jobs to get me through school. That never denied me anything, who never said: “Sorry we don’t have the money.” My true inspiration in life.

Presentations arising from this dissertation

Conference:	MRC research day 2011
Venue:	MRC Tygerberg Cape Town
Presenting:	Oral Presentation
Title:	The role of resuscitation promoting factors in peptidoglycan hydrolysis and reactivation from dormancy in *Mycobacterium smegmatis*
Authors:	Germar M Beukes, Lusanda Mapela, Bavesh D Kana

Won second prize for best oral presentation by an MSc student

Conference:	SASBMB/FASBMB 2012
Venue:	Champagne Sports Resort, Drakenberg
Presenting:	Poster Presentation
Title:	The role of resuscitation promoting factors in peptidoglycan hydrolysis and reactivation from dormancy in *Mycobacterium smegmatis*
Authors:	Germar M Beukes, Lusanda Mapela, Bavesh D Kana

Conference:	Wits Research day and Post Graduate expo 2012
Venue:	WITS medical school, Johannesburg
Presenting:	Poster Presentation
Title:	The role of resuscitation promoting factors in peptidoglycan hydrolysis and reactivation from dormancy in *Mycobacterium smegmatis*
Authors:	Germar M Beukes, Lusanda Mapela, Bavesh D Kana

Abstract

The global burden of tuberculosis (TB) has reached an alarming status with numerous countries reporting an incidence of greater than 300 cases per 100 000 population per capita. By far, the most concerning statistic regarding TB is that estimates indicate 2 billion people worldwide are infected with *Mycobacterium tuberculosis*, the causative agent of TB. Only a small proportion (10%) of these individuals progress to active disease whilst the majority control the infection in an asymptomatic state that is termed latent TB infection (LTBI). These individuals carry a lifetime risk, which is significantly enhanced in the presence of HIV co-infection, of progressing to active disease. It has been hypothesized that during LTBI, the infecting bacterial population adopts a non-growing, dormant state and that progression to active disease is a result of reactivation of these organisms from dormancy. *M. tuberculosis* encodes for 5 homologues for the resuscitation promoting factor (Rpf), designated *rpfA-E* which have been shown to be important for reactivation from dormancy and critical for virulence during TB infection. As such, these factors may play an important role in bacterial reactivation during LTBI. In this study, we further characterize Rpf function in *Mycobacterium smegmatis*, a non-pathogenic relative of *M. tuberculosis*. *M. smegmatis* encodes four *rpf*–like homologues and using sequential deletion mutagenesis, we constructed a panel of deletion mutants that were defective in one, two, three or all four *rpf*-like genes in *M. smegmatis*. The successful construction of a quadruple mutant lacking all four *rpf*-like genes demonstrated that, as observed in *M. tuberculosis*, the *rpf*-like genes are collectively dispensable for growth of *M. smegmatis*. A select group of *rpf* deficient mutant strains were then characterized further. Our analysis indicates that the double Δ*rpfA* Δ*rpfB,* triple Δ*rpfA* Δ*rpfB* Δ*rpfC*, and quadruple Δ*rpfA* Δ*rpfB* Δ*rpfC* Δ*rpfE*, mutants displayed no growth defects *in vitro* but were impaired for biofilm formation and formed abnormal colonies that lacked the surface cording which is characteristic of mycobacterial colonies. Genetic

complementation reversed these defects. Furthermore, the triple Δ*rpfA* Δ*rpfB* Δ*rpfC*, and quadruple Δ*rpfA* Δ*rpfB* Δ*rpfC* Δ*rpfE*, mutants displayed increased susceptibility to vancomycin, erythromycin and cephalosporins, suggesting some change in peptidoglycan structure or composition. Microscopic analysis of *rpf* deletion mutants revealed that the double Δ*rpfA* Δ*rpfB*, triple Δ*rpfA* Δ*rpfB* Δ*rpfC*, and quadruple Δ*rpfA* Δ*rpfB* Δ*rpfC* Δ*rpfE*, mutants displayed cells that were smaller than the wild type. In an interesting development, analysis of growth and survival in an *in vitro* model of mycobacterial dormancy indicated that the triple Δ*rpfA* Δ*rpfB* Δ*rpfC*, and quadruple Δ*rpfA* Δ*rpfB* Δ*rpfC* Δ*rpfE* mutants were unable to enter into a viable but non-culturable state. These results point to a novel role for Rpfs in the establishment of the dormant state in mycobacteria. Transmission Electron Microscopy on cells isolated from the dormancy model confirmed the progressive accumulation of inclusion bodies in the double Δ*rpfA* Δ*rpfB*, triple Δ*rpfA* Δ*rpfB* Δ*rpfC*, and quadruple Δ*rpfA* Δ*rpfB* Δ*rpfC* Δ*rpfE* mutants as these stains were passaged through our model of dormancy. Further analysis with Nile Red staining identified these inclusion bodies as lipid bodies. Collectively, our data reveal an important role for Rpfs in regulating essential growth processes and reveal a new role for Rpfs in the ordered shutdown of bacterial growth and establishment of dormancy in *M. smegmatis*.

Acknowledgements

I would like to acknowledge my funders, the Post graduate Merit Award, Medical Research Council, National Research Fund, Howard Hughes Medical Institute and the Centre of Excellence Funding for providing me with financial backing to complete this degree.

I would also like to acknowledge my supervisor Dr B.D Kana for his hard work and perseverance, without his guidance and strength none of this would have been possible. For his leadership in the unit as well as his strive to reach new heights. His willingness to stop at nothing to let us reach our dreams. Regardless of where he is in the world, he has always had an open door policy, always only a sms away.

I would also like to acknowledge all the people from different laboratories for their assistance in this project. Prof Phillips, who allowed me to use his microscopes and microtome. He was always willing to help with this project early in the morning and his knowledge, not every person you meet is able to recall that they use to use Ruthenium Red for mycobacterial cells forty years ago. Estelle Girton from Prof Phillip's lab who showed me how to prepare samples and how to use the microscope. Prof L. Scott from the Molecular Medicine and Haemotology Unit, for the use of the Flow Cytometer in her lab, as well as her reagents. I would also like to ackownledge the MMU at UCT for the use of their equipment after hours.

Mrs Pamela Sharp, my angel in the dungeon of Medical school, who was always willing to lend a helping hand. Showing me how to perform a technique that no one has done in a 10 years. Spending hours in the dark room to develop my negatives. Finding me stains from friends in the department. Always greeting me with a smile, brightening up my day. No problem seems that big after a cup of coffee with this remarkable person.

I would also like to acknowledge my friend, Samantha Scott, who was so helpful and supportive. I need to thank her for assisting me in the statistical analysis of the SEM data. Late night BBM's to make sure I'm still alive in the lab. I truly appreciate that. To my other friends in the lab at the CBTBR, who we shared lunch with every day, my cake buddies, thank you for the support and the wonderful times spend in the lab. Also my friends at the pharmacy that were always so understanding in moving a shift if I need to go to Cape Town or if I will be late for a shift due to traffic from JHB every day.

My loving family, for supporting me while studying. My brother who is always willing to wait for me to finish in the lab, even though his classes finished at 10 in the morning. My parents who have always been supportive in my career, who have always said that this is your future, do whatever you have to do. My mother for bringing an entourage to the airport after winning a prize at the MRC in Cape Town. My mother for being there after a long stressful day, with advice on how to approach a situation. I really need to acknowledge them for without them none of this would have been possible.

Table of Contents

List of Figures

Appendices

List of Tables:

Nomenclature:

A	Ampere
AAP	Accumulation-Associated Proteins
Amp	Ampicillin
BCG	Bacillus Calmette Guerin
bp	Base pairs
BSA	Bovine serum albumin
CFU	Colony forming unit
CSPD	Disodium 2-chloro-5-(4-methoxyspiro (2-dioxetane-3, 2 (2-dioxetane-3, 2'-(5'-chloro)-tricyclo decan)-. 4-yl)-1-phenyl phosphate
CTAB	Cetyltrimethylammonium bromide
DAPI	4', 6-diamidino-2-phenylindole
DCO	Double cross over
DDSA	Dodecenyl Succinic Anhydride
DIG	Digoxigenin
DMP-30	Tris-2, 3, 6-(dimethylaminomethyl) phenol, tertiary amine accelerator
DMSO	Dimethylsulphoxide
DNA	Deoxyribonucleic acid
DNTPs	Deoxynucleotide triphosphate
EDTA	Ethylene diamine tetraacetic acid
EtOH	Ethanol
F	Farad Capacitance
g	gram
HEPES	(4- (2-hydroxyethyl)-1-piperazineethanesulfonic acid)
HIV	Human Immunodeficiency Virus
HRSEM	High Resolution Scanning Electron Microscopy
hyg	Gene conferring resistance to hygromycin B
Hyg	Hygromycin
IGRA	Interferon-Gamma release assay
J	Joules
Kbp	Kilo base pair
Kan	Kanamycin
KCl	Potassium Chloride
LA	Luria-Bertani agar
lacZ	Gene encoding β-galactosidase
LB	Luria-Bertani broth
LTBI	Latent tuberculosis infection
m	milli
M	Molar
MDR-TB	Multidrug-Resistant Tuberculosis
mHdeB	modified Hartman's de Bont's media
MIC	Minimum inhibitory concentration
ml	Mililitre
MOPS	3-(N-morpholino) propane sulfonic acid
MPN	Most Probable Number
n	Nano
NPT	Nitrophenylthiocyanates
OADC	Oleic acid-albumin-dextrose-catalase
OD_{600nm}	Optical density at 600 nanometre wavelength
PBS	Phosphate Buffered Saline

PCR	Polymerase Chain Reaction
PG	Peptidoglycan
RPF	Resuscitation Promoting Factor
Rpm	Revolutions per minute
RT	Room Temperature
SCO	Single cross over
sdH_20	Sterile distilled water
sacB	Gene encoding levansucrase
SEM	Scanning Electron Microscopy
SDS	Sodium Dodecylsulphate
TB	Tuberculosis
TDR-TB	Totally Drug Resistant TB
TE	Tris-EDTA
TEM	Transmission Electron Microscopy
Tfb	Rubidium Chloride Compentent Cell solution
TLC	Thin Layer Chromatography
Tris	Tris (hydroxymethyl) aminomethane
TST	Tuberculin Skin Test
Tween	Polyoxyethylene sorbitan monooleate
UV	UltraViolet light
V	Voltage
v/v	Volume per volume
w/v	Weight per volume
WHO	World Health Organisation
XDR-TB	Extensively Drug Resistant TB
× g	*relative centrifugal force*
X-Gal	5-bromo-4-chloro-3-indolyl-β-galactoside
°C	Celsius
Ω	ohm resistance
µ	micro
2 × TY	Two times Tryptone, Yeast extract media

1. Introduction

1.1.General background

The global burden of tuberculosis (TB) has reached alarming proportions with incidents of 8.7 million people infected in 2011, and a mortality rate of 1.4 million per annum (WHO, 2012, Kana et al., 2010, Downing et al., 2004, Downing et al., 2005). *Mycobacterium tuberculosis* the causative agent of TB was first isolated by the German physician Robert Koch in 1882 (Sakula, 1983) and remains a problem today despite decades of chemotherapeutic treatment and global vaccination efforts. One of the major contributing factors to the significant morbidity and mortality associated with TB disease is the high number of individuals (34 million people) living with Human Immunodeficiency Virus (HIV) worldwide (WHO, 2012). It is estimated that of these, at least one third is infected with TB, suggesting a dreaded synergy between these two diseases (WHO, 2012). Estimates also indicate that individuals living with HIV are 21 to 34 times more likely to develop active TB (WHO, 2012) when compared to immune competent individuals. In 2011, about 500 000 people died of HIV related TB (WHO, 2013), which accounted for one quarter of the deaths in HIV patients in that year (WHO, 2012). In the same year, estimates of new TB cases in HIV positive individuals amounted to 1.1 million, a concerning statistic considering that 79% of these cases come from Africa (WHO, 2012).

A key factor that has contributed to the escalation of this epidemic is the rapid emergence of drug resistance, more importantly multi-drug resistant (MDR) TB which accounted for 310 000 of the reported TB cases in 2011 (WHO, 2013). MDR strains are resistant to the conventional first line drugs, isoniazid and rifampicin. In 2012, 9 % of the total MDR TB burden comprised of extensively-drug resistant (XDR) strains of *M. tuberculosis* which are

not only resistant to first line drug treatment but also resistant to aminoglycosides and fluoroquinolones (Loddenkemper and Hauer, 2010). More recent work that report cases of totally-drug resistant (TDR) strains, resistant to first and second line drugs, in India have fuelled global concern with regards to the control and ultimate eradication of TB (Velayati et al., 2009).

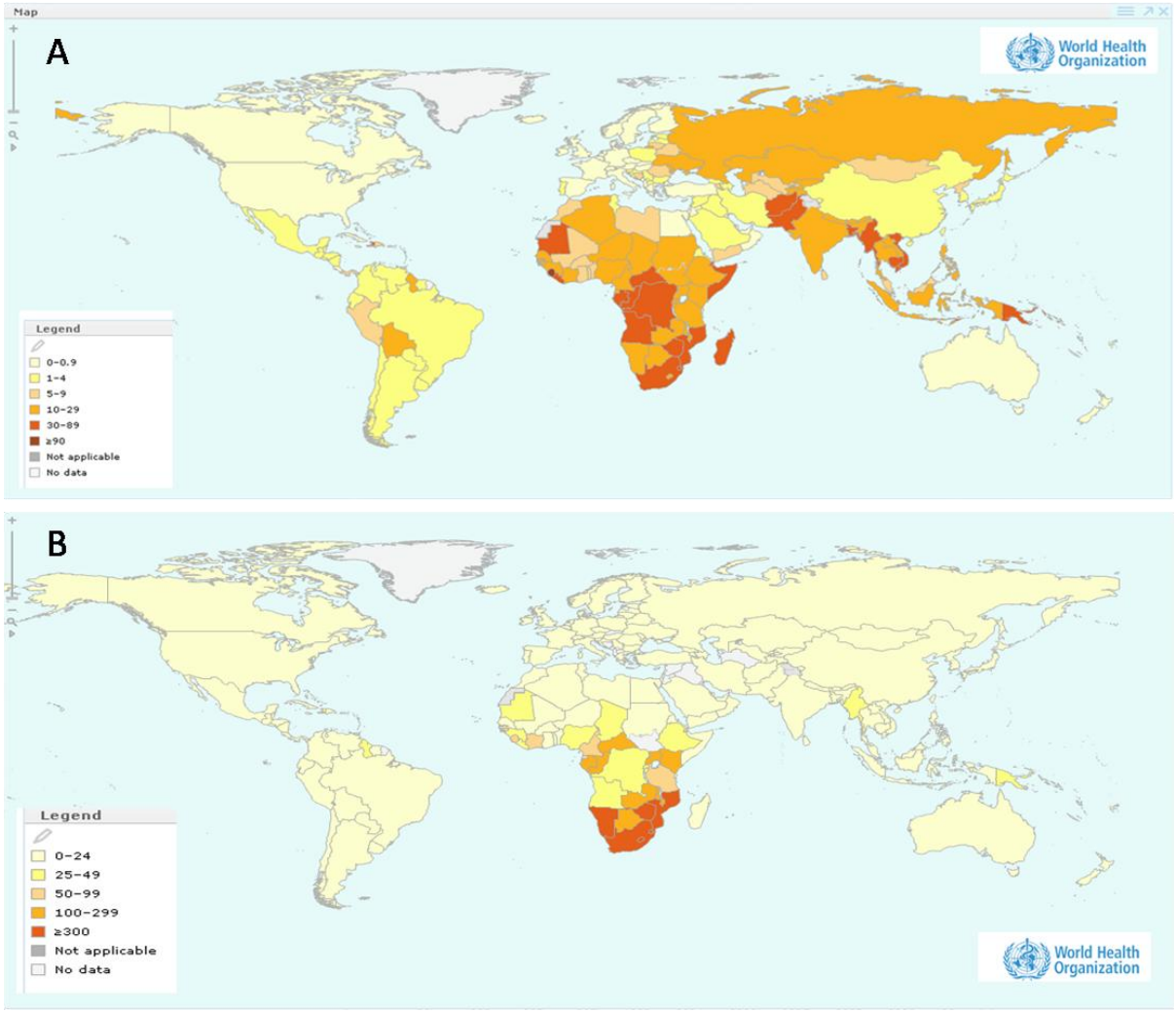

Figure 1.1: Geographical map of Estimated TB cases in 2011. A: Shown is the estimated mortality of TB cases, excluding HIV per 100 000 population, 2011. B: The estimated incidence of TB cases in HIV positive individuals, per 100 000 population, (WHO, 2013).

In the local context, with 325 321 new TB cases reported in 2011 (WHO, 2013), South Africa ranks third highest on the list of TB endemic countries (WHO, 2009) with a mortality rate of 650 / 100 000 people with only 50 of these occurring in HIV negative people (WHO, 2013).

These data confirm that the high HIV infection rate in South Africa continues to fuel the TB pandemic in the country (Pillay and Sturm, 2007). This delay in starting treatment results in community-wide transmission of drug resistance from these patients.

1.2. TB infection and pathogenesis

TB infection primarily results from the inhalation of aerosolized tubercle bacilli expectorated by an infected person during the coughing process that characterizes TB diseaese (Svenson et al., 2010). However, only in 5 % of cases does the infection result in active disease, with the remaining individuals controlling the infection by the innate immune system, which at a later stage may lead to complete inactivation or latent TB infection (LTBI) (Svenson et al., 2010). LTBI can be defined by the immune sensitization against the mycobacterial proteins in the tuberculin skin test (TST) with no associated symptoms of active TB (Barry et al., 2009). Testing for LTBI is a two-step procedure; firstly the TST is performed, which reveals if the patient has been in contact with any mycobacterial antigens, secondly interferon-gamma release assays (IGRAs), which are more accurate, (van Zyl-Smit et al., 2009) can be performed. For *M. tuberculosis* to cause disease or even start infection, tubercle bacilli have to penetrate the alveoli and be engulfed by macrophages (Frieden et al., 2003). The cell wall of the bacterium provides protection against the antibacterial effect of certain molecules produced by the macrophage (Lin and Ottenhoff, 2008). Furthermore, the bacterium interferes with the maturation of the phagocyte and prevents fusion of the phagosome with the lysosome, causing an immature phagosomal compartment which allows for bacterial replication (Stewart et al., 2003).

1.3. Latent TB infection

It is estimated that 1/3 of the world's population harbours LTBI and these individuals have defined risk of developing active disease (Young et al., 2009). The host determinants that result in reactivation of LTBI include host genetics, age, malnutrition, homelessness, drug and alcohol abuse and HIV infection (Jain and Dixit, 2008). The bacterial factors that contribute to the reactivation of clinically latent infection in people have yet to be identified. It has been hypothesized that LTBI is characterized by a population of dormant or metabolically quiescent organisms but this has not been unequivocally demonstrated (Young et al., 2009). In this regard, it is important to consider the terms "latency" and "dormancy" as well as the relative impact of these phenomena on our understanding of bacterial physiology during TB infection. LBTI is a *clinical phenomenon* that refers to state of asymptomatic disease in infected individuals whereas dormancy refers to a reversible *in vitro* state of metabolic quiescence in bacteria (Chao and Rubin, 2010). The association between latent infection and dormancy has been made on the basis of evidence that point to a harsh environment within TB granulomas, which would serve as a driving force to push the infecting organisms into a state of dormancy. In this regard, it has been demonstrated that human TB granulomas are hypoxic, suggesting that the tubercle bacilli would need to adapt to this environment, presumably by shutting down growth (Barry et al., 2009). Within the macrophage, oxygen and nutrients would be gradually become limiting and in response to this, the bacilli would enter a drug-tolerant, non-replicating state (Frieden et al., 2003). A key factor that associates LTBI with dormancy is the lack of culturable bacteria in both cases and consequently, those bacterial factors that control culturability are postulated to play an important role in LTBI (Kana and Mizrahi, 2010).

1.4. Dormancy and culturability in mycobacteria

The mycobacterial Wayne model of non-replicating persistence allows for bacteria to adapt to gradual depletion of oxygen in a closed container, giving rise to a drug-resistant, non-replicating state (Wayne and Hayes, 1996). In this system, the bacterium shuts down protein synthesis, and appears to display no net growth, as the oxygen levels are restored, the bacteria exit from this state (Hu et al., 1998). Other researchers have described a similar state in mycobacteria, for example in *M. smegmatis* (Lee et al., 1998) and *M. bovis* (Lim et al., 1999). However, these bacteria cannot be considered as dormant, due to the fact that they do not lose culturability, which is a key characteristic of the dormant state (Kaprelyants and Kell, 1993).

It has been demonstrated that different strains of Actinomycetes are able to enter into a non-culturable state when grown in batch culture under non-optimal conditions (Shleeva et al., 2002). Under these conditions these organisms are considered to be dormant, since they display reduced metabolic activity, lose culturability and are able to resuscitate from this state (Shleeva et al., 2004). Furthermore, it has been shown that a group of peptidoglycan (PG) degrading enzymes, termed resuscitation promoting factors (Rpfs) play an important role in reactivation from this dormant state (Shleeva et al., 2004). *In vivo*, the Cornell model, a murine model of TB infection, has been used to describe a state akin to dormancy *in vivo*. In this case, an established TB infection is cleared with the use of antibiotics until no bacteria are recovered, the animals are then immune suppressed which leads to the re-emergence of culturable bacteria (McCune et al., 1966). This result suggests that post-antibiotic treatment of TB infection in mice, there is a population of non-culturable and/or non-detectable bacteria that have the potential to reactivate growth under favourable conditions.

1.5. Vaccines

The current vaccine for TB is the live attenuated Bacillus Calmette-Guerin (BCG) vaccine which was developed 90 years ago and has been used for vaccination since 1921 (Malmros, 1948). However, BCG provides variable protection (between 0-80%) in adults for pulmonary TB, therefore a new protective vaccine is urgently sought after (Svenson et al., 2010). The BCG vaccine has been administered to 3 billion individuals, and is still administered to 100 million new-born infants every year.

1.6. Rpfs

Micrococcus luteus, a high GC content, gram positive bacterium is able to survive in soil due to its ability to enter into a non-spore forming, non-culturable stationary state (Kaprelyants and Kell, 1993). It also has the ability to resuscitate from this state in an autocrine manner and it is hypothesized that these stimulated cells can subsequently influence the growth of other dormant cells (Kaprelyants and Kell, 1993). In this regard, it has been demonstrated that dormant cells of *Mi. luteus* can be stimulated into rapid growth through the addition of sterile culture filtrate from actively replicating cultures (Mukamolova et al., 1998). This growth stimulatory activity observed with culture filtrate has been attributed to a small 16-17 kDa protein, termed Rpf, which is required for viability and is present in the supernatant of growing cells (Mukamolova et al., 2002a). Rpfs retain the potential to stimulate the growth of bacteria when added at very low concentrations and due to this potent activity, this molecule has been termed a bacterial cytokine (Mukamolova et al., 1998). Previous reports document that bacteria can communicate with each other using molecules such as *N*-acyl-L-homoserine lactones, in Gram negative bacteria (Fuqua and Greenberg, 1998) whereas peptides are used more frequently by Gram positives (Ohnishi et al., 1999). The actual mechanism of Rpf-mediated growth stimulation is unknown. Since these proteins are biologically active in very

low, picomolar concentrations, they do not serve as nutrients for the cell but rather stimulate cellular growth through another mechanism (Mukamolova et al., 1998).

The *rpf* gene product has a signal sequence at the N-terminus, which allows for secretion into the surrounding media or in some cases, for association with the cell wall (Mukamolova et al., 2002a). When a recombinant form of this protein which lacks this N-terminus was added to dormant cells no resuscitation was observed, this implies interaction with another protein – through the N-terminus – or that post translational processing of the Rpf may be important (Mukamolova et al., 2002a). This is supported by the observation that the protein found in the supernatant of *Mi luteus* cultures is much smaller than the predicted protein, confirming proteolytic cleavage of the nascent polypeptide (Mukamolova et al., 2002b). The fact that exogenous recombinant Rpf, lacking the secretory signal on the N-terminus, is unable to resuscitate dormant cells and that addition of anti-Rpf antibodies to Rpf-stimulated cultures reverses the growth stimulatory effect, implies that Rpfs bind extracellularly to some bacterial cell wall component, most likely the PG (Mukamolova et al., 2002b).

1.7. Rpf in *M. tuberculosis*

Bioinformatics analysis indicates that *rpf*-like genes are widely distributed within GC-rich, Gram positive bacteria, including mycobacteria (Mukamolova et al., 1998, Ravagnani et al., 2005b). *M. tuberculosis* encodes 5 *rpf*-like genes which are designated *rpfA-E,* Figure. 1.2, and have been the subject of extensive study [reviewed in (Kana and Mizrahi, 2010)].
The original observations regarding Rpf-mediated stimulation of bacterial growth suggest that Rpfs enhances bacterial culturability by acting from outside of the cytoplasmic compartment, which suggests that the cleavage of PG is an integral part of resuscitating dormant cells (Mukamolova et al., 2002a). Rpf from *Mi. luteus* has the ability to stimulate

growth of *M. tuberculosis* from an aged culture (Shleeva et al., 2002) and enhance the recovery of *M. tuberculosis* from infected macrophages (Biketov et al., 2000). The latter is evidenced by the fact that addition of Rpf from *Mi. luteus* to the culture media of bacteria recovered from macrophages results in a dramatic increase in culturable bacteria in the most probable number (MPN) assay (Biketov et al., 2000). Recombinant forms of *Mi. luteus* Rpf also have the ability to increase the growth of stationary phase *Mycobacterium bovis* and reduce the lag phase in *M. smegmatis* during batch, axenic culture (Mukamolova et al., 2002b).

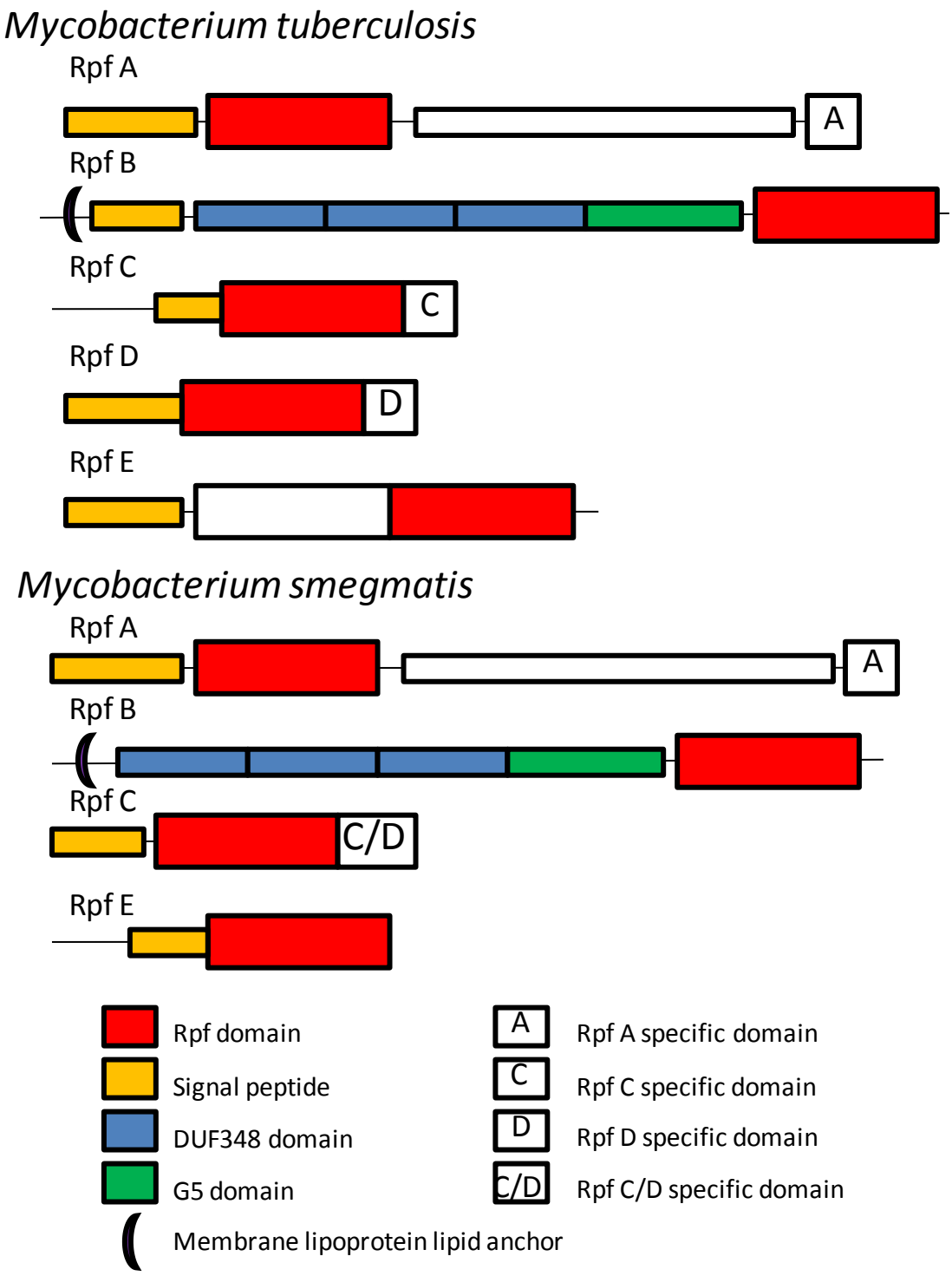

Figure 1.2: Diagrammatic presentation of Rpf proteins from *M. tuberculosis* and *M. smegmatis*. Diagram adapted from (Ravagnani et al., 2005a). Shown are the five *M. tuberculosis* proteins and the four present in *M. smegmatis*, which does not retain a RpfD homologue. The proteins are designated RpfA-E based on the presence of a distinguishing domain which allows categorization of these proteins into sub-classes (Ravagnani et al., 2005a).

1.8. Rpf function in *M. tuberculosis*.

A panel of mutants that lack between one and all five *rpf* genes in *M. tuberculosis* has been created and characterized at the CBTBR (Downing et al., 2004, Downing et al., 2005, Kana et al., 2008). An unexpected finding of this combinatorial deletion mutagenesis strategy is the ability to delete all five *rpf*-like genes in *M. tuberculosis*, suggesting that these genes are collectively dispensable for growth unlike the essentiality observed in *Mi. luteus* (Kana et al., 2008, Mukamolova et al., 2002a). Progressive *rpf* gene loss affects colony morphology on solid media and also reduced the kinetics of colony formation as evidenced by the observation that certain quadruple and quintuple *rpf*-deletion mutants formed visible colonies after 34 days, compared to the 18 days observed with the wild type strain (Kana et al., 2008). Genetic complementation of the quintuple *rpf* deletion mutant with *rpfB* and *rpfE* genes reversed this growth defect and the complementation of *rpfC* and *rpfD* did not result in any notable reversion of the phenotype (Kana et al., 2008). Moreover, this phenotype was more pronounced when the mutant strains were grown on Middlebrook 7H11 plates, which contains Malachite green, a cell wall damaging agent that could have contributed to the more pronounced phenotype (Kana et al., 2008). To further test this, the *rpf* deletion strains were grown on solid media in the presence of Sodium Dodecylsulphate (SDS). A quadruple deletion mutant which retained *rpfB* and the quintuple deletion mutant, showed increased susceptibility to SDS (Kana et al., 2008).

Assessment of resuscitation in an *in vitro* model of dormancy demonstrated that the triple, quadruple and quintuple *rpf* deletion mutants of *M. tuberculosis* did not have the ability to spontaneously resuscitate, a defect which was relieved with addition of culture filtrate from the wild type or with genetic complementation (Downing et al., 2005, Kana et al., 2008). Analysis of antibiotic susceptibility of the *rpf* deficient mutants, using a range of antibiotics,

revealed no significant increase in susceptibility with the exception of vancomycin and erythromycin where the *rpf* quintuple deletion mutant showed a 16 - and 4 - fold increase in susceptibility to these antibiotics respectively (Kana et al., 2010).

1.9. The role of Rpfs during pathogenesis

Transcriptional analyses of *M. tuberculosis* during infection in humans suggests that *rpfA* and *rpfD* are expressed in human TB infection (Rachman et al., 2006). Furthermore, *rpfB* and *rpfC* are expressed in the rabbit model of TB infection (Kesavan et al., 2009). All five *rpf*-like genes in *M. tuberculosis* are expressed in the murine model of TB infection, with their actual transcript abundance depending on the stage of infection (Tufariello et al., 2004). It has also been found that all the Rpfs, except for RpfC, are immunogenic and can be used as possible vaccine targets. In this regard, dormancy survival regulon (DosR) regulated genes and Rpfs are able to elicit a strong immune T-cell response with latently infected patients; however there is variation in responses between the European and African populations (Riano et al., 2012). Three DosR gene products (Nark2, PrkB and Rv2628) and 2 Rpfs (RpfA and RpfD) display higher levels of IFNγ production, yet no increase in CD8 cells (Riano et al., 2012). The significance of these observations to controlling TB infection is unkown.

1.10. Biochemical properties of Rpfs

In silico protein modelling revealed that the three dimensional structure of the Rpf domain has a *c*-type lysozyme fold, later confirmed by the NMR structure of RpfB from *M. tuberculosis* (Cohen-Gonsaud et al., 2004), which shares high similarity to soluble lytic transglycolases (Cohen-Gonsaud et al., 2005).

The recently reported crystal structure of a fragment of RpfB from *M.tuberculosis* describes the structure of the catalytic domain, which is conserved in all the Rpfs, three DUF 348 domains and the G5 domain. The G5 domain has been found in other proteins implicated in cell wall degradation (Ruggiero et al., 2009). The crystal-structure of RpfB, shown in Figure 1.3A and B, and some *in silico* modelling suggests that RpfB associates with the cell wall through its G5 domain (Ruggiero et al., 2009), Figure 1.3C.

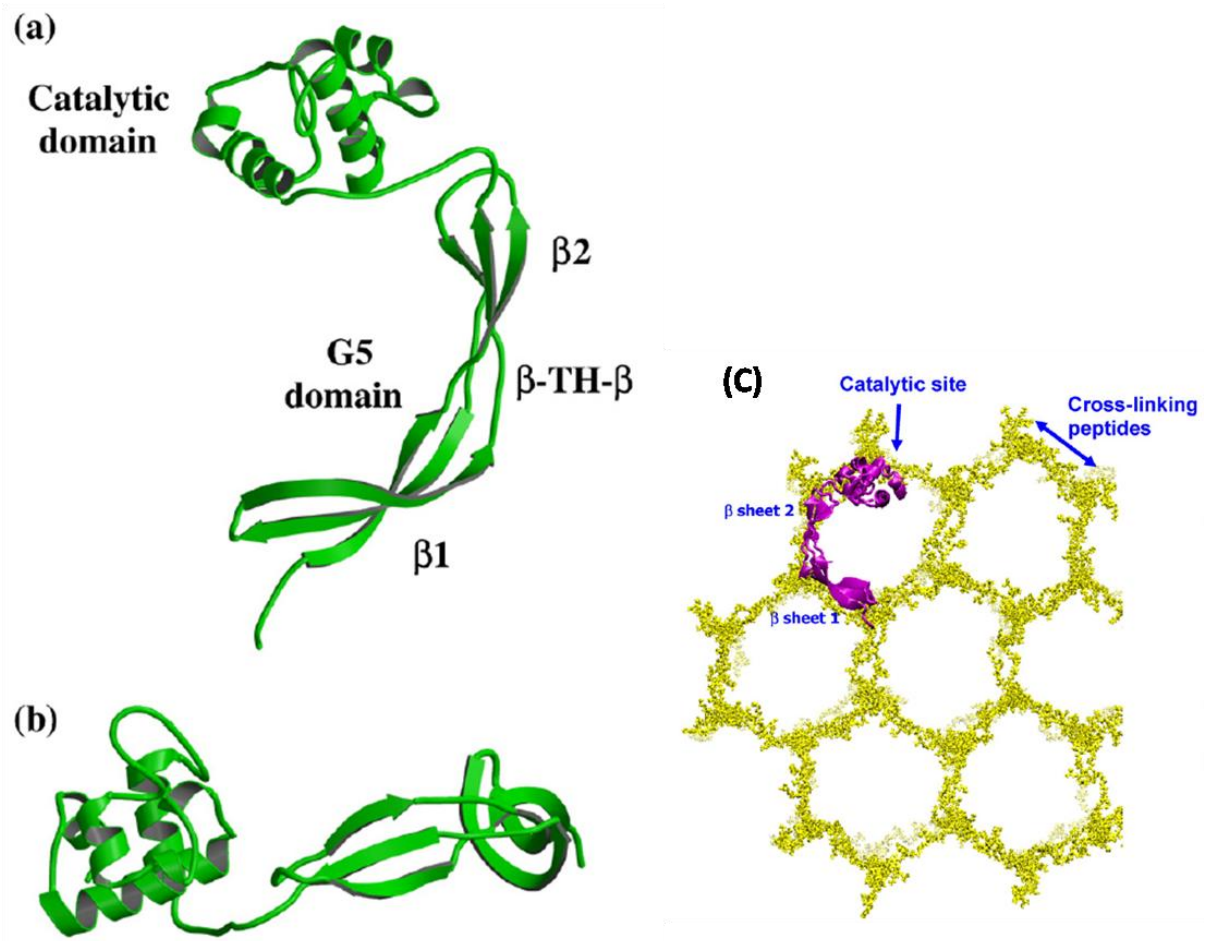

Figure 1.3: Crystal-structure of RpfB. Side view (A) and top view (B) of the crystal-structure, (C) Top view of docked RpfB molecule on the PG model. Apart from the catalytic domain, the G5 domain is clearly visible and consists of three β-sheets. The comma-like structure of RpfB, suggests the binding of RpfB to the peptide bonds inside the PG, positioning the catalytic domain close to the glycosidic bond between the NAM/ NAG molecules. Figures were taken from (Ruggiero et al., 2009), and generated using MOLSCRIPT.

The G5 domain is also present in the sequence of many accumulation-associated proteins (AAPs) (Ruggiero et al., 2009). AAPs have been shown to be important for biofilm formation (Bateman et al., 2005) and it has been suggesting that the β-triple helix-β motif of this domain confers cell wall adhesive properties to the Rpfs (Ruggiero et al., 2009). The catalytic domain which adopts a *c*-type lysozyme fold (Cohen-Gonsaud et al., 2004), was reported to retain a conserved glutamate residue, which is responsible for enzymatic activity (Mukamolova et al., 2006). Biochemical evidence indicates that Rpf from *Mi. luteus* is able to cleave tri-*N*-acetylglucosamine, a synthetic cell wall substrate, as well as other gram positive cell wall substrates (Mukamolova et al., 2006), confirming that it is a muralytic enzyme. Mutation of the conserved glutamate residue led to the inability of the protein to stimulate growth as well as degrade cell wall material (Mukamolova et al., 2006). Previous studies demonstrate that soluble lytic transglycosylases have the ability to cleave the glycosidic bonds in bacterial PG, allowing for cell wall remodelling (Scheurwater et al., 2008). Lytic transglycosylases and lysozyme share the same substrate but their enzymatic activity results in different products. Lysozymes hydrolyse PG and produce simple hydrolysis products while lytic transglycosylases cleave PG to produce a 1, 6-anhydromuramoyl conformation of the muramic acid (Mukamolova et al., 2006, Kana and Mizrahi, 2010). The association of Rpfs with the cell wall, combined with the structural information reported above, has led to the hypothesis that Rpfs cleave the β-1, 4-glycosidic bond found in PG, Figure 1.4.

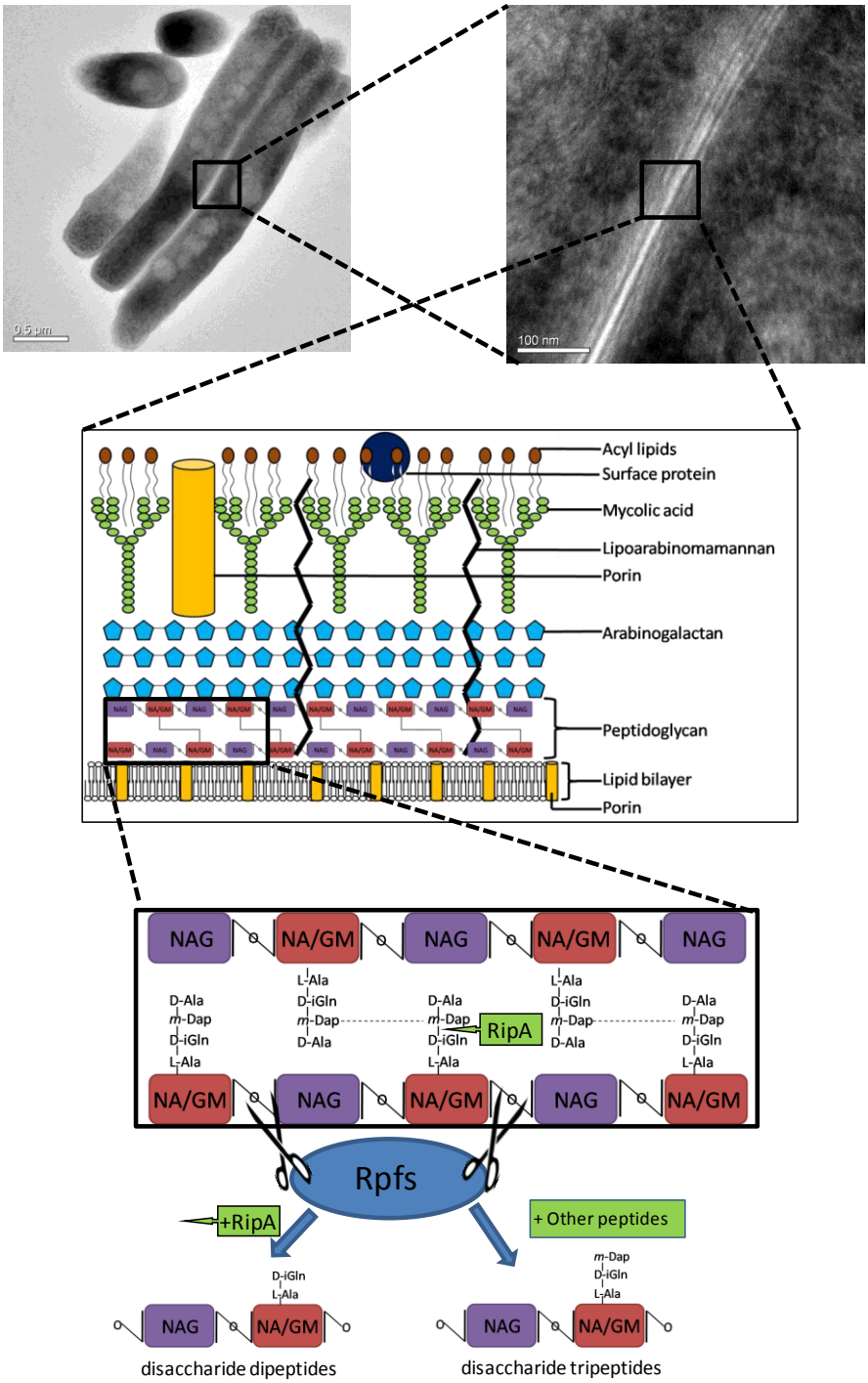

Figure 1.4: Diagrammatic representation of Mycobacterial cell wall. A. Transmission Electron Micrograph of *M. smegmatis* is used to show an experimental observation of the cell wall, which is then depicted diagrammatically to illustrate the position of the PG layer, found in this structure. PG consists of glycan and peptides, the former is made up of cross-linked *N*-acetylglucosamine (NAG) and *N*-acetylmuramic acid (NAM) and attached to these residues are the following: D-alanine, *m*-Dap, D-iGln and L-alanine. The predicted site of Rpf cleavage is shown in the diagram, at the glycosidic bond between the NAG and NAM molecules. The synergistic activity of Rpfs with other PG hydrolases will produce PG breakdown products, termed muropeptides. An interaction between Rpfs and RipA can produce disaccharide dipeptides, or an interaction between Rpfs and other enzymes could result in the production of disaccharide tripeptides (Kana and Mizrahi, 2010).

1.11. Rpf-Interacting partners and signaling

In other organisms, PG degradation and synthesis usually occurs through the combination of a group of enzymes that act together – the process is usually facilitated by protein-protein interactions. A yeast-two hybrid screen identified a partnering protein for the Rpfs, termed Rpf-interacting protein A (RipA), which has endopeptidase activity and interacts with RpfB and RpfE from *M. tuberculosis* (Hett et al., 2007). RipA and RpfB are found at the septa of dividing cells and interaction with RpfB results in synergistic PG degradation by the RipA-RpfB complex (Hett et al., 2007) which would suggest an important role for this complex in cell division, Figure 1.4. More recently the *ponA1*-encoded Penicillin Binding Protein 1 (PBP1) was also found to interact with RipA (Hett et al., 2010). The interaction of PBP1 with RipA antagonized the activity of the RipA-RpfB complex, which indicates that RipA catalytic activity is regulated by multiple proteins (Hett and Rubin, 2008). RipA is predicted to hydrolyze the bond between the D-*iso*-glutamine and *meso*-diaminopimelic acid in the PG, Figure 1.4 (Hett and Rubin, 2008). In *M. smegmatis*, depletion of RipA results in a cessation of cell division which leads to the production of long bacterial chains, brought about by the incomplete resolution of the septa (Hett and Rubin, 2008). These observations, in conjunction with the co-localization studies, suggest that RipA is essential for PG degradation at the septum and that the interaction with RpfB and PBP1 modulates its activity. The interaction of these three proteins have been proposed to control septation, Figure 1.5 (Hett et al., 2010). Both RpfB and PBP1 bind RipA in the same position, therefore these two proteins compete for the same site (Hett et al., 2010). It is hypothesized that the balance in this competition between these two proteins regulates septal synthesis and hydrolysis (Hett et al., 2010). If PBP1 binds to RipA, it inhibits PG degradation and consequently, newly synthesized PG accumulates which results in the formation of the septal bridge. When RpfB replaces the PBP1, synergistic PG hydrolysis is initiated, leading to degradation of the septum (Hett et al.,

2010). In mycobacteria, this is the first demonstration of post-translational regulation of PG degradation at the septum of dividing cells.

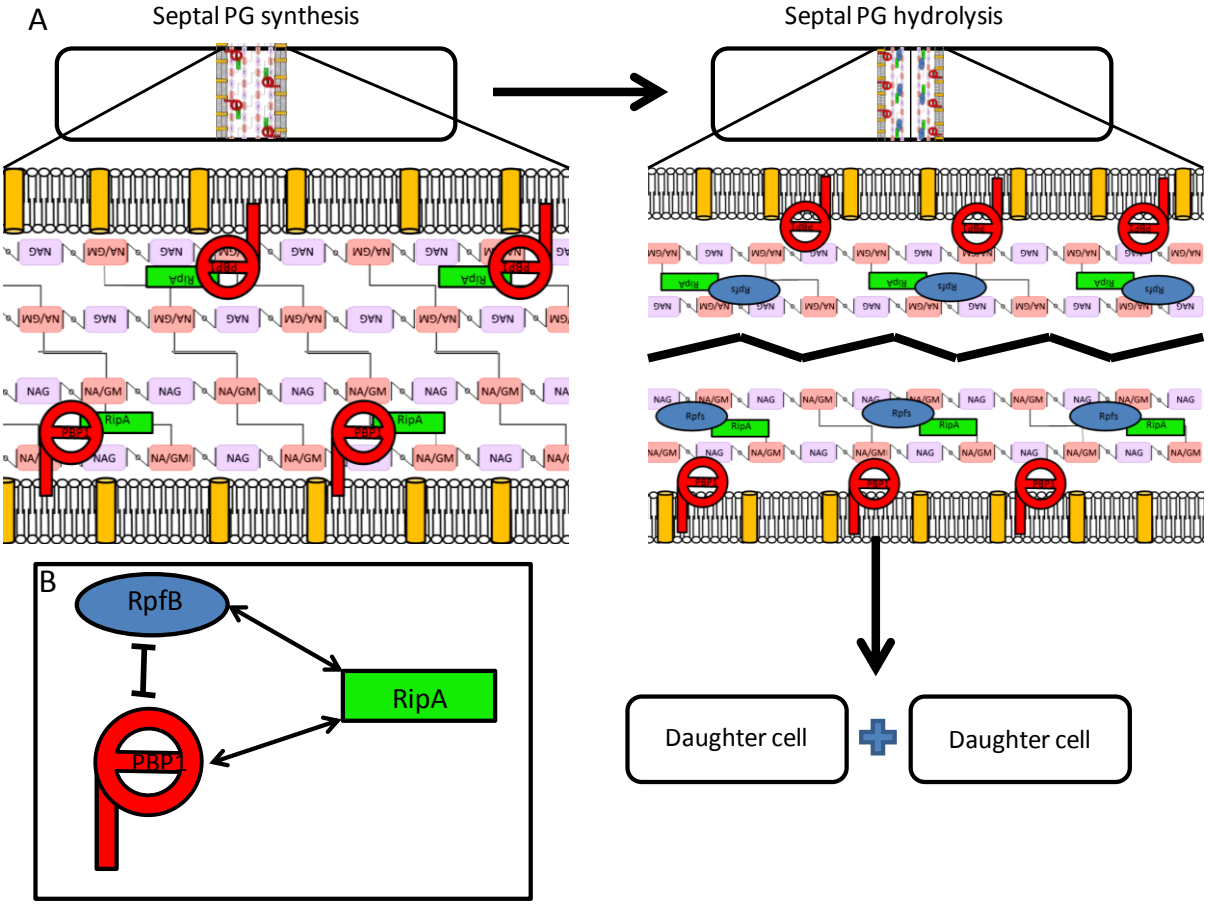

Figure 1.5: Schematic representation of interaction between RpfB, RipA and PBP1 and their role in septal synthesis and hydrolysis. A: Process of septal synthesis and hydrolysis. PBP1 binds to RipA and inhibits PG degradation resulting in the formation of new PG which constitutes the septal bridge. RpfB then replaces PBP1 and binds to RipA, the complex is now able to degrade PG hydrolysis which leads to daughter cell separation. B: An illustration of the interaction between the three proteins. Both RpfB and PBP1 compete for the same site on RipA – it is currently unknown whether PBP1 and RpfB interact with one another. Binding of these proteins to RipA regulates septal PG hydrolysis. Adaptation from Hett et al, 2010.

Emerging data suggest that all five of the Rpfs in *M. tuberculosis* may have the same biological activity on PG, however there might be some specialization in their function or substrate specificity (Mukamolova et al., 2002b, Kana and Mizrahi, 2010). The mechanism of Rpf mediated growth stimulation is currently unknown. There are two possibilities: (I) Rpf cleavage of PG in dormant cells directly results in growth or (II) Rpf cleavage of PG results in the release of PG breakdown products such as muropeptides that then serve as signaling molecules for reactivation from dormancy (Keep et al., 2006). With regards to the latter, eukaryotic-like serine/threonine protein kinases (STPKs) and associated serine/threonine protein phosphotase systems would be of critical importance. This is evidenced by a study that reports the reactivation of growth in *Bacillus subtilis* spores in response to muropeptides through the activity of PrkC, a STPK conserved in mycobacteria (Shah et al., 2008). Mutants of *Enterococcus faecalis* that lack PrkC show sensitivity to cephalosporins and vancomycin, as well as the inability to maintain normal cell morphology (Kristich et al., 2007). The mycobacterial homologue of PrkC is designated as PknB and has been shown to be essential for growth (Fernandez et al., 2006). PknB has many substrates, most of which are associated with cell wall synthesis such as PknA, Wag31 and PpbA (Kang et al., 2008). All of these proteins are localized to the bacterial poles and disruption of anyone of them causes morphological defects (Kang et al., 2008).

1.12. Other proteins involved in cell division

FtsZ is a cytoskeletal protein and a GTPase which is able to initiate cytokinesis by the assembly of a Z-ring (Adams and Errington, 2009), and is phosphorylated by PknA (Thakur and Chakraborti, 2006). Known interactions between FtsZ and other cell division proteins are shown in Figure 1.6. The Z-ring initiates cell division by constriction the ring structure and pulling together the newly formed poles of the daughter cells (Adams and Errington, 2009).

FtsZ has been found to be essential in *M. tuberculosis* (Dziadek et al., 2002) and was shown to interact with FtsW (Datta et al., 2002), FipA (Sureka et al., 2010) and CrgA (Plocinski et al., 2012). Other proteins that have been found to have an effect on FtsZ is ClpX (Chauhan et al., 2006) and ChiX (Dziedzic et al., 2010). Not only does FtsZ interact with ClpX and ChiX, but it also forms part of a trimeric complex with FtsW and FtsI (Datta et al., 2006). PknA phosphorylates this trimeric complex through an interaction with FtsI (Thakur and Chakraborti, 2006). More recently, Wag31 was discovered as the TB homolog of DivIVA (Kang et al., 2008). This is a cell division protein and is localized at the septa and poles (Kang et al., 2005). Wag31 is phosphorylated indirectly by PknA through PknB (Kang et al., 2005), and also forms a complex with CrgA and CrwA, both of which have been found to play a role in the localization of FtsI (Plocinski et al., 2012). CrgA also retains the ability to interact with the FtsZ complex at the septa (Plocinski et al., 2011).

1.13. Inhibitors for Rpfs

Rpfs have attracted significant interest as potential drug targets due their role in reactivation from dormancy, as well as in cell division. Of particular note in this regard, is a group of compounds, known as the 2-Nitrophenylthiocyanates (NPT), which show inhibitory activity against RpfB (Demina et al., 2009). NPT7 (4-benzoyl-2-Nitrophenyl thiocyanate) was further studied and three-dimensional structural modelling revealed that NPT7 binds to the catalytic cleft of RpfB, through the benzene rings of the drug, with the thiocyanate group of the drug being of utmost importance to inhibit the function of RpfB (Ruggiero et al., 2009, Ruggiero et al., 2012).

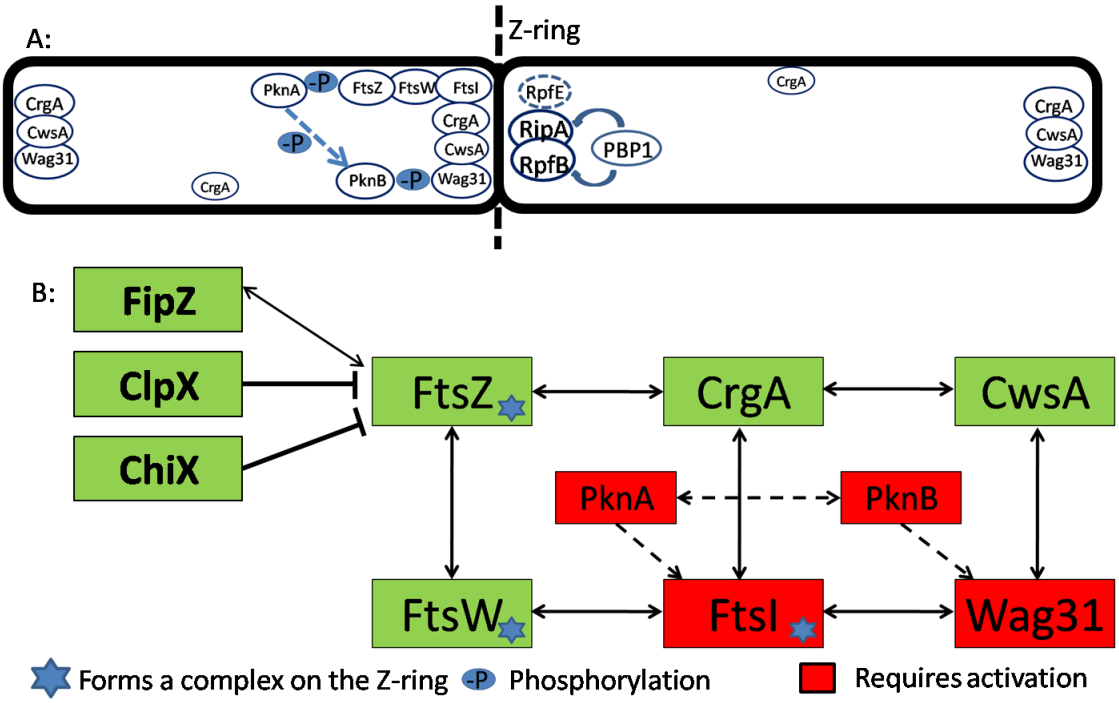

Figure 1.6: Schematic of protein-protein interacting partners in cell division in mycobacteria. A: Diagram of cytokinesis in the mycobacterial cell. The diagram illustrates the interaction between the proteins as well as their location at the Z-ring and elsewhere in PG synthesis. RpfB and RpfE interact with RipA. The RipA-RpfB synergistic complex is modulated by PBP1. FtsZ, FtsW and FtsI form a complex which is phoshorylated by PknA. Wag31 is phosphorylated indirectly by PknA through PknB. The location of CrgA, CwsA and Wag31, which form a complex to help coordinate the FtsZ-ring assembly at septa, is shown on the diagram. B: Schematic illustration of protein interactions. Shown are the interactions of CrgA, CwsA, FipZ, FtsI and Wag31. PknA and PknB phosphorylate FtsI and Wag31 respectively. ClpX and ChiX regulate FtsZ assembly and cell division potential. Adaptation from (Plocinski et al., 2012).

1.14. Problem statement

In this study we will assess the role of Rpfs in a model organism *M. smegmatis* mc^{2}155 to further understand the biological functions of these proteins in mycobacteria. *M. smegmatis* is a good model system for TB research as it is closely related to *M. tuberculosis* but grows much faster. It is also non-infectious making it amenable to specialized microscopy and other technically challenging experiments that have limited further study of these proteins in *M. tuberculosis*. Deletion mutants in *M. smegmatis* will allow for a comprehensive study of the

role of Rpfs in bacterial growth and cell division by providing the opportunity to microscopically study *rpf* mutants – outside of the Biosafety Level III environment. In the CBTBR some work has already been done in this regard. An MSc student, Ms. Lusanda Mapela, has created *M. smegmatis* deletion mutants deficient in Δ*rpfA* or Δ*rpfB* individually, followed by the construction of a double *rpfA rpfB* mutant. In this study, the phenotype of this double mutant will be further assessed. Moreover, further deletions will be introduced into this background to create a panel of mutants that lack between one and all four *rpf* genes in *M. smegmatis*.

1.15. Aims

The specific aims for this study are as follows:

1. To create a panel of *rpf* deficient mutants that lack various *rpf* genes in different combinations.
2. To assess the effect of deleting these genes on growth of *M. smegmatis.*
3. To determine the effect of *rpf* gene deletion on antibiotic susceptibility in *rpf* deficient strains.
4. To assess the effect of Rpfs on cell wall integrity *in vitro* in *M. smegmatis*, by visually assessing the cell wall of *rpf* deficient strains.
5. To assess the ability of these mutants to form biofilms.
6. To assess the effect of deleting *rpf* genes on dormancy and resuscitation in *M. smegmatis*

2. Methods and materials

2.1. General recombinant DNA manipulations

2.1.1. Bacterial strains, plasmids and culture conditions

All cloning vectors and bacterial strains used in this study are listed in Table 2.1 and Table 2.2 respectively. Glycerol stocks of bacterial strains were prepared in 33.3 % glycerol (v/v) and stored at -80 °C.

Table 2.1: Plasmid vectors used in this study

Plasmids	**Genotype**	**Reference**
pGEM	*E. coli* cloning vector; Amp^R	Promega Medicine WI
pMV306	*E. coli* - Mycobacterium integrating shuttle vector	Stover *et al*., 1991
pMV306H	*E. coli* - Mycobacterium integrating shuttle vector; derivative of pMV306 carrying a *hyg* gene; Hyg^R	H. Boshoff
pMVrpfA	Derivative of pMV306H carrying *M. tuberculosis* H37Rv *rpfA* gene and upstream native promoter region; Hyg^R	Lusanda Mapela
pMVrpfB	Derivative of pMV306H carrying *M. tuberculosis* H37Rv *rpfB* gene and upstream promoter region; Hyg^R	Lusanda Mapela
pMVrpfArpfB	Derivative of pMVrpfA carrying *Mycobacterium tuberculosis* H37Rv *rpfA* and *rpfB*; Hyg^R	Lusanda Mapela
pINSCE	Knockout construct for the in-frame deletion of *rpfC and rpfE*, 427 bps deleted from *rpfC* and 289 bps deleted from *rpfE*; Km^R	E. Machowski
pCEM	Derivative of pINSCE carrying the *lacZ* and *sacB* marker gene casette from pGOAL17, Km^R	E. Machowski

Amp^R: Ampicillin Resistance, Hyg^R: Hygromycin Resistance, Km^R: Kanamycin Resistance

Table 2.2: Bacterial strains

Strain	Genotype	Reference
Esherichia coli DH5α	Strain used for cloning, *sup*E44 Δ*lac*U169 *hsd*R17 *rec*A1 *end*A1*gyr*A96 *thi*-1 *rel*A1	Promega Medicine WI
mc^2155	High-frequency transformation mutant of *M. smegmatis* ATCC 607	Snapper *et al*., 1990
Δ*rpfA*	Derivative of mc^2155 carrying an in-frame, unmarked deletion in *rpfA*	Lusanda Mapela
Δ*rpfB*	Derivative of mc^2155 carrying an in-frame, unmarked deletion in *rpfB*	Lusanda Mapela
Δ*rpfC*	Derivative of mc^2155 carrying an in-frame, unmarked deletion in *rpfC*	This study
Δ*rpfE*	Derivative of mc^2155 carrying an in-frame, unmarked deletion in *rpfE*	This study
Δ*rpfA* Δ*rpfB*	Derivative of Δ*rpfA* carrying an in-frame, unmarked deletion in *rpfB*	Lusanda Mapela
Δ*rpfC* Δ*rpfE*	Derivative of mc^2155 carrying an in-frame, unmarked deletion in *rpfC and rpfE*	This study
Δ*rpfA* Δ*rpfB* Δ*rpfC*	Derivative of Δ*rpfA* Δ*rpfB* carrying an in-frame, unmarked deletion in *rpfC*	Lusanda Mapela
Δ*rpfA* Δ*rpfB* Δ*rpfE*	Derivative of Δ*rpfA* Δ*rpfB* carrying an in-frame, unmarked deletion in *rpfE*	This study
Δ*rpfA* Δ*rpfB* Δ*rpfC* Δ*rpfE*	Derivative of Δ*rpfA* Δ*rpfB* carrying an in-frame, unmarked deletion in *rpfC* and *rpfE*	This study
Δ*rpfA* Δ*rpfB*::pMVrpfArpfB	Derivative of Δ*rpfA* Δ*rpfB* carrying the *rpfA* and *rpfB* genes in pMVrpfArpfB integrated at the *attB* locus; Hyg^R	Lusanda Mapela
Δ*rpfA* Δ*rpfB* Δ*rpfC*:: pMVrpfA	Derivative of Δ*rpfA* Δ*rpfB* Δ*rpfC* carrying the *rpfA* gene in pMVrpfA integrated at the *attB* locus; Hyg^R	This study
Δ*rpfA* Δ*rpfB* Δ*rpfC*:: pMVrpfB	Derivative of Δ*rpfA* Δ*rpfB* Δ*rpfC* carrying the *rpfB* gene in pMVrpfB integrated at the *attB* locus; Hyg^R	This study
Δ*rpfA* Δ*rpfB* Δ*rpfC*:: pMVrpfArpfB	Derivative of Δ*rpfA* Δ*rpfB* Δ*rpfC* carrying the *rpfA* and *rpfB* genes in pMVrpfArpfB integrated at the *attB* locus; Hyg^R	This study
Δ*rpfA* Δ*rpfB* Δ*rpfC* Δ*rpfE*:: pMVrpfA	Derivative of Δ*rpfA* Δ*rpfB* Δ*rpfC* Δ*rpfE* carrying the *rpfA* gene in pMVrpfA integrated at the *attB* locus; Hyg^R	This study
Δ*rpfA* Δ*rpfB* Δ*rpfC* Δ*rpfE*:: pMVrpfB	Derivative of Δ*rpfA* Δ*rpfB* Δ*rpfC* Δ*rpfE* carrying the *rpfB* gene in pMVrpfB integrated at the *attB* locus; Hyg^R	This study
Δ*rpfA* Δ*rpfB* Δ*rpfC* Δ*rpfE*:: pMVrpfArpfB	Derivative of Δ*rpfA* Δ*rpfB* Δ*rpfC* Δ*rpfE* carrying the *rpfA* and *rpfB* genes in pMVrpfArpfB integrated at the *attB* locus; Hyg^R	This study

Amp^R: Ampicillin Resistance, Hyg^R: Hygromycin Resistance, Km^R: Kanamycin Resistance

a.) *E. coli* DH5α strains

E. coli strains containing plasmids were grown in Luria-Bertani (LB) media containing appropriate antibiotics at 37 °C, with exception of pCEM which was grown at 30 °C to avoid plasmid rearrangement, in an INCO COOL incubator overnight with shaking at 110 rpm. For selection on solid media, all strains containing plasmids were grown overnight on Luria-Bertani agar (LA) containing appropriate antibiotics at 37 °C except for pCEM which was grown at 30°C for 48 hours in Incotherm Labotec Incubator. For selection of *E. coli* cells containing plasmids, the antibiotics were used at the following concentrations: ampicillin (Amp) 200 μg/ml, kanamycin (Kan) 50 μg/ml, hygromycin (Hyg) 200 μg/ml.

b.) Mycobacterial strains

All strains were grown in Middlebrook 7H9 supplemented media, containing 0.5 % glycerol and a detergent, either 0.01 % Tyloxypol or 0.05 % Tween 80, unless otherwise stated. The media was also supplemented with 100 ml oleic acid-albumin-dextrose-catalase (OADC) enrichment (Difco) per litre of media, or a glucose-salt mixture (0.085 % $NaCl_2$, 0.2 % glucose). Antibiotics were added to media when appropriate. Strains were also grown in Sauton's media with detergents Tyloxypol or Tween at the above mentioned concentrations. All the strains were grown on solid Middlebrook 7H10 media supplemented with a glucose-salt mixture (0.085 % $NaCl_2$, 0.2 % glucose) and 0.5 % glycerol. For selection of strains carrying pMV306-based vectors, 50 μg/ml Hyg was used in the growth media. For counter selection of clones carrying the *sacB* and *lacZ* genes, 2 % w/v sucrose was included in plates containing 40 μg/ml 5-bromo-4-chloro-3-indolyl-β-galactoside (X-gal).

2.1.2. DNA extraction

a.) Plasmid preparation from *E.coli*

For small scale plasmid preparation, 1 ml of stationary phase culture was transferred to 1.5 ml Eppendorf tubes and harvested by centrifugation at 16 110 × g for 1 minute. Cells were resuspended in 100 µl of solution 1 (50 mM glucose, 25 mM Tris-Cl pH 8.0, 10 mM EDTA), followed by addition of 200 µl solution 2 (1 % SDS, 0.2 M NaOH). The cell suspension was then mixed and incubated on ice for 5 minutes. To neutralize, 150 µl of solution 3 (3 M Potassium acetate, pH5.5) was added, mixed and left on ice for 10 min before cellular debris was removed by centrifugation at 16 110 × g for 10 minutes at 4 °C. The supernatant was transferred to a new Eppendorf tube followed by treatment with 2 µl of RNaseA (10 µg/ml) for 20 minutes at 42 °C. The plasmid DNA was precipitated by the addition of 350 µl of isopropanol followed by incubation at room temperature for 10 minutes before centrifugation at 16 110 × g for 10 minutes. The DNA pellet was washed with 70 % Ethanol, dried at 65 °C in a vacuum centrifuge (SpeedVac, Savant, Farmingdale, NY, USA) and resuspended in 20 µl sterile distilled water (sdH_2O).

For large scale DNA extractions, *E. coli* cultures were grown overnight in 50 ml LB with shaking at 110 rpm followed with harvesting by centrifugation in a Beckmann J2-21 centrifuge at 4 500 × g for 10 minutes. The DNA was extracted by a combination of solutions found in Macherey and Nagel DNA plasmid extraction kit as per the manufacturer's instructions. Cells were resuspended in buffer S1 (50 mM Tris-HCl, 10 mM EDTA, 100 µg/mL RNase A, pH 8.0) before being lysed by Lysis buffer S2 (200 mM NaOH, 1 % SDS) at room temperature for 5 minutes. The solution was then neutralized with Neutralization buffer S3 (2.8 M potassium acetate, pH 5.1) and placed on ice for 5 minutes. A NucleoBond® AX drip column was equilibrated with equilibration solution N2 (100 mM Tris, 15 % ethanol,

900 mM KCl, 0.15 % Triton X-100, adjusted to pH 6.3 with H_3PO_4) before loading the plasmid extract to column. The column was washed with buffer N3 (100 mM Tris, 15 % ethanol, 1.15 M KCl, adjusted to pH 6.3 with H_3PO_4) twice, before being eluted with elution buffer N5 (100 mM Tris, 15 % ethanol, 1 M KCl, adjusted to pH 8.5 with H_3PO_4). The plasmid DNA was then precipitated with an equal amount of isopropanol and pelleted by centrifugation. The pellet was washed with ethanol (70 %) and dried at 65 °C in a vacuum centrifuge. The DNA was dissolved in sdH_2O, before being stored at -20 °C.

b.) Chromosomal extraction from mycobacteria

An actively growing culture of *M. smegmatis* was streaked onto solid agar as discussed above and grown to confluence. Bacterial cells were then scraped and resuspended in 500 µl of TE buffer (10 mM Tris-HCl pH 8.0, and 1mM EDTA) and heat killed by incubating at 65 °C for 35 minutes. The solution was cooled and 50 µl of lysozyme (10 mg/ml) was added. After incubating at 37 °C for 1 hour, 70 µl of 10 % SDS and 6 µl of proteinase K (10 mg/ml) were added followed by incubation for 2 hours at 65 °C. To this solution, 100 µl of NaCl (5 M) was added and mixed. This was followed by addition of 80 µl of cetyltrimethylammonium bromide (CTAB) made up in a NaCl mixture (10 % CTAB in 0.7 M NaCl). The solution was then incubated at 65 °C for a further 10 minutes. Chloroform:isoamyl alcohol (24:1 v/v) was added in equal volume before centrifugation at 16 110 × g for 10 minutes. The aqueous phase was removed and transferred to a new Eppendorf tube. The DNA was precipitated by adding 1/10 volume of sodium acetate (5.3 M pH 5.2) and 2.5 × volume ethanol (100%), this mixture was then incubated at - 20 °C for an hour. The DNA was pelleted by centrifugation at 16 110 × g for 30 minutes at 4 °C, the pellet was washed with ice cold ethanol (70 %) and dried by vacuum centrifugation. The DNA was resuspended in sdH_2O.

2.1.3. DNA manipulations

a.) Restriction enzyme digestions

All restriction enzymes were obtained from New England Biolabs, Inc., Roche Applied Science, or Fermentas. All digests were performed at 37 °C with the appropriate buffer as per manufacturer's instructions. Up to 5 µg of plasmid DNA was digested in 20 µl reaction volumes for 1 hour and up to 10 µg of mycobacterial chromosomal DNA was digested overnight in 50 µl reaction volumes.

b.) Ligation reactions

DNA ligations were performed using the T4 DNA Ligase (Roche Applied Science), as per manufacturer's instructions. Briefly, 10 × T4 DNA Ligase buffer, T4 ligase and linear plasmid DNA (50 ng) were made up to a 50 µl reaction volume which was incubated at room temperature for 10 minutes. For transformation into *E. coli* DH5α cells, 5 µl of this ligation reaction was used.

2.1.4. Agarose gel electrophoresis

All gels were made in 1 × TAE buffer (1mM EDTA, 40 mM Tris-acetic acid pH 8.5), depending on the size of the DNA fragments either a 0.8 % agarose (>1kb) or a 1.5 % agarose (<1kb) concentration was used. All gels contained 0.5 µg/ml ethidium bromide and the DNA samples were loaded with a tracking dye (0.025 % bromophenol blue in 30 % glycerol). Lambda DNA molecular weight markers (IV and VI; Roche Applied Science) were used to assess DNA fragment sizes. The agarose gels were electrophoresed at 80 V in a Mini-Sub Cell GT minigel horizontal submarine unit (BIO-RAD) and visualized under UV-light using the Gel Doc 2000 system (BIORAD).

2.1.5. DNA fragment recovery from agarose gels and quantification

The required DNA fragment was excised from the gel and purified using the Nucleospin kit (Macherey-Nagel) as per manufacturer's instructions. Briefly, the excised gel fragment was melted, loaded onto the provided column, and washed. The DNA was then eluted using pre-warmed sterile distilled water. The DNA was quantified either on agarose gels by comparison to DNA molecular weight markers or on the NanoDrop ND-1000 Spectrophotometer, as per manufacturer's instructions (Thermo Scientific).

2.1.6. Transformation of bacteria

a.) *E. coli* DH5α transformations

E. coli DH5α competent cells were used for transformation of plasmids. Rubidium chloride competent cells were prepared as follows. One ml of a stationary phase overnight culture was inoculated in 100 ml 2 × TY and grown to an (Optical Density at 600 nm) OD_{600nm} of between 0.48 - 0.52. The cells were placed on ice for 15 min and centrifuged at 3 900 × g for 5 min at 4 °C. The pellets were gently resuspended in 20 ml TfbI solution (30 mM potassium acetate, 100 mM rubidium chloride, 10 mM calcium chloride, 50 mM manganese chloride, and 15 % v/v glycerol - pH 5.8), and placed on ice for 15 min. The cells were then centrifuged again at 3 900 × g for 5 min at 4°C, resuspended in 2 ml TfbII solution (10 mM MOPS, 75 mM calcium chloride, 10 mM rubidium chloride and 15 % v/v glycerol-pH 6.5) and 500 µl aliquots were flash-frozen in ethanol and stored at -80 °C.

For transformations, *E. coli* DH5α competent cells were thawed on ice and 100 µl of cells used per transformation. The plasmid DNA was incubated with the cells on ice for 20

minutes, heat-shocked for 90 seconds at 42 °C and chilled on ice for 2 minutes. The cells were rescued by adding 800 µl of 2 × TY, before incubating at 37 °C for 1 hour, for phenotypic expression of antibiotic resistance. The cells were centrifuged for 5 minutes at 2 360 × g and resuspended in 200 µl of LB media before being serially diluted and plated on LA plates containing the appropriate antibiotics.

b.) Transformation of *Mycobacterium smegmatis* mc^{2}155

One millilitre of a stationary phase *M. smegmatis* culture was inoculated in 100 ml Middlebrook 7H9 supplemented with a glucose-salt mixture (0.085 % $NaCl_2$, 0.2 % glucose), 0.5 % glycerol and 0.05 % Tween 80, and grown to an OD_{600nm} of 0.6. The cells were centrifuged at 2 360 × g for 10 minutes at 4 °C and the pellet was washed twice by resuspending in 10 ml of ice-cold 10 % glycerol and centrifuging at 2 360 × g for 10 minutes at 4 °C. The final pellet was resuspended in 2 ml ice-cold 10 % glycerol and these competent cells were used immediately. The plasmid DNA was added to 400 µl aliquots of *M. smegmatis* competent cells before being transferred to a 0.2 cm electroporation cuvette and pulsed using the following conditions: 2500 V, 25 µF and 1000 Ω in Gene Pulser Xcell BioRad laboratories. After electroporation, 800 µl 2 × TY was added and incubated for 3 hours at 37 °C. The cells were then plated on Middlebrook 7H10 media with glucose salts (0.085 % $NaCl_2$, 0.2 % glucose). Plates were incubated for 7-14 days at 37 °C before scoring CFUs.

2.1.7. Polymerase Chain Reaction (PCR)

a.) General PCR

For all PCR for screens, either the Roche FastStart kit or the Fermentas HotStart kit was used. When amplifying for cloning, Phusion high-Fidelity DNA polymerase (Finnzymes) was used to prevent the insertion of mutations during PCR, discussed below. All reactions were conducted as per manufacturer's instructions. For screening reactions using the Roche FastStart Taq DNA polymerase, 20 – 50 µl reactions were set up containing: 1 × reaction buffer, 2 µl genomic DNA, 200 µM of each dNTP, 0.5 - 1.0 µM of each primer, 1.5 mM $MgCl_2$, 1 × GC rich solution and 0.5 µl of the DNA polymerase. DNA amplification was performed using the following cycling parameters: denaturation at 94 °C for 5 minutes; followed by 30 cycles of denaturation at 94 °C for 30 seconds, annealing at 62 °C for 30 seconds and an extension at 72 °C for 30 seconds with a final extension at 72 °C for 7 minutes.

b.) High Fidelity PCR

For reactions using the Phusion High-Fidelity DNA polymerase (Finnzymes), 50 µl reactions were set up containing: 1 × reaction buffer, 200 ng plasmid or genomic DNA, 200 µM of each dNTP, 0.5 µM of each primer, 3 % DMSO and 0.5 µl of the DNA polymerase. DNA amplification was then performed using the following cycling parameters: denaturation at 98 °C for 30 seconds; followed by 30 cycles of denaturation at 98 °C for 30 seconds, annealing at 72 °C for 30 seconds, and extension at 72 °C for 2 minutes with a final extension at 72 °C for 7 minutes. For each amplification reaction, three control reactions were set up (I) a no DNA control reaction (II) a reaction containing only the forward primer (III) a reaction containing only the reverse primer. All PCR reactions were performed using the MyCyclerTM thermal cycler (BIO-RAD) machine with oligonucleotide primers listed in Table 2.3, obtained from Inqaba Biotech Ltd.

c.) Probe synthesis for Southern Blotting

For synthesis of probes to be used for southern blotting, the PCR DIG Probe Synthesis Kit from Roche Applied Science was used. The alkali-labile digoxigenin (DIG)-dUTP was incorporated into the probe by PCR as per the manufacturer's instructions. Probe synthesis was performed using the following cycling parameters: denaturation at 94 °C for 5 minutes; followed by 40 cycles of denaturation at 94 °C for 30 seconds, annealing at 60 °C for 30 seconds and an extension at 72 °C for 30 seconds with a final extension at 72 °C for 7 minutes.

2.1.8. Sequencing

DNA was extracted as discussed in section 2.1.5, sequencing was conducted by the DNA Sequencing Facility of Stellenbosch University. Sequencing was performed using the Big Dye terminator v3.1 Cycle Sequencing kit and Bioline Half Dye Mix. Oligonucleotides used in sequencing reactions are listed in Table 2.3. All sequences received from the unit were analyzed, and aligned using DNAMAN version 7 (Lynnon Corporation, Copyright 2012).

Table 2.3: Oligonucleotides used in this study, with applications and expected sizes.

Target	Name	Sequence	Application	Expected size
694 bps up-stream of *rpfC*, 828 bps down-stream of *rpfE*	rpfdupF1	5'-GCGGGGGTACCGCTAGCCCGCCTAACTAACC-3'	sequencing of deletion allele	2563 bps (wild type)
				2103 bps (Δ*rpfC*)
	rpfdupR3	5'- CGGCGTCGACTCGGTCGTGGCGCGC -3'		2239 bps (Δ*rpfE*)
				1779 bps (Δ*rpfC* Δ*rpfE*)
Screening primers				
*rpf*A	rpf A F1	5'-GAGGACCTCGACGCTTATGA-3'	screen for *rpfB* allele	300 bps (wild type)
	rpf A R1	5'-TCCTTGGTGGCCATGTACGC-3'		
	rpf A R2	5'-CATCGTGGACGAAGTTCTGT-3'		100 bps (mutant)
*rpf*B	rpf B F1	5'-AGGACCACACGACAGAAGTG-3'	screen for *rpfC* allele	300 bps (wild type)
	rpf B R1	5'-CGGCTGCGGCGCAACACGAT-3'		
	rpf B R2	5'-CATCGTGGACGAAGTTCTGT-3'		100 bps (mutant)
*rpf*C	MutC F1	5' -GAACGTTTGTACGGCAGTGA- 3	screen for *rpfA* allele	300 bps (wild type)
	MutC R1	5' -GCCAGACCCTGGGTGCGCAG- 3'		
	MutC R2	5' -GCGCGACCGTGCTGGTGCCC- 3'		100 bps (mutant)
*rpf*E	MutE F1	5'-TGGCGAAAGGAACGAAGTGA- 3'	screen for *rpfE* allele	300 bps (wild type)
	MutE R1	5'-TGGGTACGCAGCACGTTCTC- 3'		
	MutE R2	5'-GCAGAAGGGCCTGGAGAGGA- 3'		100 bps (mutant)
Complementation vectors				
*rpf*A	rpf A F1	5'-ATAGCACGCCGAACTCCATC-3'	screen for complementing *M. tuberculosis rpfA* allele	1150 bps *rpfA* (Mtb)
	rpf A R2	5'-GTGGCGGAGGTAGCTGAAGA-3'		
*rpf*B	rpf B F1	5'-TTATGGGCTAGGGTGGATGC-3'	screen for complementing *M. tuberculosis rpfB* allele	1150 bps *rpfB* (Mtb)
	rpf B R2	5'-GCAGCCGAGAAGCCAGTAGT-3'		
Southern Blotting Probe primers				
Up-stream	MutC F1	5' -GAACGTTTGTACGGCAGTGA- 3	Southern blot probe synthesis Figure 3.7	1160bps
	rpfdupR3	5'- CGGCGTCGACTCGGTCGTGGCGCGC -3'		
Down-stream	rpfdupF1	5'-GCGGGGGTACCGCTAGCCCGCCTAACTAACC-3'	Southern blot probe synthesis Figure 3.6	1242bps
	MutE R2:	5'-GCAGAAGGGCCTGGAGAGGA- 3'		
Sequencing				
pCEM, pINSCE, homo-logous rpfC/rpfE	seqGBR1	5' TCGTTGCGCAGCACGTCG 3'	Sequence confirmation of pCEM, pINSCE, homologous *rpfC/rpfE regions*	not applicable
	seqGBR2	5' GTCGGCAGATCCGGCTCC 3'		not applicable
	seqGBR3	5' TTCGCGGTCCTCGTGTCG 3'		not applicable
	seqGBR4	5' GCCTGGACACAGGTAGCC 3'		not applicable
	seqGBR5	5' GCGATGACGCTGTGTGCC 3'		not applicable
	seqGBF6	5' CGGGACTTCGACTCTGGC 3'		not applicable
	seqGBR7	5' TCTCGGCGTGCGTTCTGC 3'		not applicable

2.1.9. Southern blot analysis

Approximately 5 μg of genomic DNA was digested overnight at 37°C with the restriction enzyme *Not*I and appropriate buffer. The DNA fragments were separated on a 0.8 % agarose gel at 80 V. The DNA in the agarose gel was depurinated by soaking the gel in a 0.25 M HCl solution for 15 minutes and then denatured by soaking in a 0.5 M NaOH/1.5 M NaCl solution for 15 minutes and finally equilibration in 1 × TBE buffer (Tris-Borate-EDTA pH 8.0, Sigma). The agarose gel was then overlayed with a Hybond-N nitrocellulose membrane, sandwiched between two pre-soaked 3 MM Whatmann filter papers, and two pre-soaked sponges. After ensuring no air bubbles were present, this "sandwich" was placed carefully in a TE 22 Mini Transphor cassette and the cassette transferred to a TE 22 Mini Transphor unit (Hoefer) containing 1 × TBE buffer. The DNA was then transferred to the nitrocellulose membrane (0.5 A for two hours at 4 °C), and cross-linked by irradiation at 1200 mJ/cm^2 in a UV Stratalinker 1800 (Stratagene).

Hybridisation of the probe to the membrane was done as per manufacturer's instruction for the DNA High Prime DNA labelling Kit and Detection Starter Kit II (Roche Applied Science). Briefly, the membrane was pre-hybridised with 12 ml DIG Easy Hyb solution (1 hour at 52 °C) in Hybaid HB-OV-BM roller bottles incubated in a hybridization oven (Hybaid Micro-4). The probe, synthesized by PCR as discussed in section 2.1.7, was denatured at 95 °C for 10 minutes and then added to the pre-hybridisation solution and hybridized overnight at 52 °C. The membrane was then washed twice with Solution I (2 × SSC, 0.1 % SDS) at room temperature for five minutes and then once with Solution II (0.5 × SSC, 0.1 % SDS) at 65 °C for 30 minutes. Following these stringency washes, the labeled DNA was detected as per the manufacturer's protocol (Roche Applied Science). Briefly, detection of the DIG-labelled hybrids was achieved by dephosphorylation of the CSPD

substrate upon addition of a specific DIG alkaline phosphatase-conjugated antibody, which resulted in chemiluminescence, visualized on X-ray film after one hour incubation at room temperature.

2.2. Construction of knockout mycobacterial strains

The pCE knockout vector was obtained from Lusanda Mapela a former MSc student in the CBTBR. This vector was electroporated into mc^2155 (Section 2.1.6.b) and mutants were obtained by homologous recombination using a two step selection method as previously described (Gordhan and Parish, 2001). Briefly, Electroporation of the construct was followed by selection on kanamycin and X-gal containing media. The suicide vector contains a *LacZ* gene that allows for the degradation of X-gal by the β-galactosidase enzyme which will result in blue colony colour (Tubb and Liljestroem, 1986). The homologous recombination with the pCEM knockout vector can have more than one possible outcome resulting in single or double mutants, Figure 3.3, The two-step allelic replacement strategy used in this study is shown in Figure 2.1. The suicide vector is electroporated in *M. smegmatis*. After selection of a single crossover recombinant, a second crossover is facilitated by further growth and selection on sucrose containing plates. The suicide vector contains a *sacB* gene which encodes for a secreted enzyme levan sucrase which hydrolyses sucrose to levans, a high molecular weight fructose that is toxic to the bacteria (Pelicic et al., 1996). To survive, the bacteria will then facilitate the second cross over to remove the plasmid that is causing toxicity. During the second crossover event, the bacterium can either regenerate the wild type allele or incorporate the mutant allele, Figure 2.1.

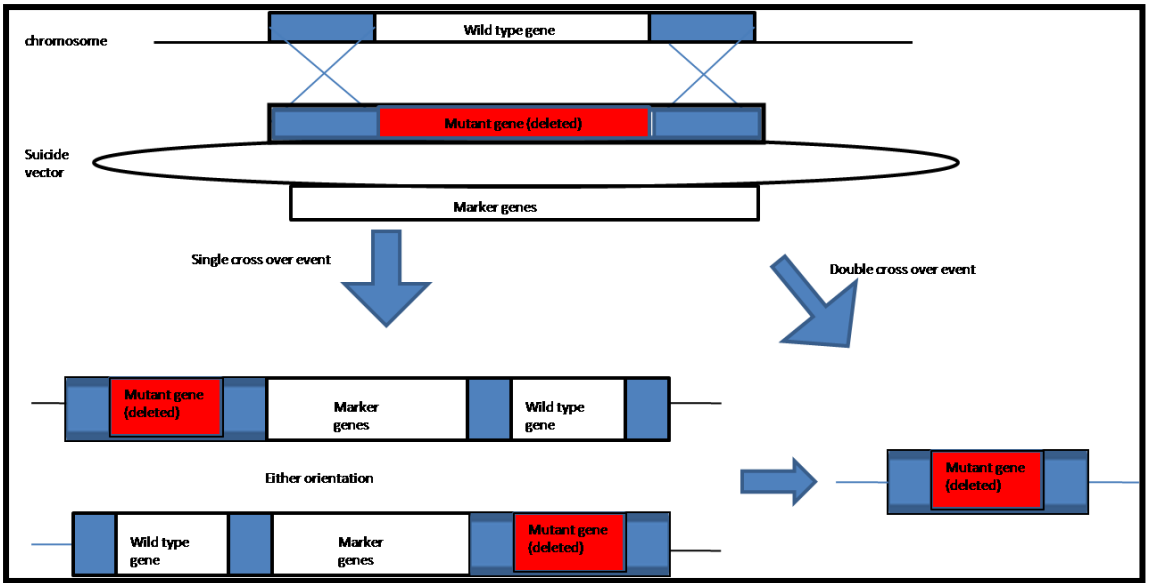

Figure 2.1: Allelic replacement by homologous recombination. Adapted from (Gordhan and Parish, 2001).

2.3. Minimal Inhibitory Concentration (MIC) determination

The role of *rpf*'s in mycobacterial drug susceptibility was determined in liquid media using the broth microdilution method (Domenech et al., 2005). *M. smegmatis* wild type and mutant strains were grown to an OD_{600nm} of 0.3. Before inoculation, the cells were diluted 500 times. The assay was set up in 96 well plates using the following antibiotics: vancomycin, erythromycin, rifampicin, D-cycloserine, and the following individually as well as with 2.5 µg/ml clavulanate: meropenem, carbenicillin, imipenem, ampicillin, cefamandole, cefapirin, cefoxitin, cefotaxime. The plates were visually read after 7 days of incubation at 37 °C, with the MIC scored as the lowest drug concentration that completely inhibited visible growth.

2.4. Thin Layer Chromatography (TLC)

Cultures were grown as described previously in a volume of 20 ml to stationary phase before being centrifuged at 3 900× g for 5 minutes. Cells were washed in 0.1 % PBS by repeated resuspending and centrifugation three times. Cells were weighed and chloroform: methanol solution (2:1) was added to cells at 20 µl / mg of cells. This mixture was incubated at room temperature with shaking overnight. The suspension was centrifuged at 3 900 × g for 30

minutes, before the supernatant was transferred to a new tube, along with 0.2 volumes of $NaCl_2$ (0.9 %). This mixture was then further centrifuged at 1150 ×g for 5 minutes. The organic phase was collected and evaporated at 65 °C. The remaining residue was resuspended in 60 µl of chloroform: methanol solution (2:1). There after, 5µl of the extract was spotted onto a TLC plate Silica Gel 60 F_{254} (Merck). Plates were run in TLC chamber for 25 minutes in chloroform: methanol solution (100:7), and air dried. Dried plates were sprayed with a mixture of Orcinol (0.1 %) and sulphuric acid (40 %) before being charred at 140 °C for 2-3 minutes.

2.5. Sodium dodecylsulphate (SDS) susceptibility testing

Strains were grown up to an OD_{600nm} of 0.5 before being serial diluted and spotted on solid Middlebrook 7H10 plates supplemented with 0.001 % SDS, 0.05 % SDS and no SDS as a control. Plates were then incubated for 5 days before visually scored for growth.

2.6. Microscopy

a.) Scanning Electron Microscopy

Assessment of Colony morphology

Actively growing culture were spotted onto solid media and grown for 4 days at 37 °C. Spots were floated off plates by pouring PBS (0.1 %) onto colonies. Colonies were transferred to microfuge tubes where they were treated with glutaldehyde (2.5 %) in PBS (0.1 %) overnight at 4 °C. Fixed cells were centrifuged at 3 900 × g for 10 minutes, and then washed with PBS (0.1 %) three times by centrifugation. The pellet was resuspended in Osmium tetra oxide (2 %) in PBS for an hour. After this, cells were washed three times with PBS (0.1 %), before being dehydrated with an alcohol series ranging from 30% EtOH to 99% EtOH. Cells were

stored after a dehydration series in ethanol (100 %). Dehydrated cells were transferred to gold coated filters (Millipore 0.22 μm pores, Merck), and dried. Filters were stuck onto a carbon disk, before being further coated with gold scatter. Colonies were visualized on JEOL JSM-5600 SEM.

Effect of imipenem on cell wall morphology

Cultures were grown from preculture to OD_{600nm} of 0.3 at 37 °C. The culture was then split into two; one half of the culture was treated with imipenem (2.5 μg / ml) for a further 3 hours. Both cultures were then treated with glutaldehyde (2.5 %) in PBS (0.1 %) overnight at 4 °C. Cultures were centrifuged at 3 900× g for 10 minutes before being washed in PBS (0.1 %) three times, by centrifugation. The pellet was resuspended in Osmium tetra oxide (2 %) in PBS for an hour. Thereafter, the cells were washed three times with PBS (0.1 %), before being dehydrated in an alcohol series ranging from 30 % EtOH to 99 % EtOH. The cells were stored after dehydration in ethanol (100 %) for viewing. All samples were couriered down to University of Cape Town, where they were visualized on the High resolution (HR) SEM, FEI Nova nanoSEM 230. Dehydrated cells were spotted onto filter papers (Millipore 0.22 μm pores, Merck), which were stuck down onto stubs for visualization after carbon coating.

Statistical analysis of HRSEM

The micrographs were visually scored to allow for descriptive statistics to be done. Five fields of view from each strain were scored at 20 000 × magnification. Descriptive statistics were done by scoring in a binary fashion the presence or absence of the following characteristics: Binary fusion, > 50 % binary fusion, bulging at ends of bacterium, bulging along the length of the bacterium, wrinkles, pitting, rings at binary fusion, V-form, Y-form, division scars and buds. The surface wrinkles were also scored on the severity: low, medium,

high. The average lengths of non-dividing cells were also measured. Normality of data was tested by the Kolmogorov Smirnov test (Statsoft.inc., 2004). The group average was used to do a cluster analysis according to the Bray-Curtis similarity method without a pre-treatment. To show the similarity between groups, a dendrogram was drawn. Analysis was done using the Primer version 6.1.5, software (Clarke and Gorley, 2006). The Mann-Whitney U test was performed on data, which was non-parametric and independent, to determine the significance of differences between lengths of wild type compared to *rpf* deficient mutants. STATISTICA version 6.1 (Statsoft.inc., 2004), was used to perform the Mann-Whitney U test. Lengths were plotted individually to determine the distribution of data.

b.) Transmission Electron Microscopy

Aliquots were taken from the modified Hartman's de Bont (mHdeB) media, Section 2.12, cultures at the required time points and centrifuged. The volume of culture taken depended on the visibility of the resulting cell pellet at the bottom of the Eppendorf tube. Volumes differed from 2 ml to 6 ml. After centrifugation, cells were washed three times with PBS (0.1 %). The pellet was resuspended in 500 µl of Ruthenium Red Fixative solution (0.1 M HEPES, 2.5 % Glutaldehyde, 2 % Formaldehyde, 0.005 % Ruthenium Red) for an hour. The cells were washed in PBS (0.1 %) and stained in Osmium tetra oxide (2 %) for an hour, before being dehydrated in an alcohol dehydration series ranging from 30 % EtOH to 99 % EtOH. Samples were transferred to Propylene Oxide and stored till they were fixed in resin. Cells were fixed in resin consisting of 5.62 g of Araldite, 7.75 g Epon 812 and 15 g DDSA. Cells in Propylene Oxide were transferred to 1:1 propylene oxide and resin for one hour, before being resuspended in 100 % resin overnight. Cells were transferred to new resin containing the accelerator DMP30 (1:40), which allows for hardening of resin, for an hour and then incubated at 60 °C for 48 hours. Solidified resin was sectioned with a diamond knife to have

a thickness of between 70 nm and 150 nm. The sections were removed from water and placed onto copper grids to dry. Once dried, grids were stained with Uranyl acetate. The Uranyl acetate was a saturated solution in 100 % methanol, and was spun down for 10 minutes before every use. Uranyl acetate was placed in a drop like fashion onto wax and staining was achieved by placing the grid, containing cells, onto the droplet for 3 minutes. After the 3 minutes, samples were rinsed in aqueous methanol (50 %) for three times before being left to dry for an hour. Lead citrate, 1 % aqueous solution, 4 % NaOH (25:1), also spun down before use, was placed in similar fashion onto wax. The grid was then once again placed on top of the droplet for 2 minutes, then rinsed with water for three times and left to dry.

c.) Confocal Microscopy

Cultures were grown to OD_{600nm} of 0.3 as discussed before. A vancomycin mixture, 1:1 vancomycin : fluorescent BioDIPY vancomycin (1 μg/ml) was added to culture and grown at 37 °C for another 90 minutes. The culture was then centrifuged and resuspended in media, before being stained with 4', 6-diamidino-2-phenylindole (DAPI) (200 μg/ml), and CellMask™ Orange (5 μg/ml), for 5 minutes. Cells were washed with media by centrifugation before being resuspended in media and streaked onto glass coverslips. The cells were heat-fixed to coverslips at 65°C on a heating block for 2 minutes before being permanently fixed with drop of fluoromount (Sigma) onto a glass slide. All slides were visualized on Zeiss LSM-780 Confocal and images processed with ZEN black software. Nile red staining was done by taking samples from the dormancy model at different time points and streaking cells directly onto glass slides. Slides were then heat fixed at 65 °C for an hour before being sprayed with Merckofix® spray and stored in the dark. When the samples were ready for processing, slides were treated with Ethanol (95 %) for 10 minutes and air-dried to remove fixative. Slides were then treated with nile red (10 μg/ml) in Ethanol

(99.9 %) for 10 minutes before being rinsed with water. The slides were permanently fixed with a drop of fluoromount (Sigma) under a coverslip. This entire process is done in a dark room. Slides were then visualized as before on Zeiss LSM-780 Confocal and images processed with ZEN black software.

2.7. Flow Cytometry

Aliquots (1000 µl) were taken from ongoing dormancy experiments, at different time points and washed in $NaCl_2$ (0.9 %) by centrifugation at 16 110 × g for 1 minute. The pellet was resuspended in 1 ml $NaCl_2$ (0.9 %) before being stained with the LIVE/DEAD® *Bac*Light™ Bacterial Viability Kit (Invitrogen). The kit contains two types of dyes, Propidium Iodide and Syto9. Both these dyes were added to microfuge tubes (1.5 µl each), containing the $NaCl_2$ solution, and incubated at room temperature for 15 minutes in the dark. The solution was decanted into a flow cytometry tube and inserted into the Beckman and Coultier Flow cytometer Gallios AN10032, Software: Gallios version 1.0. The suspension was excited at 470 nm, and emission is measured in red and green for live (green) and dead (red) cells. Results are gated and values are given as a percentage of viability.

2.8. Biofilms

Cultures were grown from pre-culture to stationary phase. The OD_{600nm} was adjusted to 1, to normalize the concentration of cells. Cells were then serially diluted and 100 µl of culture was added to 10 ml of Sauton's media in 6-well plates. Plates were sealed and incubated at 37 °C for 10 days, before being visually scored. Plates were then placed under Zeiss Stemi 200 microscope and images were taken at different magnifications, using the AxioVision software.

2.9. Motility

All strains were streaked on Middlebrook 7H10 plates and incubated for 4 days at 37 °C. Single colonies were picked from agar plates and placed on Middlebrook 7H9 media which was solidified with 0.3 % agar and left to dry on the bench overnight before use. Plates were sealed with parafilm and incubated at 37 °C for 5-10 days. Sliding was scored visually.

2.10. Neutral red staining

Strains were grown on Middlebrook 7H10 plates (as discussed) at 37 °C for 4 days. The bacterial colonies were picked from 4 day old Middlebrook 7H10 plates with an inoculation loop, resuspended in aqueous methanol (50 %) and incubated for an hour at room temperature. The solution was then washed by centrifugation and resuspended in aqueous methanol (50 %). After centrifugation at 2 360 × g for 10 minutes, the pellet was resuspended in Neutral red (0.002 %) in Barbital buffer (1 % sodium barbital, 5 % $NaCl_2$, pH 9.8), incubated overnight.

2.11. Growth on Tween 80 and Congo red staining

Strains were grown in liquid culture to an OD_{600nm} of 0.5 before being spotted and streaked onto Middlebrook 7H10 plates containing either Tween 80 (0.05 %) or Congo red (100 μg/ml) and incubated at 37 °C for 5 days. Plates were visually scored for absorption of stain or changes in morphology.

2.12. Dormancy

Strains were streaked onto solid Nutrient Broth E (NBE) (5 g $NaCl_2$, 1.5 g yeast extract, 3 g Beef extract, 7.5 g peptone, 15 g Agar per litre) and incubated for 4 days at 37°C. Single

colonies were picked and transferred to 75 ml of liquid NBE media in a 500 ml Erlenmeyer flask and grown at 37 °C, rotating at 200 rpm. After 30 hours, 400 µl of the culture was transferred to 50 ml of modified Hartman de Bont's media (mHdeB) (17.9 g Na_2HPO_4, 1.2 g citric acid, 5 ml trace element solution 1 [0.15 g Ethylenediaminetetraacetic acid (EDTA), 3 g $MgCl_2$, 0.03 g $CaCl_2$, 0.15 g $FeSO_4$ in 150 ml of water, filtered], 5 ml trace element solution 2 [0.15 g EDTA, 0.012 g $CoCl_2$, 0.037 g $MnCl_2$, 0.006 g Na_2MoO_4, 0.006 g $ZnSO_4$, $CuSO_4$ in 150 ml of water, filtered], 0.025 % Tween 80, 5 g $(NH_4)_2SO_4$, 30 ml of Glycerol, 0.025% bovine serum albumin (BSA). The solution was adjusted to pH 7 with citric acid, 0.025%). The culture was grown at 37 °C in a 250 ml Erlenmeyer flask, rotating at 200 rpm. Aliquots were taken to determine colony forming units (CFU) for viability when streaked onto solid NBE plates.

2.13. Resuscitation

Aliquots of dormant cells were taken at 72 hours (Shleeva et al., 2004), after being transferred to mHdeB media, and washed in Sauton's media by gentle centrifugation. Spent media was made by growing *M. smegmatis* mc^2155 and the quadruple *rpf* mutant, from starter cultures, for 30 hours to OD_{600nm} of 0.5 at 200 rpm at 37 °C. The cultures were then centrifuged and filtered to remove cells. The spent media was diluted with an equal volume Sauton's media, containing 0.6 % Glycerol and 0.025 % yeast extract. Most Probable Number (MPN) assay was performed by adding 1 ml of spent media (containing different dilutions of "dormant" cells) into 48-well plates. The plates were incubated at 37 °C for 10 – 14 days and scored visually for growth.

3. Results

3.1. Analysis of the *rpf*-like gene complement in *M. smegmatis*.

Previous work from the CBTBR demonstrated that five *rpf*-like genes in *M. tuberculosis* are dispensable for growth *in vitro*. At this point, no information was available on *rpf*-like gene function in the closely related *M. smegmatis* strain. In this context, the CBTBR undertook to characterize the *rpf* genes in *M. smegmatis* by creating a panel of mutant strains that could be used for specialized microscopic analysis, and other technically challenging experiments, that could not be done with the *M. tuberculosis* Rpf mutants. The genomic complement and organization of the *rpf* genes in these two mycobacterial strains is shown in Figure 3.1 and further again in Figure 3.2 as alignments with the corresponding genes in *M. tuberculosis*. Two features distinguish *M. smegmatis* from *M. tuberculosis*: (I) *M. smegmatis* encodes only four *rpf*-like genes and does not retain a homologue for *rpfD*. The entire region encoding *rpfD* is deleted from the genome of *M. smegmatis*, when compared to *M. tuberculosis*, this can be seen in the genomic region comparison for *rpfD* shown in Figure 3.2. (II) The genomic context of *rpfC* and *rpfE* is different in *M. smegmatis* relative to *M. tuberculosis* where both genes are arranged proximal to each other in the former and in contrast, they found at distinct, distal chromosomal loci in the latter, Figure 3.1 and Figure 3.2. Considering the genomic context, an important point to note here is that there is no clear homologue of *rpfC* in *M. smegmatis* with a sequence similarity of 65%, compared to the *rpfA* and *rpfB* homologues that have a sequence similarity of 67% and 78% respectively, between *M. smegmatis* and *M. tuberculosis*. Rather, there seems to be a gene duplication at the *rpfE* locus in this organism, which has a sequence similarity of 80% between these two organisms. BLAST searches with the *M. tuberculosis rpfC* identified this duplicated gene, MSMEG-_4643, as an "*rpfC*-family-like" homologue (Ravagnani et al., 2005a). Hence, in *M. smegmatis* we have designated this gene as *rpfC* and the associated homologue,

MSMEG_4640, as *rpfE*. The chromosomal context of *rpfA*, *rpfB* and *rpfE* is similar in *M. smegmatis* and *M. tuberculosis*, Figure 3.1 and Figure 3.2. As mentioned previously, the five *rpf*-like genes in *M. tuberculosis* are dispensable for growth *in vitro* (Kana et al., 2008). Interestingly, the two *rpf*-like genes in *Corynebacterium glutamicum* ATCC 13032 are also dispensable for growth *in vitro* (Hartmann et al., 2004). These data contrast with the essentiality of the single *rpf* gene in *Mi. luteus* (Mukamolova et al., 2002a), suggesting a divergence of Rpf associated function in other actinomycetes which may form the basis of the genetic multiplicity associated with these genes in many bacteria. Preliminary work by an MSc student at the CBTBR resulted in the construction of a mutant strain (Δ*rpfA* Δ*rpfB*) of *M. smegmatis* that was deficient in two of the four *rpf*s in this model organism. To further test *rpf* gene essentiality in mycobacteria, the first aim of this work was to delete all *rpf* –like genes in *M. smegmatis*, using the previously constructed *M. smegmatis* Δ*rpfA* Δ*rpfB* double mutant and a knockout vector that allows for the simultaneous deletion of *rpfC* and/or *rpfE*. As mentioned earlier, the *rpfE* and *rpfC* genes occur together on the chromosome of *M. smegmatis*, with an intervening gene that is predicted to be transcribed on the complement strand, Figure 3.1. Considering the distance between the two genes, it is unlikely that *rpfC* and *rpfE* are operonic and would hence require individual deletion.

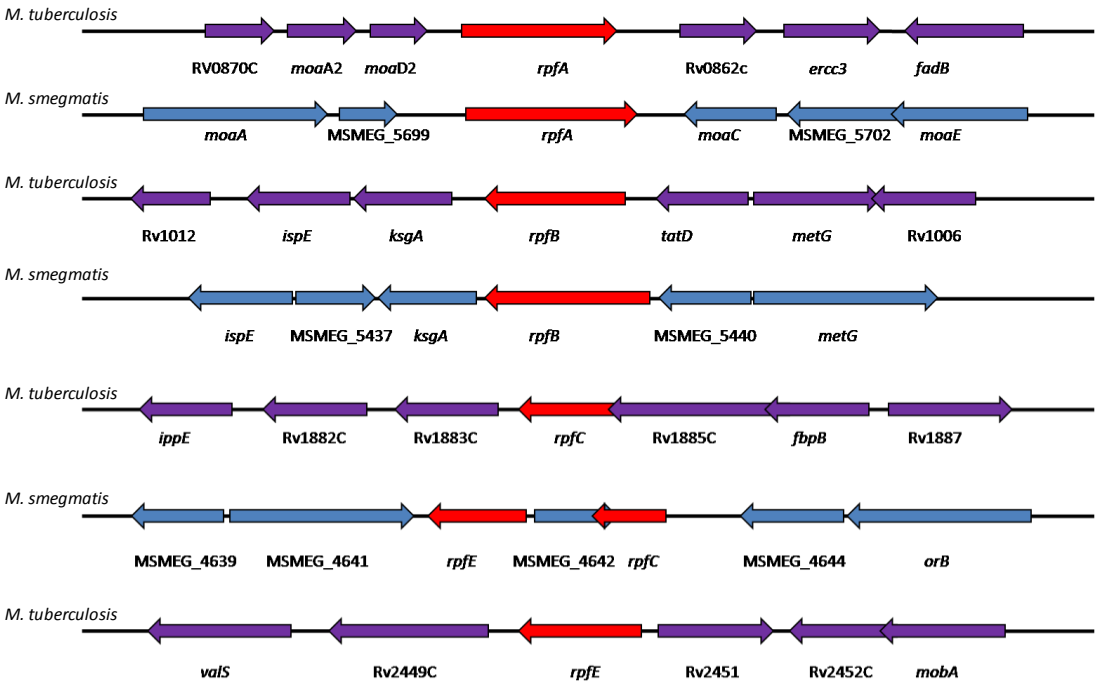

Figure 3.1: Schematic presentation of genomic context of *rpf*-like genes in *M. smegmatis* compared to the corresponding genes in *M. tuberculosis.* Genomic organization was determined by interrogating the Smegmalist (Kapopoulou et al., 2010) and Tuberculist databases (Lew et al., 2011) and using the Artemis Comparison Tool (Carver et al., 2005).

rpfA

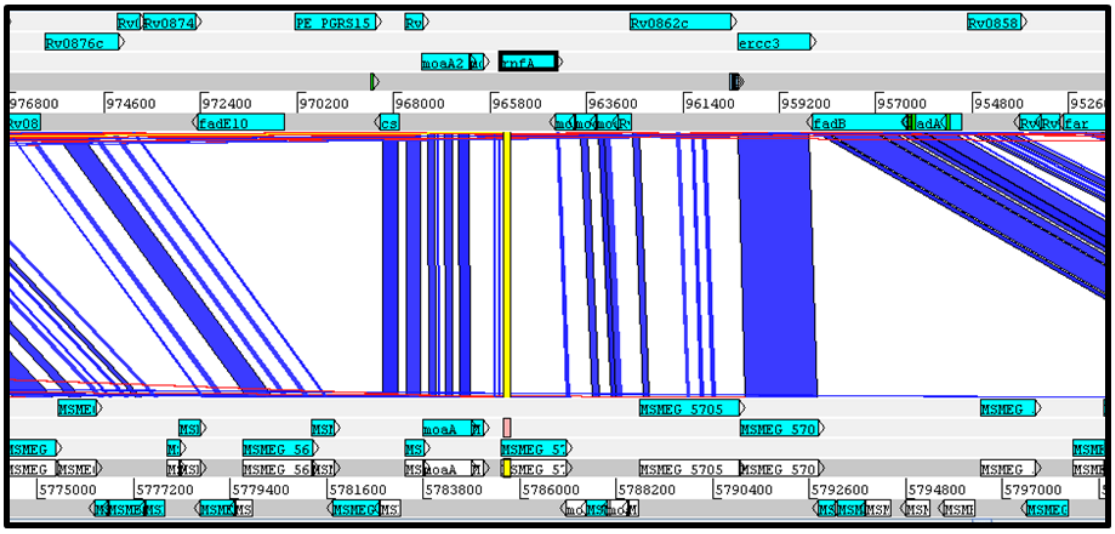

rpfB

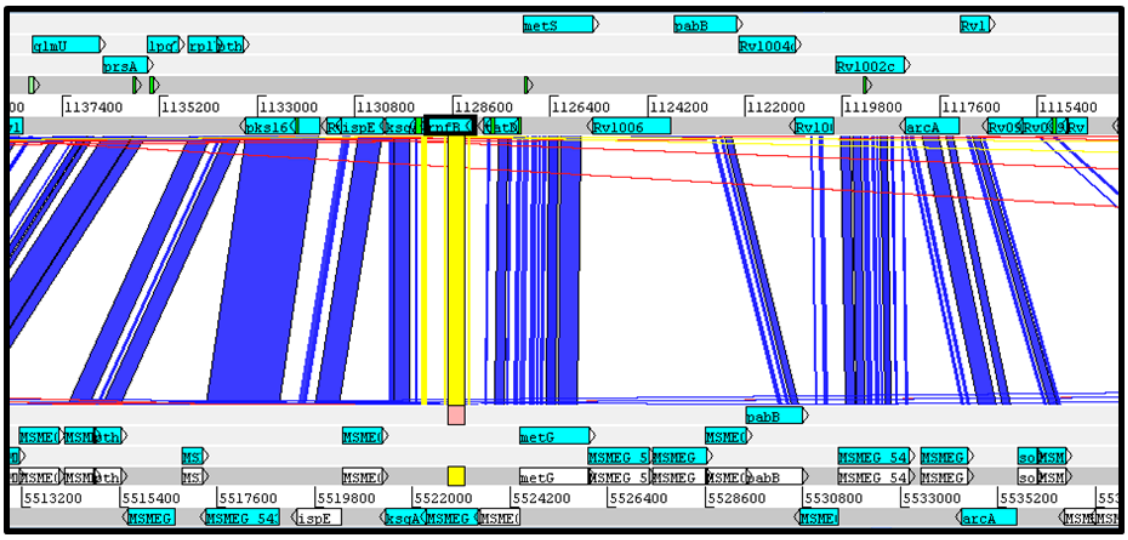

rpfD

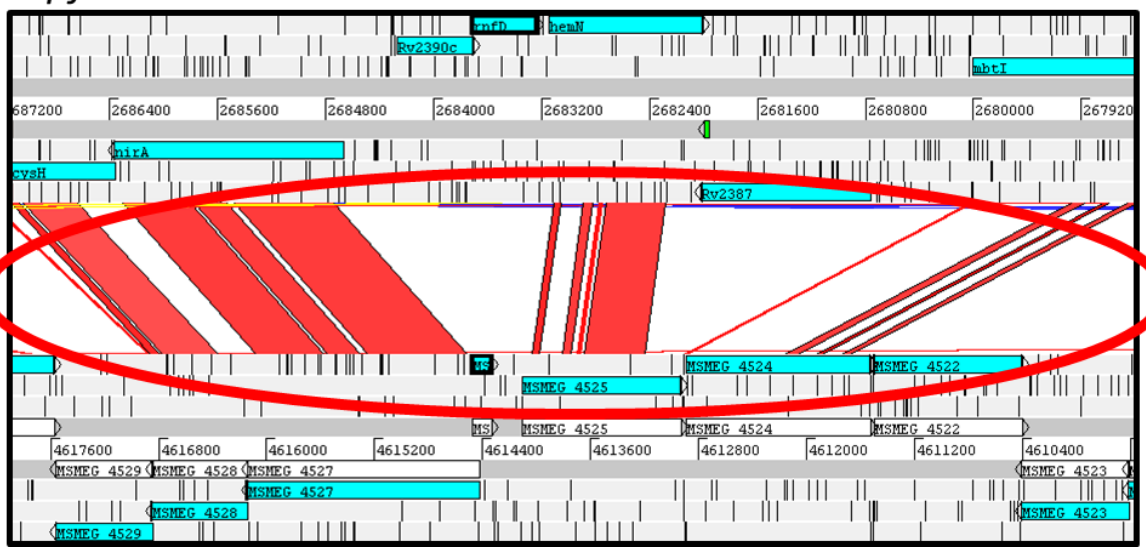

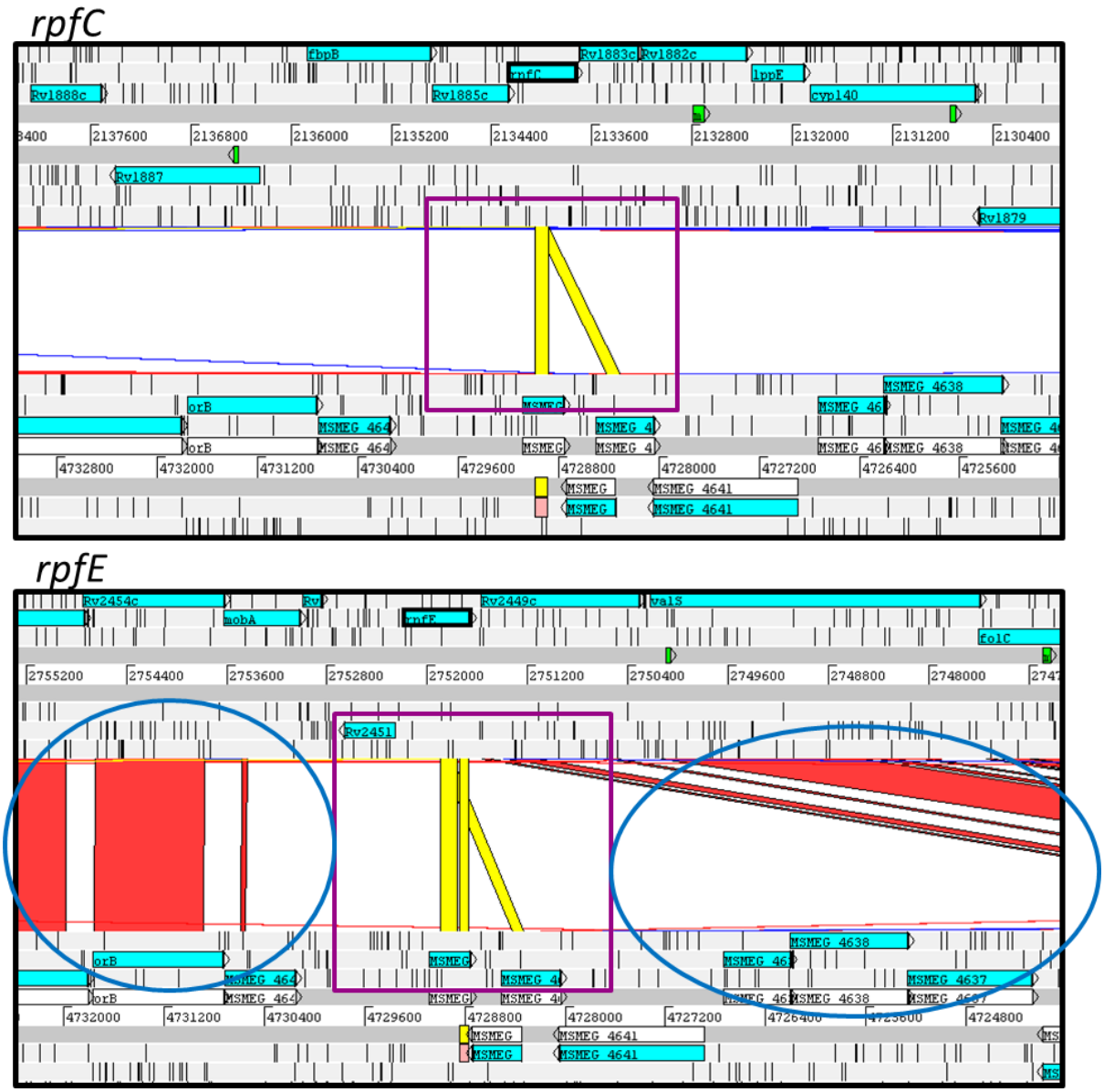

Figure 3.2: Gene alignment snapshots from the Artemis Comparison Tool (ACT) program (Carver et al., 2005). Shown are alignments of the genomic context of *rpf*-like genes in *M. smegmatis* compared to *rpf*-like genes in *M. tuberculosis.* Screen snaps were taken to show the alignment of the *rpf* genes and moreover, the homology between the associated upstream and downstream regions. Blue, red and yellow shaded areas that connect the two genomes indicate areas of homology and confirm that gene synteny is conserved. Yellow lines specifically represent the alignment of the *rpf* genes. Both *rpfA* and *rpfB* have a similar genomic context between the two organisms as is indicated by the blue lines. The red circle shows that the genomic context of *rpfD* is similar between the two organisms but the actual *rpfD* gene and some associated sequence has been lost. For the *M. tuberculosis rpfC/rpfE*, BLAST searches and ACT comparisons identify the same region (purple squares) in the *M. smegmatis* genome. This region looks similar to the *rpfE* region of *M. tuberculosis* (blue circles), suggesting that in *M. smegmatis*, *rpfE* has been duplicated. However, for simplicity and because MSMEG_4643 displays higher homology to the *M. tuberculosis rpfC*, we have designated the duplicated gene as "*rpfC*".

To facilitate individual and combinatorial deletion of *rpfC* and *rpfE*, the knockout vector pCEM was designed, using the homologous regions upstream and downstream of *rpfE* locus in *M. smegmatis*, in a way that would allow for deletion of *rpfC* or *rpfE* or both genes simultaneously, Figure 3.3. Homologous regions upstream and downstream of the *rpfC*/*rpfE* locus were cloned, along with the intervening segment into a suicide vector, which resulted in the production of a deletion cassette that carried unmarked deletions in both *rpfC* and *rpfE*, Figure 3.3. This strategy removes the end of MSMEG_4642, however blast gene searches and ACT comparison did not identify this as a functional gene with homology to known protein. Hence the annotation of MSMEG_4642 as an ORF in *M. smegmatis* may be incorrect. Removal of the end of MSMEG_4642 was necessary to ensure that functional domains from *rpfC* were deleted.

The knockout vector, PCEM was created by former MSc student, Ms Lusanda Mapela, but was not characterized and confirmed extensively by restriction analysis. The first step of this MSc was to characterize this vector by restriction analysis and sequencing.

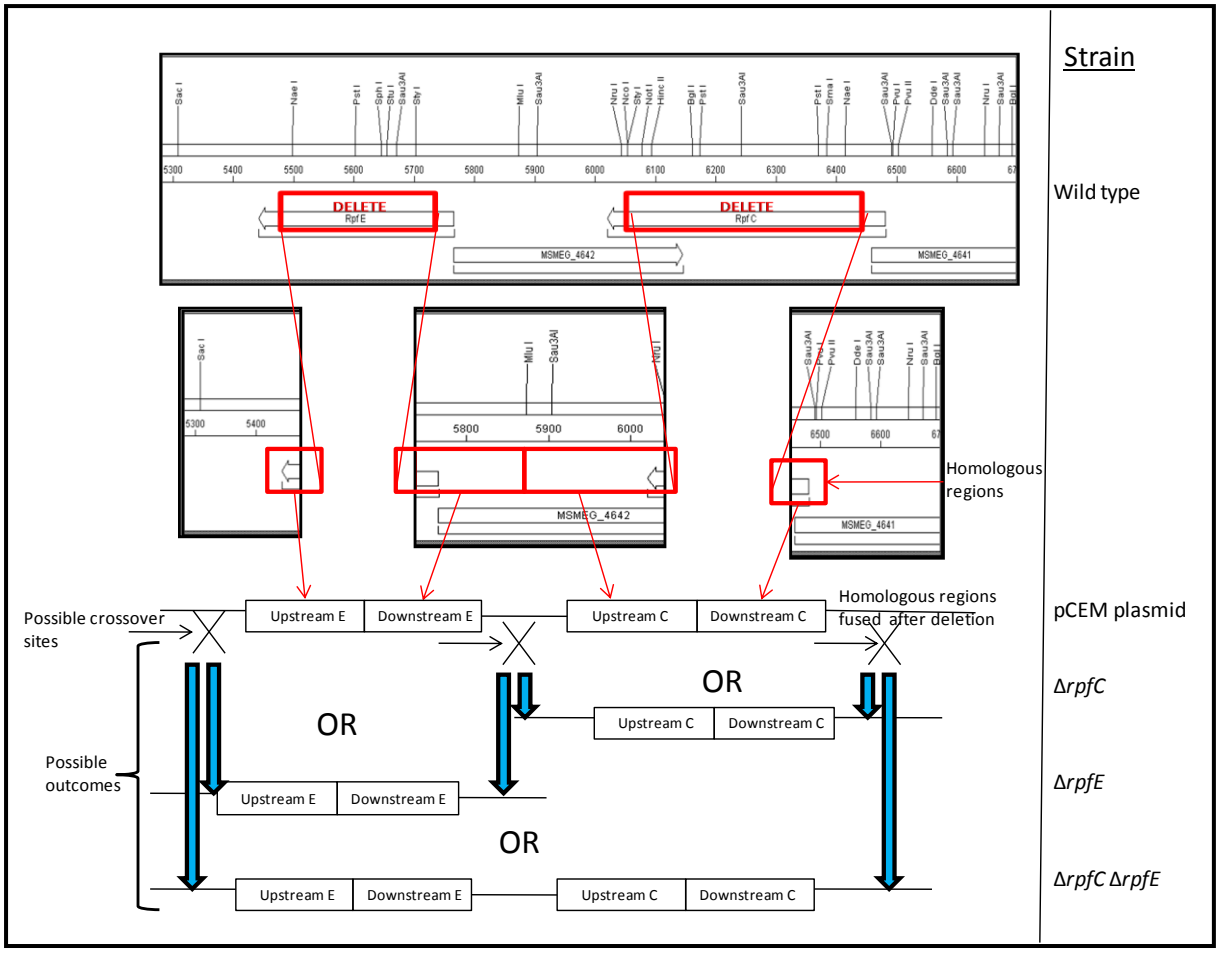

Figure 3.3: The construction of the Δ*rpfC* and/or Δ*rpfE* mutant with possible outcomes of deletion mutagenesis when using the pCEM construct. Wild type gene sequences for *rpfC* and *rpfE* were used to determine the homologous region to be incorporated into the suicide vector, adapted from Smegmalist (Kapopoulou et al., 2010). Homologous regions were fused together to facilitate a crossover between the suicide vector and the chromosome (Gordhan and Parish, 2001). The construction of the pCEM construct is such that there are three possible places where homologous recombination and crossover can occur, these are shown as crossed lines. Considering this, there are three possible allelic exchange outcomes when using this vector, the first is crossover between the upstream and downstream regions of *rpfE* give rise to an Δ*rpfE* mutant. The second is crossover between the upstream and downstream regions of *rpfC*, which would yield an Δ*rpfC* mutant. Finally, crossover between the upstream region of *rpfC* and the downstream region of *rpfE* will result in replacement of the entire chromosomal region to yield a Δ*rpfC* Δ*rpfE* double deletion. Map generated using Mapdraw (Clewley, 1995).

3.2. Analysis of the pCEM knockout vector to delete *rpfC* and *rpfE* in *M. smegmatis*.

3.2.1. Plasmid restriction mapping and sequencing

Restriction mapping was carried out on bulk plasmid preparations of pCEM to determine the orientation of the genes in the plasmid as well as to make sure that no rearrangement of the plasmid occurred during amplification in the *E.coli* host. The predicted restriction map, from

in silico analysis of the cloned PCR fragments, can be seen in Figure 3.4, as well as the expected and actual sizes of fragments obtained during restriction analysis.

A.

Enzyme	Expected (size bp)
*Acc*1	3694, 2897, 2541, 2012, 1505
*Bam*H1	9574, 3072
*Eco*R1	9867, 1863, 766, 150
*Pst*1	5696, 3937, 3013
*Pvu*1	5527, 2384, 1907, 1169, 726, 480, 453

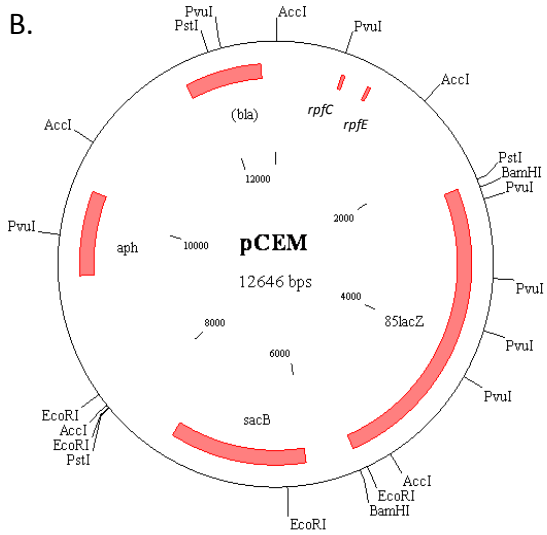

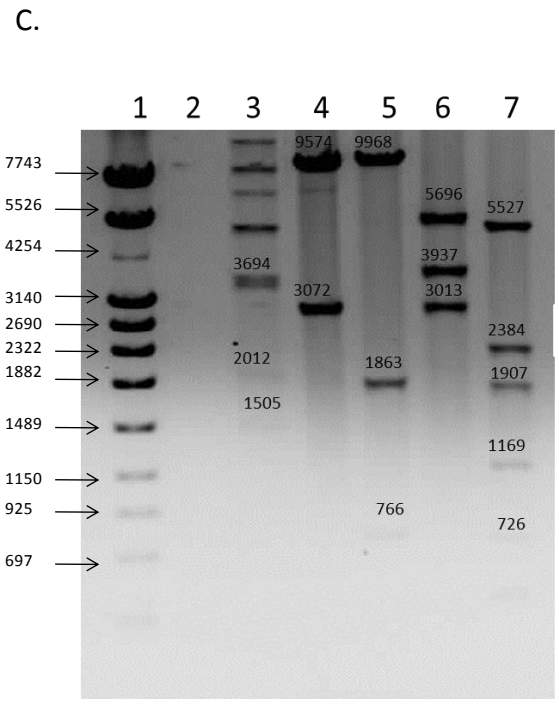

Figure 3.4: Restriction mapping of knockout vector, pCEM. A: Table of Restriction enzymes with their expected sizes. B: The predicted map of pCEM, with the restriction enzymes indicated on the map. C: Gel image of restriction digests electrophoresed on a 1% agarose gel. Lane 1: Marker IV, Lane 2: Blank, Lane 3: *Acc*I, Lane 4: *BamH*I, Lane 5: *Eco*RI, Lane 6: *Pst*I, Lane 7: *Pvu*I, fragment sizes shown in bp.

The restriction fragment pattern that was obtained for *Pvu*I, *Pst*I, *Eco*RI and *Bam*HI were all correct and as expected, Figure 3.4, small fragments (700 bp and below) were very light and difficult to visualize, but were visible when the gel was overexposed (not shown). Restriction digest with *Acc*1 yielded products of incomplete digestion which could not be interpreted. Repeated digestion did not improve this result suggesting that there was a problem with the preparation of the enzyme. To further test the integrity of the vector and to make absolutely sure that the correct fragments were cloned, the region that would be used to facilitate the homologous recombination was digested from the plasmid along with the plasmid backbone, purified and ligated to itself for further restriction analysis – this process removed the *lacZ*/*sacB* cassette. A positive clone was selected on kanamycin containing plates and the

plasmid DNA extracted and subjected to extensive restriction analysis, Figure 3.5. The fragments observed for restriction digest with *Acc*I, *Eag*I, *Nar*I, *Nru*I, *Pvu*I, *Sal*I and *Mlu*I all corresponded to the predicted sizes from the restriction map of pINSCE, Figure 3.5. There was still some incomplete digestion with *Acc*I. The restriction pattern from Acc651 suggests that this enzyme did not digest the DNA, since the banding pattern looked similar to the uncut vector control. These data confirm the genetic integrity of the vector however, one digest pattern – for *Pvu*II, did not match the predicted fragment sizes. Analysis of the map suggested that the discrepancy in this case came from sites introduced during the sub-cloning steps that were not accounted for in the predicted map (data not shown). Collectively, the data from Figure 3.4 and Figure 3.5 confirmed the genetic integrity of the homologous region in the knockout vector. However, for further and absolute confirmation, the entire deletion allele cassette, including upstream and downstream homologous regions were sequenced from the final knockout vector. The sequence analysis (Figure 3.10) confirmed that the homologous regions were intact, with no mutations, and that the deletion alleles were present as expected, with the correct amount of sequence deleted from both the *rpfC* and *rpfD* genes. This extensive analysis yielded unequivocal confirmation of the genetic integrity of the homologous regions, vector backbone and marker cassettes in pCEM for use in allelic exchange mutagenesis.

A.

Enzyme	Expected (size bp)
*Acc*I	2773, 2012, 1502
*Eag*I	4737, 1039, 256, 145, 110
*Nar*I	5635, 352, 187, 113
*Acc*651	6287
*Nru*I	3229, 2740, 318
*Pvu*I	2734, 2384, 1169
*Pvu*II	5390, 897
*Sal*I	6287
*Mlu*I	6287

B.

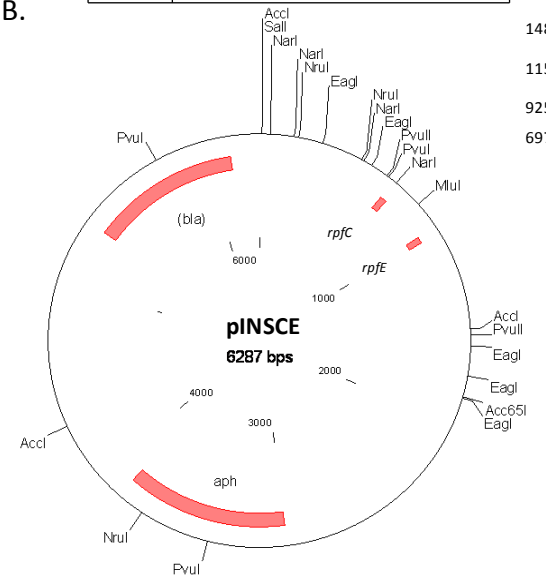

C.

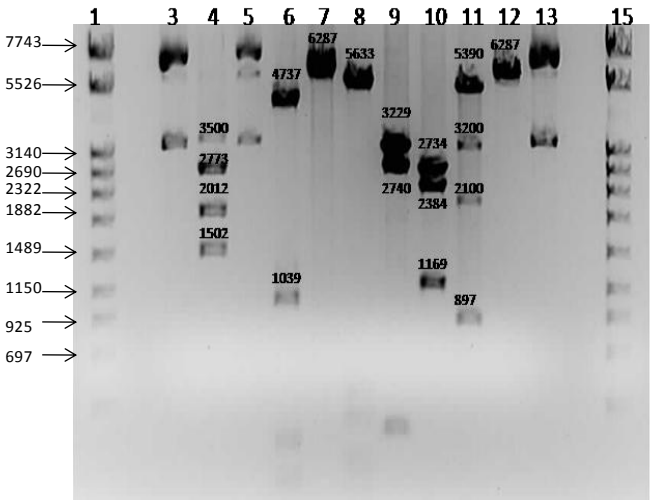

Figure 3.5: Restriction mapping of knockout vector, pINSCE. A: Table of Restriction enzymes with their expected sizes. B: The predicted plasmid map of pINSCE, with the restriction enzymes indicated on the map. C: Gel image of restriction digests electrophoresed on a 1% agarose gel. Lane 1, 15: Marker IV, Lane 3, 13 uncut plasmid, Lane 4: *Acc*I, Lane 5: *Acc*651, Lane 6: *Eag*I, Lane 7: *Mlu*I, Lane 8: *Nar*I, Lane 9: *Nru*I, Lane 10: *Pvu*I, Lane 11: *Pvu*II, Lane 12: *Sal*I, Lane 13 uncut plasmid, fragment sizes shown in bp.

3.2.2. Allelic Exchange mutagenesis

After obtaining sequence confirmation, the pCEM vector was used for allelic exchange mutagenesis by electroporating the vector into both the wild type and Δ*rpfA* Δ*rpfB* background strains. The two-step selection method described in section 2.2 of the Material and Methods section was used to select for mutant clones. In the wild type strain, this process resulted in the production of Δ*rpfC* and Δ*rpfE* single deletion mutants and a Δ*rpfC* Δ*rpfE* double mutant, Figure 3.3. In the Δ*rpfA* Δ*rpfB* mutant background, deletion mutagenesis with the pCEM vector resulted in the production of Δ*rpfA* Δ*rpfB* Δ*rpfC* and Δ*rpfA* Δ*rpfB* Δ*rpfE* triple mutants as well as a Δ*rpfA* Δ*rpfB* Δ*rpfC* Δ*rpfE* quadruple mutant. The production of the

quadruple mutant confirmed that, as in *M. tuberculosis* and *C. glutamicum*, the entire complement of *rpf*-like genes in *M. smegmatis* was dispensable for *in vitro* growth. After counter selection, the putative knockout clones were analysed by Southern Blotting to determine the genetic integrity of these clones at the *rpfC*/*rpfE* locus.

3.2.3. Southern Blotting to confirm mutant genotypes.

Southern Blotting on the putative knockout clones was done to ensure site-specific integration of the knockout vector, and subsequent deletion of the genes of interest with no added chromosomal rearrangements or inadvertent second site effects. For comparison, the strains used in this analysis were, wild type mc^{2}155, Δ*rpfA*, Δ*rpfB*, Δ*rpfC*, Δ*rpfE*, Δ*rpfA* Δ*rpfB*, Δ*rpfC* Δ*rpfE*, Δ*rpfA* Δ*rpfB* Δ*rpfC*, Δ*rpfA* Δ*rpfB* Δ*rpfE*, Δ*rpfA* Δ*rpfB* Δ*rpfC* Δ*rpfE*.

Analysis of the *rpfC* deletion region

For this analysis, chromosomal DNA was extracted from putative clones or wild type and subjected to restriction digest with *Not*I, which was chosen since it has a restriction site within the deleted region of *rpfC* as well as sites in the upstream and downstream regions, which are outside of the regions used for homologous recombination. This latter point ensures site-specificity of the analysis. Southern blotting with a probe that was homologous to the region upstream of *rpfC*, green box shown in Figure 3.6, revealed that the mc^{2}155, Δ*rpfA*, Δ*rpfB*, Δ*rpfE*, Δ*rpfA* Δ*rpfB*, and Δ*rpfA* Δ*rpfB* Δ*rpfE* strains all displayed the wild type genotype for the *rpfC* locus and the Δ*rpfC*, Δ*rpfC* Δ*rpfE*, Δ*rpfA* Δ*rpfB* Δ*rpfC*, Δ*rpfA* Δ*rpfB* Δ*rpfC* Δ*rpfE* retained the mutant *rpfC* genotype, as expected. These results provided confirmation that knockout mutagenesis of the *rpfC* gene in *M. smegmatis* was successful.

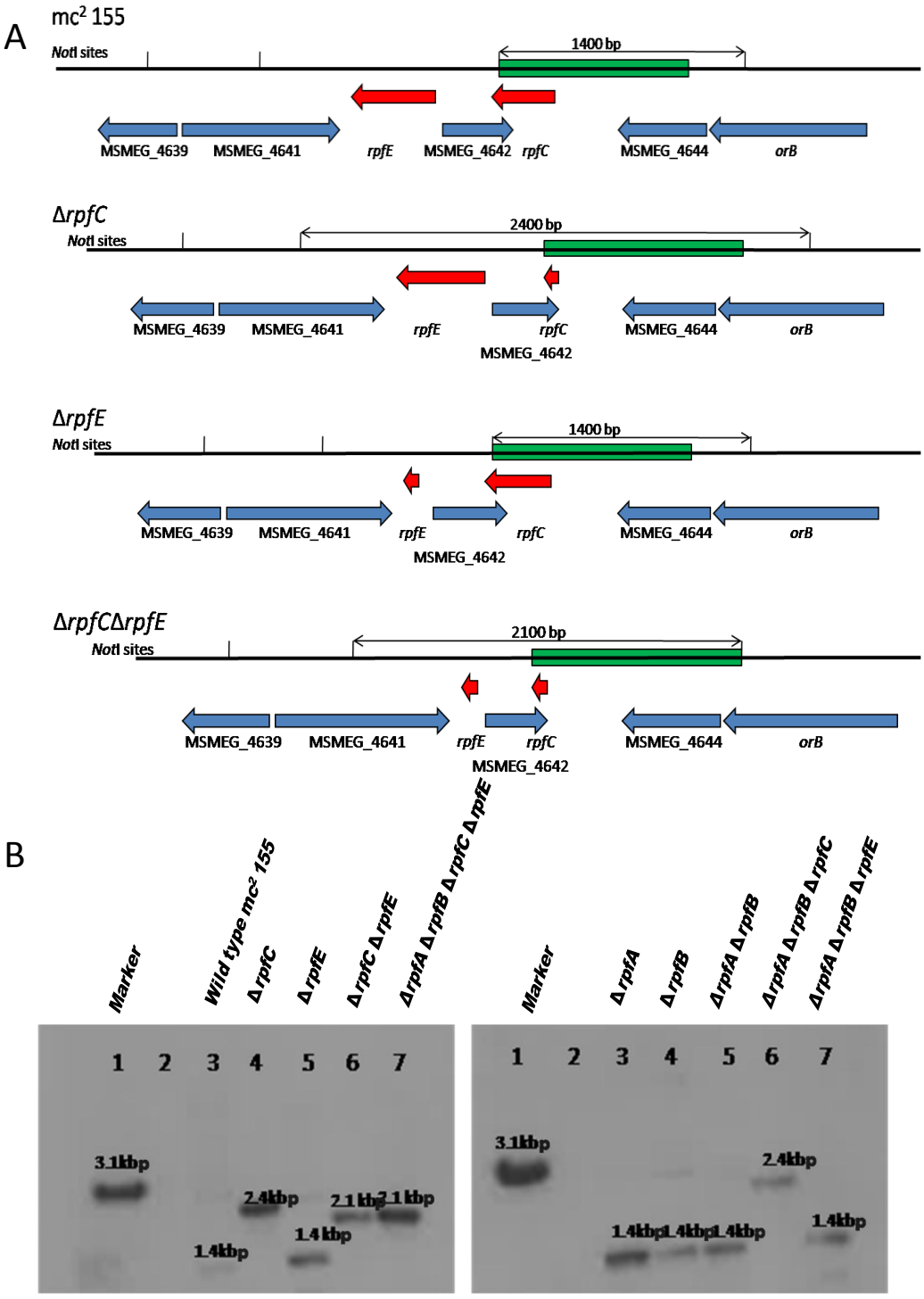

Figure 3.6: Southern blot analysis of the *rpfC* region in wild type and mutant strains. A. Diagram showing the genomic context of *rpfC* and *rpfE*. Green box indicate the region of probe homology and arrows indicate the sizes of fragments that the probe is expected to hybridize to. B: Southern blot showing the hybridization pattern. LEFT: Lane 1: Marker 4, Lane 2: Blank, Lane 3: wild type, Lane 4: Δ*rpfC*, Lane 5: Δ*rpfE*, Lane 6: Δ*rpfC* Δ*rpfE*, Lane 7: Δ*rpfA* Δ*rpfB* Δ*rpfC* Δ*rpfE*. RIGHT: Lane 1: Marker 4, Lane 2: Blank, Lane 3: Δ*rpfA*, Lane 4: Δ*rpfB*, Lane 5: Δ*rpfA* Δ*rpfB*, Lane 6: Δ*rpfA* Δ*rpfB* Δ*rpfC*, Lane 7: Δ*rpfA* Δ*rpfB* Δ*rpfE*.

Analysis of the *rpfE* deletion region

For analysis of the *rpfE* region, chromosomal DNA was digested again with *Not*I, as described above since the *Not*I sites flank the *rpfE* gene and consequently, the deletion in this gene can be measured by a reduction in the size of the *Not*I fragment, Figure 3.7, as well as confirming the presence of the Δ*rpfC* gene in combinatorial mutants. The southern blotting analysis, shown in Figure 3.6 revealed that the mc^2155, Δ*rpfA*, Δ*rpfB*, Δ*rpfC*, Δ*rpfA* Δ*rpfB*, Δ*rpfA* Δ*rpfB* Δ*rpfC* strains all displayed the wild type genotype for the *rpfE* locus and the Δ*rpfE*, Δ*rpfC* Δ*rpfE*, Δ*rpfA* Δ*rpfB* Δ*rpfE*, Δ*rpfA* Δ*rpfB* Δ*rpfC* Δ*rpfE* displayed the mutant *rpfE* genotype, as expected. These results provided confirmation that knockout mutagenesis of *rpfE* gene in *M. smegmatis* was also successful. From the Southern blotting, it is evident that the regions flanking the *rpfC/rpfE* locus were not subjected to any inadvertent rearrangements except for the in-frame deletions in *rpfC* and *rpfE*, which have resulted from homologous recombination.

3.2.4. PCR confirmation of mutant genotypes.

Whilst the Southern Blotting analysis unequivocally confirmed the deletion genotypes, a PCR screen (Figure 3.9) that simultaneously allowed for detection of both the wild type and mutant alleles for all four *rpf*-like genes in *M. smegmatis* was also designed and used for further confirmation of genotypes. This strategy was designed for routine use throughout the MSc project to ensure that there was no inadvertent mixing of mutant strains. PCR primers were designed to bind the genomic DNA as illustrated in Figure 3.8. One forward primer situated upstream of the gene of interest and two reverse primers were used. The first reverse primer binds inside the gene of interest (within the deleted region) whereas the other binds downstream of the gene, Figure 3.8. If the gene of interest is deleted, a ~100 bp band would be obtained. This will be compared against the wild type strain, which will produce a 300 bp fragment for *rpfE* or *rpfC*. Similarly, further sets of primers for the detection of *rpfA* and *rpfB*

wild type and mutant genotypes were also used, these are shown in Figure 3.8. Genotypic analysis using these primers and PCR confirmed that the genotypes of all mutant strains were as expected, Figure 3.9.

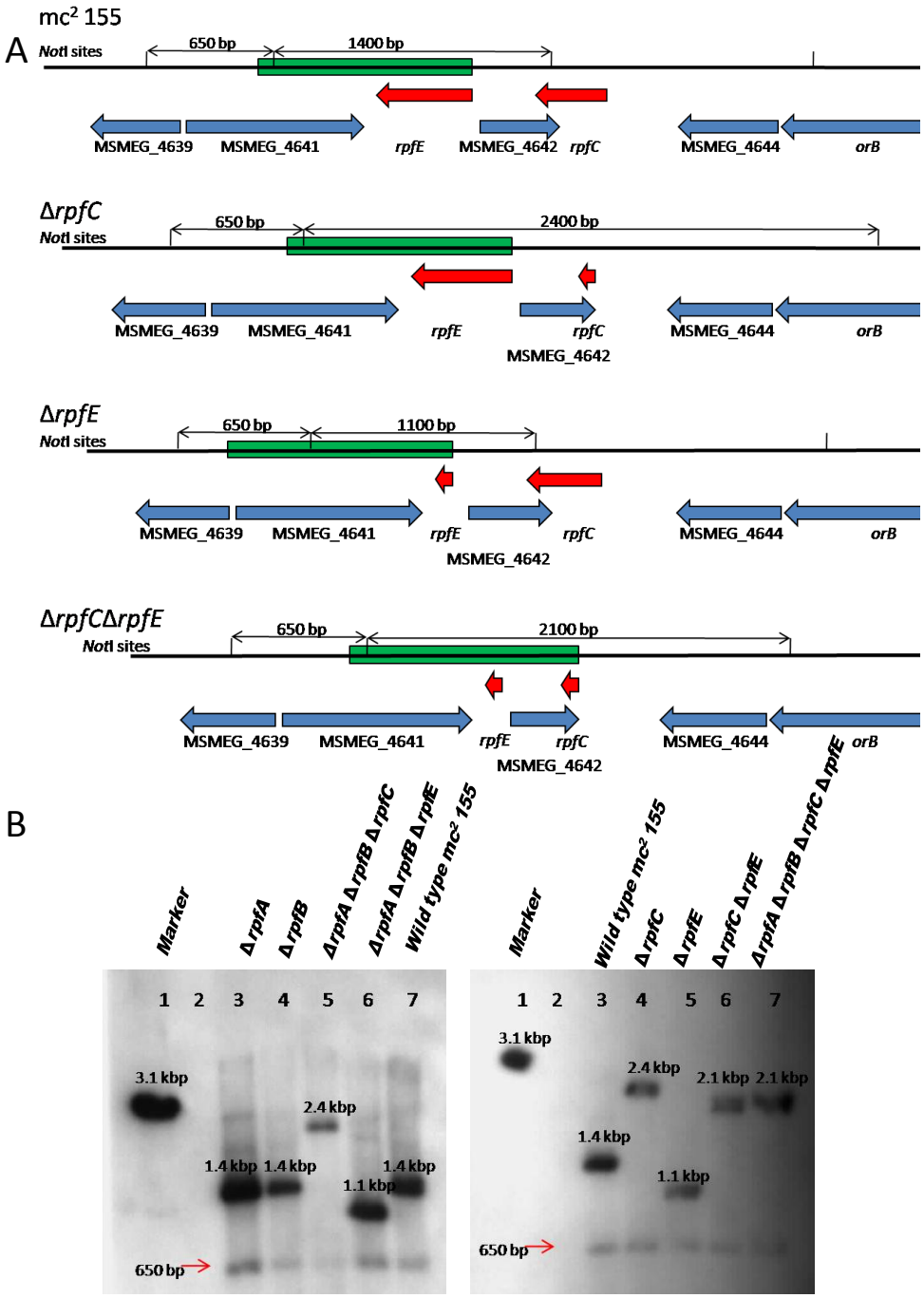

Figure 3.7: Southern blot analysis of the *rpfE* region in wild type and mutant strains. A. Diagram showing the genomic context of *rpfC* and *rpfE*. Green box indicates the region of probe homology and arrows indicate the sizes of fragments that the probe is expected to hybridize to. B: Southern blot showing the hybridization pattern. LEFT: Lane 1: Marker 4, Lane 2: Blank, Lane 3: Δ*rpfA*, Lane 4: Δ*rpfB*, Lane 5: Δ*rpfA* Δ*rpfB* Δ*rpfC*, Lane 6: Δ*rpfA* Δ*rpfB* Δ*rpfE*, Lane 7: wild type. RIGHT: Lane 1: Marker 4, Lane 2: Blank, Lane 3: wild type, Lane 4: Δ*rpfC*, Lane 5: Δ*rpfE*, Lane 6: Δ*rpfC* Δ*rpfE*, Lane 7: Δ*rpfA* Δ*rpfB* Δ*rpfC* Δ*rpfE*.

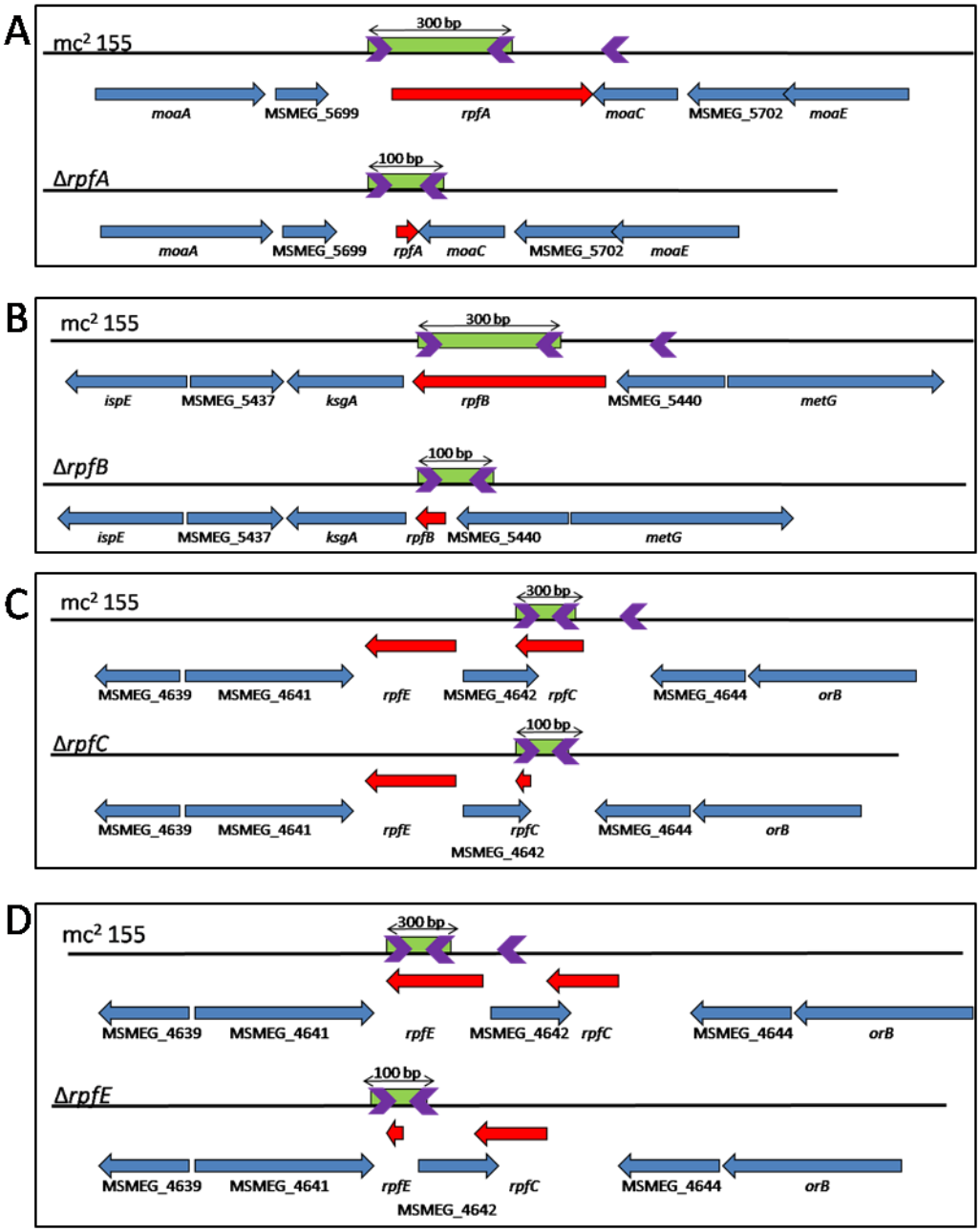

Figure 3.8: PCR screen for deletion genotypes. Screening primer location on genomic regions for *rpfA* (A), *rpfB* (B), *rpfC* (C) and *rpfE* (D) are shown. Purple arrows indicate primer location, one forward and two reverse. These are located upstream, downstream and within the gene of interest - within the deleted region. Green box: If the gene is present a 300 bp band would be seen on the gel, if the gene is deleted a 100 bp band will be created by the primers which bind outside of the gene. Gene annotation from Smegmalist (Kapopoulou et al., 2010).

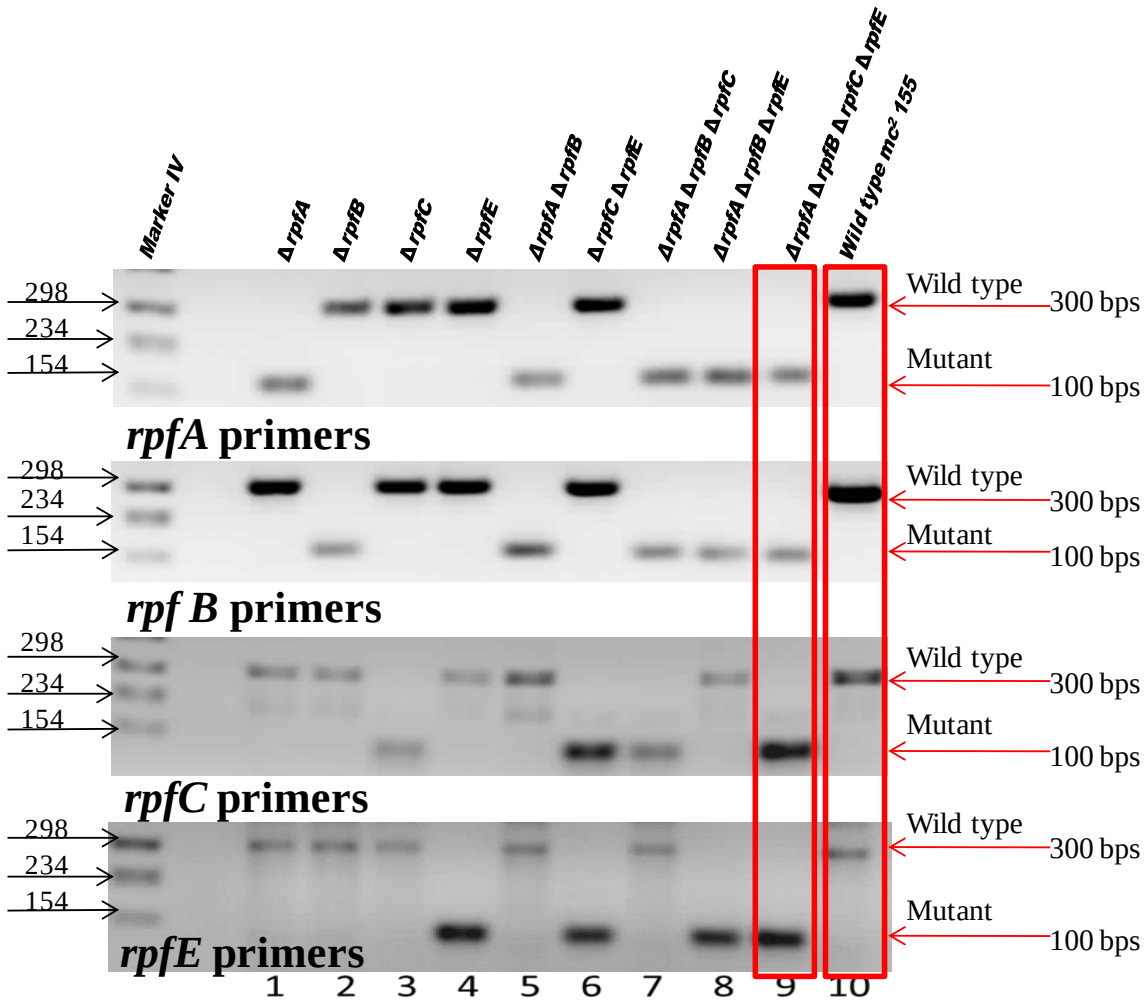

Figure 3.9: Genotypic confirmation of *rpf* deletion strains using a PCR screen designed to differentiate mutant alleles. Primers are placed upstream, downstream and inside the gene to give different size PCR products. If the gene is deleted the reverse primer inside the gene will not bind and the reverse primer further downstream will be brought closer to the upstream primer, giving a smaller PCR product. Lane 1: Δ*rpfA*, Lane 2: Δ*rpfB*, Lane 3: Δ*rpfC*, Lane 4: Δ*rpfE*, Lane 5: Δ*rpfA* Δ*rpfB*, Lane 6: Δ*rpfC* Δ*rpfE*, Lane *7:* Δ*rpfA* Δ*rpfB* Δ*rpfC*, Lane *8:* Δ*rpfA* Δ*rpfB* Δ*rpfE*, Lane *9:* Δ*rpfA* Δ*rpfB* Δ*rpfC* Δ*rpfE*, Lane 10: *M. smegmatis mc*^{2}155. Red blocks indicate the quadruple *rpf*-deficient mutant and wild type, to demonstrate the difference in banding pattern. The grid below summarizes the genotypes for these strains, - indicates the presence of a deletion allele and + indicates the presence of the wild type allele.

3.2.5. Sequence confirmation of the *rpfC* and *rpfE* mutant genotypes.

As discussed in section 3.1.1 plasmid pINSCE was confirmed by restriction analysis and sub-cloning to ensure the integrity of the region used for deletion mutagenesis. To further assess this region, and the mutant strains that resulted from use of this deletion cassette, oligonucleotides (Table 2.3) were designed to sequence this region to determine the sequence in the knockout vector and in the resulting mutant strains. In the case of the latter, the *rpfC*/*rpfE* locus from wild type and mutant strains was amplified by PCR and subjected to sequencing. The sequences obtained were combined in DNAMAN (Lynnon.Corp., 2007) to determine the consensus sequence for this region. This sequence was then compared to the published sequence for this region, Figure 3.10. As mentioned before, the sequence of the entire homologous region and the deletion alleles proved to be correct with no mutations. However, we found that a TG and GG were inserted into the sequence of the plasmid at the cloning junction sites; this explained the discrepant restriction banding pattern obtained for one restriction digest in Figure 3.5. To ensure that these were not introduced into the chromosome during recombination, this region was sequenced in all mutant strains that were generated in this study. The sequences were once again aligned to determine the sequence of each strain using DNAMAN. All of these sequences were then aligned with one another for comparison. The wild type sequence was obtained from the Smegmalist website (Kapopoulou et al., 2010) for comparison. This comparison is shown in Figure 3.10. Sequencing of the *rpfC*/*rpfE* locus from mutant strains and wild type confirmed that the up- and downstream regions used to create all the *rpfC/rpfE* deletion mutants have no discrepant sequences in this area. Furthermore it is evident that the deletion of the genes did not cause inadvertent changes to the regions flanking the *rpfC/rpfE* locus in the genome.

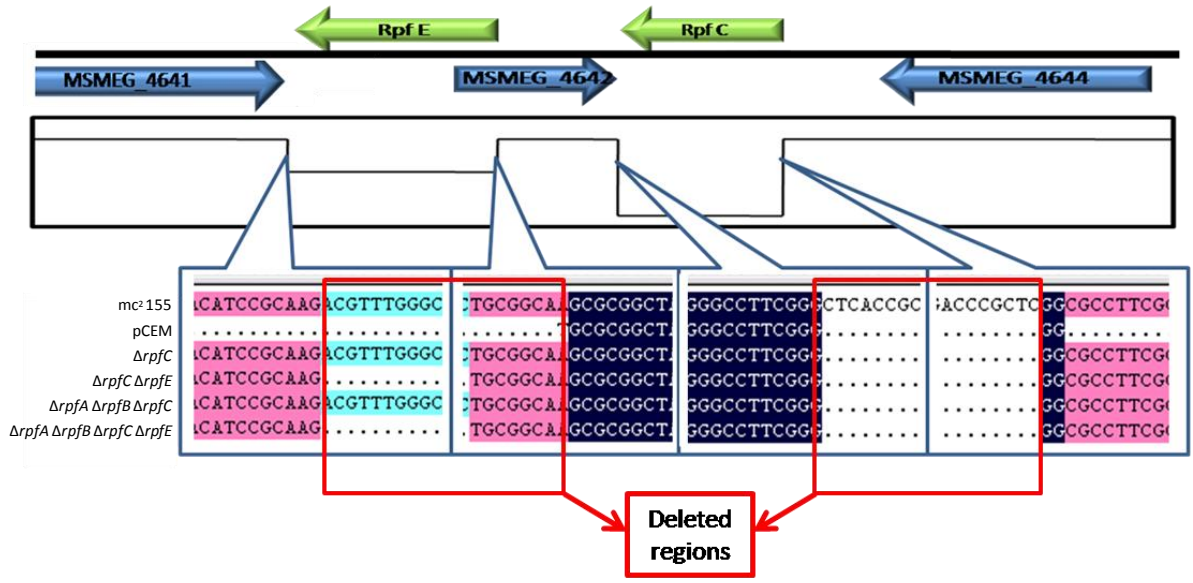

Figure 3.10: Schematic representation of the alignment of the *rpfC*/*rpfE* loci from the four *rpfC/rpfE* deletion mutant strains. For comparison both the plasmid sequence as well as the wild type sequence was included in this analysis. All four strains aligned perfectly to the wild type sequence for the homologous regions upstream and downstream of the deletions, shown in the red blocks. This confirmed the genomic integrity of all strains and provided final, unequivocal confirmation of the mutant genotypes.

3.3. Complementation of mutant strains

Genetic complementation, by insertion of the wild type gene back into the genome of a mutant strain is an important part of determinining function using gene deletion strains. Upon genetic complementation, if the phenotype, which has been observed with a knockout, is restored back to that seen in wild type, one can associate any effects seen with the gene of interest. In our panel of mutants, the *rpfA* and *rpfB* genes from *M. tuberculosis* were used for genetic complemention by introduction into the genome of the mutant strains.

3.3.1. Vectors used for complementation

For genetic complementation, vectors, pMVrpfA (carrying the *rpfA* gene and native promoter region from *M. tuberculosis*), pMVrpfB (carrying the *rpfB* gene and native promoter region from *M. tuberculosis*) and pMVrpfArpfB (carrying both the *rpfA* and *rpfB* genes and their

native promoter regions from *M. tuberculosis*) were used. These vectors were created by Dr. Edith Machowski at the CBTBR and restriction mapped in this study for confirmation. This restriction analysis is reported in Figure 3.11 and 3.12. In all three cases, all fragment sizes predicted from the *in silico* plasmid maps were observed, confirming the genetic integrity of these vectors for use in genetic complementation of deletion mutants.

A.

pMVrpfA	
Enzyme	Expected (size bp)
*Not*I	6741, 1000, 796
*Sca*I	7181, 1442
pMVrpfB	
Enzyme	Expected (size bp)
*Bgl*II	2749, 2105, 1039
*Pst*I	4257, 897, 739
*Sal*I	2614, 2200, 870, 134, 75

B.

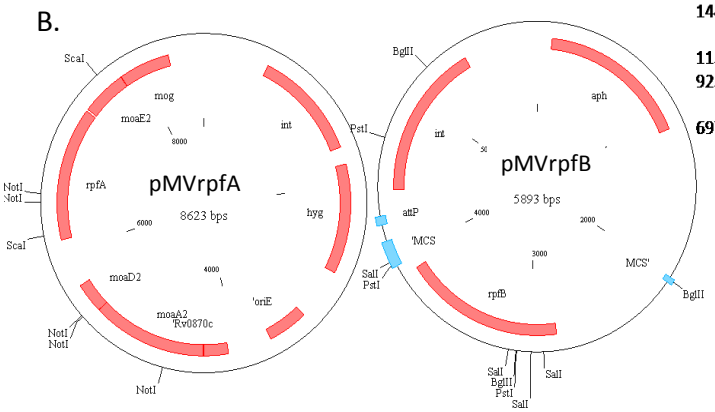

C.

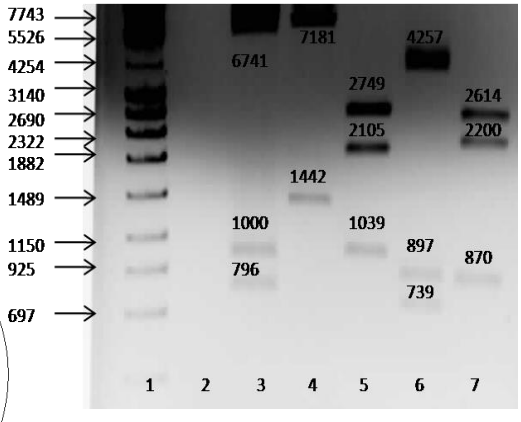

Figure 3.11: Restriction mapping of complementation vectors, pMVrpfA and pMVrpfB. A: Table of Restriction enzymes with their expected sizes. B: The predicted maps of pMVrpfA and pMVrpfB, with the restriction enzymes indicated on the map. C: Gel image of restriction digests electrophoresed on a 1% agarose gel. Lane 3&4 pMVrpfA, Lane 5-7 pMVrpfB; Lane 1: Marker 4, Lane 3: *Not*I, Lane 4: *Sca*I, Lane 5: *Bgl*II, Lane 6: *Pst*I, Lane *7: Sal*I. Restriction map of plasmids correspond to *in silico* maps provided, therefore no rearrangement has occurred during amplification, fragment sizes shown in bp.

A.

Enzyme	Expected (size bp)
*Bgl*II	4804, 3608, 2111
*Eco*RI	4948, 2858, 2717
*Kpn*I	7875, 2648
*Pci*I	5981, 4542
*Sma*I	8610, 1913

B.

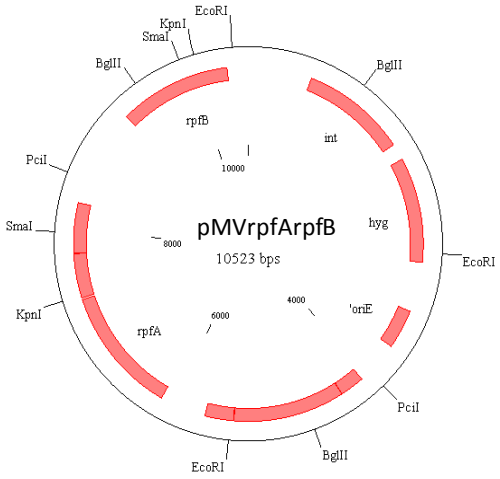

C.

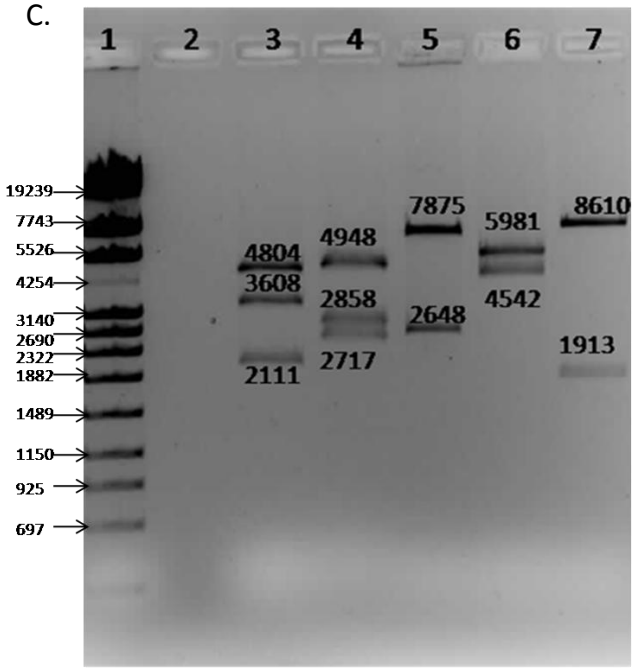

Figure 3.12: Restriction mapping of complementation vector, pMVrpfArpfB. A: Table of Restriction enzymes with their expected sizes. B: The plasmid map of pMVrpfArpfB, with the restriction enzymes indicated on the map. C: Gel image of restriction digests electrophoresed on a 1% agarose gel. Lane 1: Marker 4, Lane 3: *Bgl*II, Lane 4: *Eco*RI, Lane 5: *Kpn*I, Lane 6: *Pci*I, Lane 7: *Sma*I. Restriction banding pattern corresponded to the predicted plasmid, fragment sizes shown in bp.

3.3.2. Construction of complemented derivative strains

The three complementation vectors described above were electroporated into a panel of mutant strains which consisted of some pre-existing strains and the deletion mutants generated in this study. The outline of the complementation process is shown in Figure 3.13. Complementation with *rpfA* and *rpfB* genes (red in figure 3.13) in the single mutants, and both of these genes in the double mutant, regenerates the wild type genotype. Complementation of more advanced triple and quadruple mutants with the *rpfA* and *rpfB* genes generates new mutant genotypes, Figure 3.13.

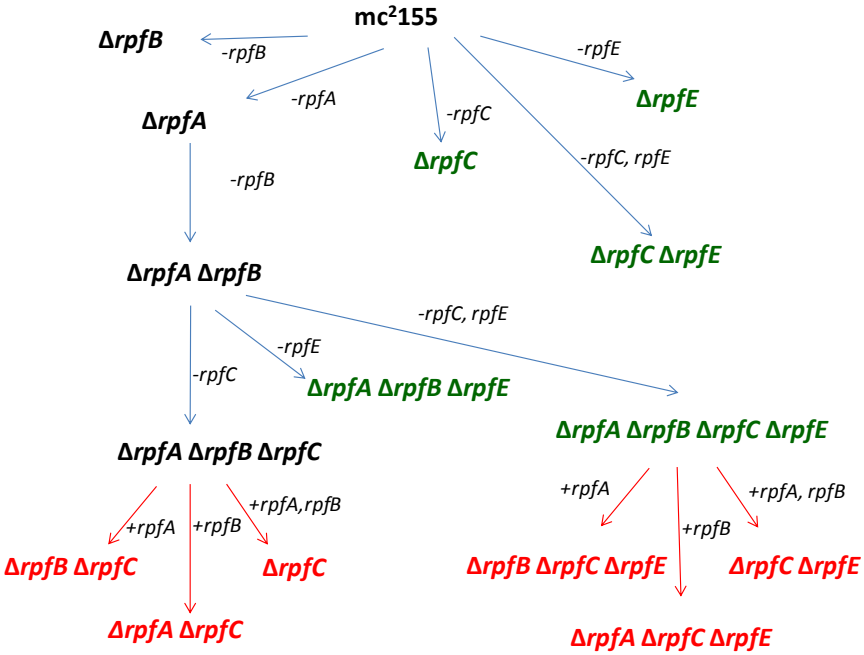

Figure 3.13: Schematic showing the combinatorial deletion of *rpf* genes in *M. smegmatis mc*^{2}155 and genetic complementation. **BLACK**: Pre-existing strains created (Lusanda Mapela). **GREEN**: strains generated in this study. **RED**: Complemented strains (this study).

3.3.3. Confirmation of genetic complementation

The pMV-based plasmid used for genetic complementation in this study is an integrating vector that inserts into the bacterial *attB* phage attachment site in the chromosome. To confirm the presence of the complementing *M. tuberculosis rpfA* and *rpfB* genes, gene-specific primers (Table 2.3) were used to detect these genes in the complemented derivatives, Figure 3.14. As expected, the *rpfA* and *rpfB* complementing genes were detected in all strains that were expected to be carrying complementing vectors.

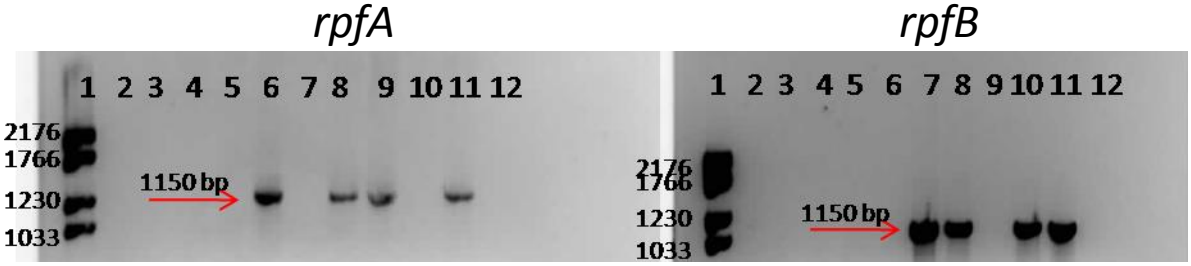

Figure 3.14: PCR confirmation of complementation strains. Left: *M. tuberculosis rpfA* primers. Right: *M. tuberculosis rpfB* primers. Lane 1: Marker VI, Lane 3-5: genomic DNA Lane 3: wild type, Lane 4: Δ*rpfA* Δ*rpfB* Δ*rpfC*, Lane 5: Δ*rpfA* Δ*rpfB* Δ*rpfC* Δ*rpfE*, Lane 6: Δ*rpfA* Δ*rpfB* Δ*rpfC*::pMV*rpfA*, Lane 7: Δ*rpfA* Δ*rpfB* Δ*rpfC*::pMV*rpfB*, Lane 8: *ΔrpfA* Δ*rpfB* Δ*rpfC*::pMV*rpfArpf B*, Lane 9: Δ*rpfA* Δ*rpfB* Δ*rpfC* Δ*rpfE*::pMV*rpfA*, Lane 10: Δ*rpfA* Δ*rpfB* Δ*rpfC* Δ*rpfE*::pMV*rpfB*, Lane 11: Δ*rpfA* Δ*rpfB* Δ*rpfC* Δ*rpfE*::pMV*rpfArpfB*, Lane 12: No DNA

3.4. Phenotypic Characterization of *M. smegmatis rpf* deletion mutants

The combinatorial deletion mutagenesis strategy used in this study, together with genetic complementation, resulted in the production of a panel of 14 mutant strains. This large number of mutant strains proved difficult to work with for any single phenotypic screen. Hence, a subset of mutant strains was selected for further characterization in this MSc study. These included wild type mc^{2}155, Δ*rpfA*, Δ*rpfB*, Δ*rpfA* Δ*rpfB*, Δ*rpfC* Δ*rpfE*, Δ*rpfA* Δ*rpfB* Δ*rpfC*, Δ*rpfA* Δ*rpfB* Δ*rpfC* Δ*rpfE*, Δ*rpfA* Δ*rpfB*::pMV*rpfArpfB*, Δ*rpfA* Δ*rpfB* Δ*rpfC*::pMV*rpfA*, Δ*rpfA* Δ*rpfB* Δ*rpfC* Δ*rpfE*::pMV*rpfA*, Δ*rpfA* Δ*rpfB* Δ*rpfC* Δ*rpfE*::pMV*rpfArpfB*. However, due to the sequential production of strains over a period of two years, not all the strains were used for all analyses. These strains were selected since they represented a progressive deletion of *rpf* genes from wild type to the quadruple mutant. The complemented strains were selected to confirm the association of any phenotype with loss of *rpf* genes. Complementation vectors containing only the *M. tuberculosis rpfA* and *rpfB* genes were used and in some cases the genetic complementation did not completely restore the wild type genotype. Our reasoning for using these vectors was that if a particular phenotype is exacerbated by the sequential deletion of *rpf* genes, then the complementation of one or two of the *rpf* genes, may alleviate the effects. We currently do not have the correct combination of all four *M. smegmatis rpf* genes on complementing vectors.

3.4.1. Growth curves

Growth curve analysis was conducted to determine if any of the *rpf*-like genes in *M. smegmatis* play a role in bacterial growth, *in vitro*. The Δ*rpfA* and Δ*rpfB* single mutants were analyzed extensively for growth defects by another MSc student, Ms Lusanda Mapela, with no differences being observed. These mutants were hence excluded from the growth curve analysis but included for other analyses later on. For growth analysis, the Δ*rpfA* Δ*rpfB* double

mutant was characterized, with wild type and a complemented derivative Δ*rpfA* Δ*rpfB*::pMV*rpfArpfB*. Rpfs have been implicated in stimulating bacterial growth from very low initial bacterial numbers. To assess this effect comprehensively in the double mutant, cultures were started with a 10-fold serial reduction in initial bacterial inoculum (that is either at OD_{600nm} = 0.01, 0.001 and 0.0001), after being washed extensively to remove residual Rpfs. The data from three independent experiments are shown in Figure 3.15, no effect was observed on initial growth rate or bacterial biomass in stationary phase. However, measurement of the optical densities at the initial time points in these experiments was challenging since the double Δ*rpfA* Δ*rpfB* mutant clumped severely, early in culture, this effect was abrogated to some extent as the culture aged. In one case (double mutant Δ*rpfA* Δ*rpfB*, experiment 3) there seemed to be delay in exit from lag phase but the clumping associated with this strain prevented any further interpretation. To circumvent this problem the surfactant, Tyloxypol was used in culture instead of Tween 80, we also included the *rpf* quadruple deletion mutant, Δ*rpfA* Δ*rpfB* Δ*rpfC* Δ*rpfE*, in subsequent growth analysis. Tyloxypol, at a concentration of 0.002%, eliminated the clumping to a certain extent but residual clumping was still present in the early logarithmic phase of bacterial growth however, despite these anomalies no difference in growth rate was observed, Figure C1. In an attempt to completely eliminate clumping and get an accurate measure on growth, the Tyloxypol concentration was increased to 0.003%. Again no differences in growth were observed with two independent experiments, Figure C2, but the clumping problems persisted.

In a final attempt to eliminate clumping, the glucose-salt mix was substituted with Middlebrook OADC enrichment, with either 0.002% (Figure C3) or 0.0003% Tyloxypol (Figure C4). In both cases, the clumping was completely eliminated and once again there was

no difference in growth rates between the wildtype, Δ*rpfA* Δ*rpfB*, Δ*rpfA* Δ*rpfB* Δ*rpfC* Δ*rpfE* strains.

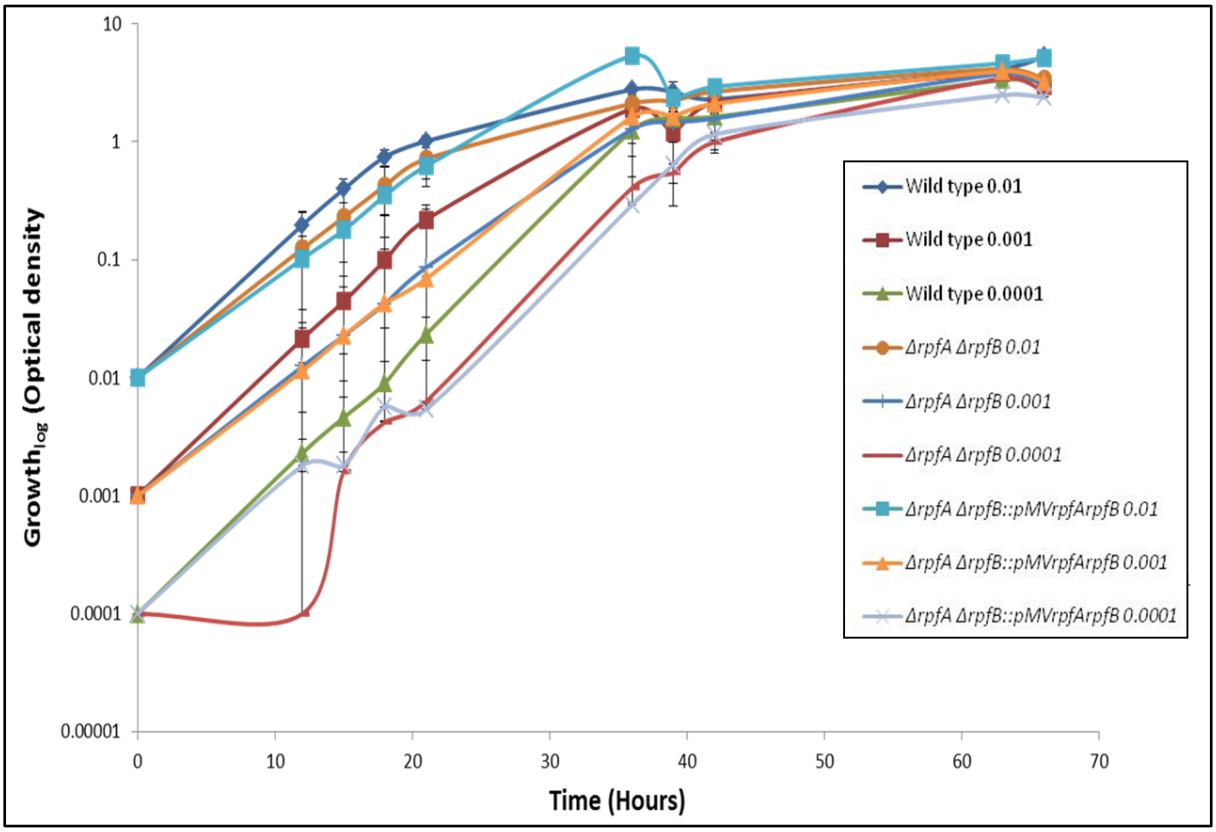

Figure 3.15: Growth curve analysis using Tween 80. Growth curve showing optical density versus time for growth in 7H9 media, supplemented with glucose, salt, and 0.05% Tween. Strains were grown with different starting bacterial numbers and monitored at 3 hourly time intervals to determine growth. Strains used in this experiment were wild type, Δ*rpfA* Δ*rpfB* and Δ*rpfA* Δ*rpfB*::pMV*rpfArpfB*. This graph is the average of three experiments.

To further assess the consequences of *rpf* gene loss on *in vitro* growth, the above mentioned strains were grown in Sauton's Minimal media, with Tyloxypol supplementation, Figure S5. In this case, we reasoned that a more restrictive growth environment in minimal media may unmask a growth defect in the mutant strains. Under these conditions, no significant effect on growth rates was noted with any of the strains thus providing further confirmation that all four *rpf*-like genes in *M. smegmatis* are dispensable for growth *in vitro*. However, in numerous experiments significant clumping was seen with both the double mutant Δ*rpfA* Δ*rpfB* and the quadruple mutant Δ*rpfA* Δ*rpfB* Δ*rpfC* Δ*rpfE*, suggesting some change in the

structure, overall charge and hydrophobicity of the cell wall. These possible effects were studied further and the data is reported below.

3.4.2. Congo red staining

A study by Nguyen et al, reports that mutation of the *mar2* gene results in differential permeability of mycobacterial strains as measured by uptake of the Congo Red stain (Nguyen et al., 2010). To test the hypothesis that the cell wall or permeability thereof in *rpf* deficient mutants is altered, these mutants were strained with Congo Red as per the previously published protocol (Nguyen et al., 2010). Only the *rpf* quadruple mutant was included in this analysis. Uptake was measured visually after four days, with no significant difference observed with quadruple *rpf* deletion mutant when compared to wild type, Figure 3.16.

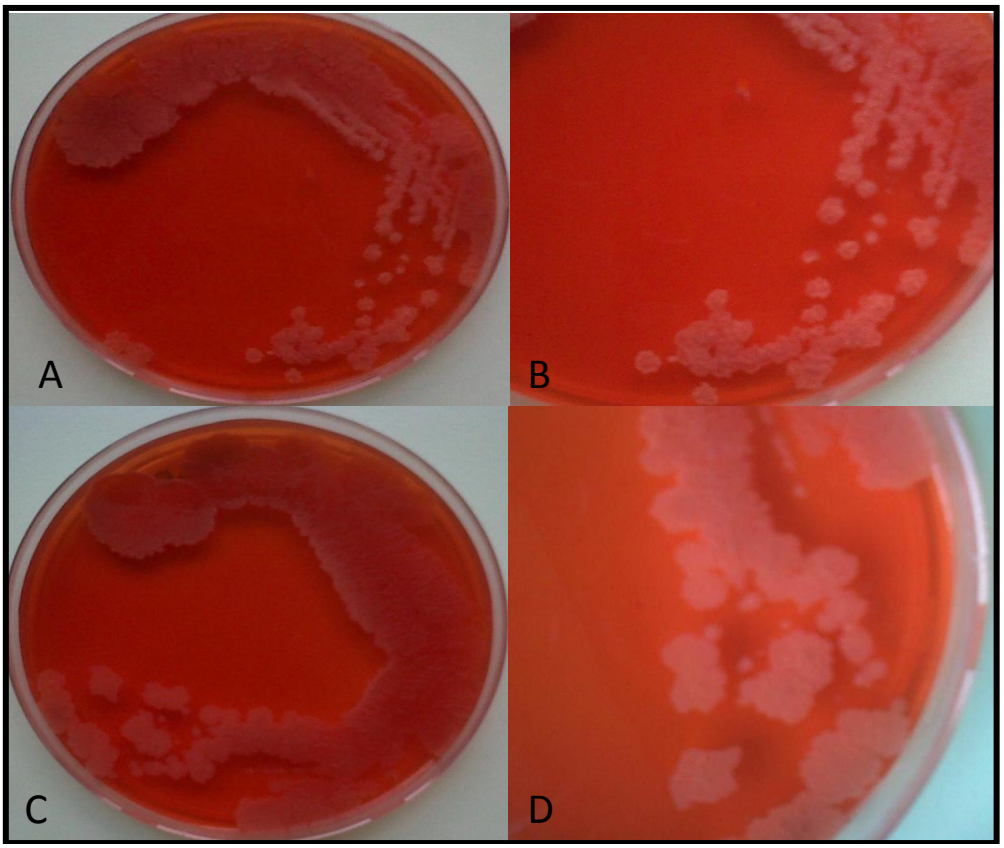

Figure 3.16: Congo red staining in the quadruple *rpf* mutant. Shown are photographs of mycobacterial strains streaked on 7H10 supplemented plates containing Congo red (100µg/ml). Image A and B (× 2 Magnification) represents wild type *M smegmatis* mc^2 155, Image C and D (× 2 Magnification) represents the quadruple *rpf* mutant. If the permeability of strain is affected, the Congo red stain would be absorbed from the media and colonies will appear red. The quadruple mutant did not show any increase in red colour.

3.4.3. Neutral red staining

Previous work has demonstrate that staining of *M. tuberculosis* with Neutral red, provides a mechanism of determining virulence and changes in cell wall structure/lipid composition and report that only virulent strains of *M. tuberculosis* would stain with the neutral red (Soto et al., 2002). Since *rpf* deficient mutants of *M. tuberculosis* have reduced virulence (Kana et al., 2008), and have lost neutral red staining (Kana B., unpublished), we decided to test whether the *M. smegmatis rpf* deficient mutants stained with neutral red. However, unlike wild type *M. tuberculosis*, no significant uptake of neutral red was noted with the *M. smegmatis* wild type or *rpf* deficient strains, Figure C6, and from these observations no conclusions can be made regarding changes in cell wall structure in these mutant strains.

3.4.4. Tween supplementation

In addition to Congo Red, it has been reported that the use of Tween 80 on agar plates can be used as a measure of cell wall permeability and work done on mutants defective in *mar2* displayed a glossy, flat morphology on Tween-containing plates (Nguyen et al., 2010). We performed a similar experiment with our *rpf* deficient quadruple mutant and found no significant difference between the wild type and the *rpf* deficient mutant, Figure 3.17.

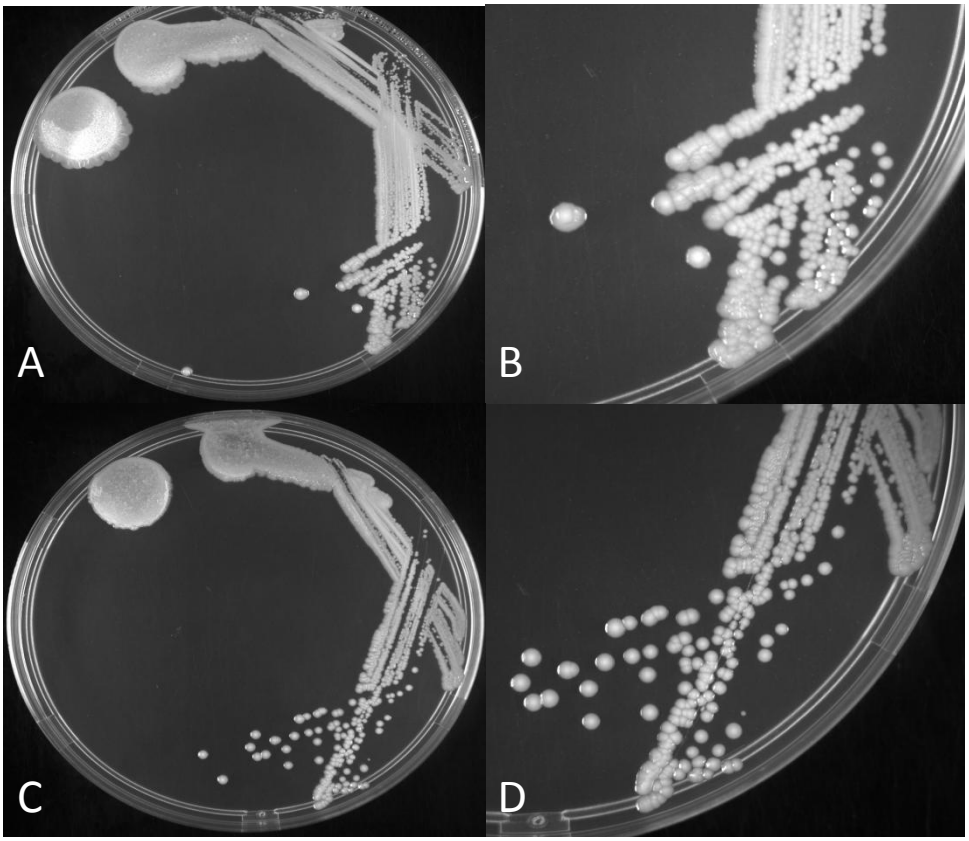

Figure 3.17: Tween supplementation of solid media in the quadruple *rpf* mutant. Image A and B (× 2 Magnification) represent wild type *M. smegmatis* mc^2155, Image C and D (× 2 Magnification) represent the quadruple *rpf* mutant. If cell wall integrity was affected, the strain would appear to be glossier. The quadruple mutant did not show any increase in gloss appearance compared to wild type.

3.4.5. Susceptibility to SDS

Previous work done in our lab reported that *M. tuberculosis rpf* deficient mutants were sensitive to cell wall damaging agents in the form of SDS. To further assess this in *M. smegmatis* double Δ*rpfA* Δ*rpfB* and quadruple deletion mutants were tested for sensitive to SDS on agar plates. As shown in Figure 3.18, there is a significant, 3 log reduction in viability of the both mutant strains when grown on plates supplemented with 0.005% SDS, with no differential effect observed. However on plates supplemented with 0.01% SDS, the wild type strain showed a 4 log reduction compared to a 5 log reduction for Δ*rpfA* Δ*rpfB* and the quadruple mutant (red square). Of particular importance is that in the complemented double mutant strain, Δ*rpfA* Δ*rpfB*::pMV*rpfArpfB*, the phenotype was restored back to the

wild type level of susceptibility (blue square), confirming that this observation was due to the loss of *rpf* genes.

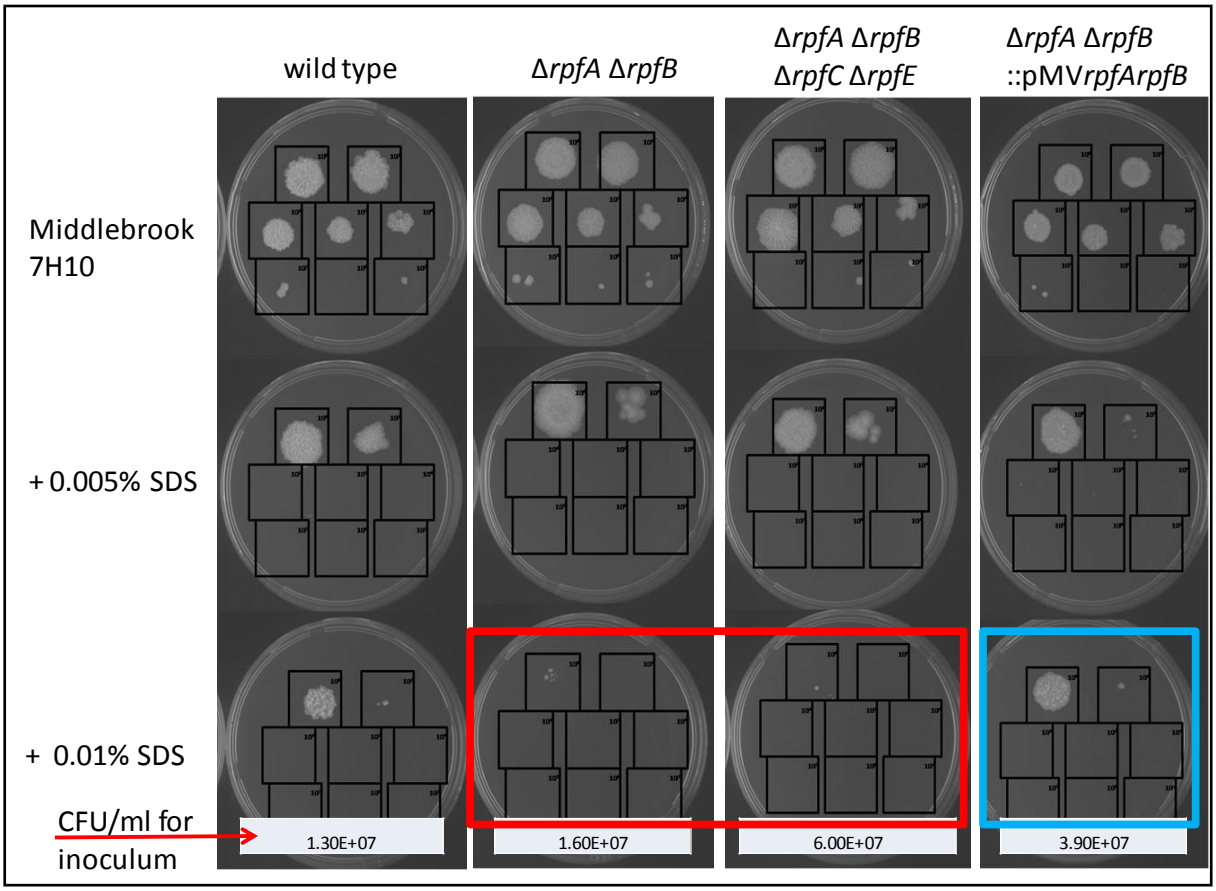

Figure 3.18: SDS susceptibility of *rpf* deficient mutants. Shown are photographs of Middlebrook 7H10 plates supplemented with different concentrations of SDS comparing a serial dilution of the wild type *M. smegmatis* mc^{2}155, Δ*rpfA* Δ*rpfB*, Δ*rpfA* Δ*rpfB* Δ*rpfC* Δ*rpfE* and Δ*rpfA* Δ*rpfB*::pMV*rpfArpfB*. Cultures were serially diluted 10-fold and 10 µl was spotted onto agar plates.

3.4.6. Analysis of drug susceptibility by broth microdilution.

To gain a better understanding of Rpf function in mycobacteria, we decided to use drugs as a probe for function by testing the drug susceptibility of various *rpf* mutant strains. We attempted to infer some functionality by identifying those drugs that displayed synthetic lethality in the *rpf* deletion mutants tested here. The choice of drugs in this case included cell wall damaging agents such as penicillin, vancomycin, D-cycloserine, imipenem, and general TB drugs, the latter to test if the permeability of the cell wall was altered to certain drugs. We tested drug susceptibility by broth microdilution and MIC determination (Domenech et al.,

2005). Table 3.1A. reports all the antibiotics tested that did not give significant, differential survival between the wild type and the *rpf* deficient mutants. The antibiotics that did show some difference are listed in Table 3.1B. There is a significant increase in susceptibility to vancomycin and erythromycin, as was reported for the *M. tuberculosis rpf* deficient mutants in a previous study (Kana et al., 2010). Interestingly the *rpf* deficient mutants have an increase in resistance to ampicillin, but no difference in susceptibility to carbenicillin. In *M. tuberculosis*, *rpf* deficient mutants have increased susceptibility to cefalosporins and with the use of labeled antibiotics, it was demonstrated that this difference in susceptibility was due to altered diffusion of these drugs across the cell (Wivagg and Hung, 2012). In this study *M. smegmatis*, triple and quadruple *rpf* deficient mutants, show a 32 to 64 fold increase in susceptibility to three of the cefalosporins tested, compared to wild type, Table 3.1B. We also found that the *rpf* deficient strains are more sensitive to imipenem. These data provide further evidence that Rpfs play an important role in PG stability and possibly, cell permeability. In some, but not all, cases genetic complementation restored susceptibility, albeit not precisely to wild type levels. Hence, these data should be interpreted with caution.

Table 3.1A: MIC of mycobacterial strains for antibiotics with no significant differential killing of *rpf* mutants. Concentration of antibiotics are given in µg/ml.

	wild type mc^2155	Δ*rpfA*	Δ*rpfA* Δ*rpfB*	Δ*rpfA* Δ*rpfB* Δ*rpfC*	Δ*rpfA* Δ*rpfB* Δ*rpfC* Δ*rpfE*	Δ*rpfA* Δ*rpfB* ::pMV*rpfArpfB*
Carbenicillin	>1200	>1200	>1200	>1200	>1200	>1200
Rifampicin	0.625	0.625	0.625	0.625	0.625	0.625
d-Cycloserine	50	50	50	50	50	50
Clavulanate	>320	>320	>320	>320	>320	>320
Meropenem	>600	>600	>600	>600	>600	>600
Meropenem + clavulanate	>600	>600	>600	>600	>600	>600

* Data are representative of at least three experiments

Table 3.1B: MIC of mycobacterial strains for antibiotics that display differential killing of *rpf* mutants.

	wild type mc^{2}155	Δ*rpfA*	Δ*rpfB*	Δ*rpfA* Δ*rpfB*	Δ*rpfC* Δ*rpfE*	Δ*rpfA* Δ*rpfB* Δ*rpfC*	Δ*rpfA* Δ*rpfB* Δ*rpfC* Δ*rpfE*	Δ*rpfA* Δ*rpfB*::pMV*rpfArpfB*	Δ*rpfA* Δ*rpfB* Δ*rpfC* Δ*rpfE*::pMV*rpfArpfB*
Vancomycin	3.125	6.25	3.125	0.781	0.781	0.39	0.39	1.562	1.562
Erythromycin	6.25	6.25	3.125	3.125	6.25	6.25	0.39	1.56	0.78
Ampicillin	18.75	75	18.75	75	75	75	150	300	600
Imipenem	20	20	0.625	0.156	0.31	0.625	0.31	1.25	0.625
Cefamandole	64	512	128	32	32	8	64	256	128
Cefapirin	100	50	25	50	12.5	25	25	25	25
Cefoxitin	80	80	40	40	20	5	2.5	80	80
Cefotaxime	100	100	6.25	25	12.5	3.125	3.125	100	100

*Data are representative of at least three experiments. RED Column indicates the triple and quadruple *rpf* deficient mutants, compared to the BLUE Column, which is wild type or genetically complemented strains. The GREEN columns, shows the increase in susceptibility, with the successive loss of the *rpf* genes. The PURPLE column shows the decrease in susceptibility, with the successive loss of the *rpf* genes.

3.4.7. Biofilm formation in *rpf* deficient mutants.

It has previously been reported that *M. smegmatis* has the ability to form biofilms when grown in Sauton's minimal media (Ojha et al., 2005). The deletion of the two heat shock protein 60 - class chaperones, *groEL* paralogs, *groEL1* and *groEL2*, resulted in the inability to switch from planktonic growth to biofilms (Ojha et al., 2005). Biofilm formation was assayed in this MSc study to determine if the deletion of *rpf* genes has any effect on the ability of mycobacteria to switch from planktonic growth to biofilms. From Figure 3.19, it can be seen that there is a major reduction in the ability of the Δ*rpfA*, Δ*rpfA* Δ*rpfB*, Δ*rpfA* Δ*rpfB* Δ*rpfC*, Δ*rpfA* Δ*rpfB* Δ*rpfC* Δ*rpfE* deficient strains to form biofilms when compared to wild type. With the deletion of *rpfA*, there is a notable reduction in the ability of the strain to

form a biofilm. This is further exacerbated in the Δ*rpfA* Δ*rpfB* double mutant. The deletion of *rpfC* and *rpf*E in this double mutant did not have any additional effect on biofilm formation. Genetic complementation of the Δ*rpfA* Δ*rpfB* double mutant, Δ*rpfA* Δ*rpfB*::pMV*rpfArpfB*, restored the phenotype completely to wild type levels. The other two complemented strains however did not restore the phenotype and since these were only complemented with *rpfA*, these data suggested that further complementation with other *rpf* genes would be necessary to revert the phenotype in these strains. It is also important to note that these phenotypes were not due to differences in initial bacterial inoculum since all these experiments were started with equivalent bacterial numbers. This was determined by plating the CFU/ml immediately after inoculation for biofilm formation, Table 3.2.

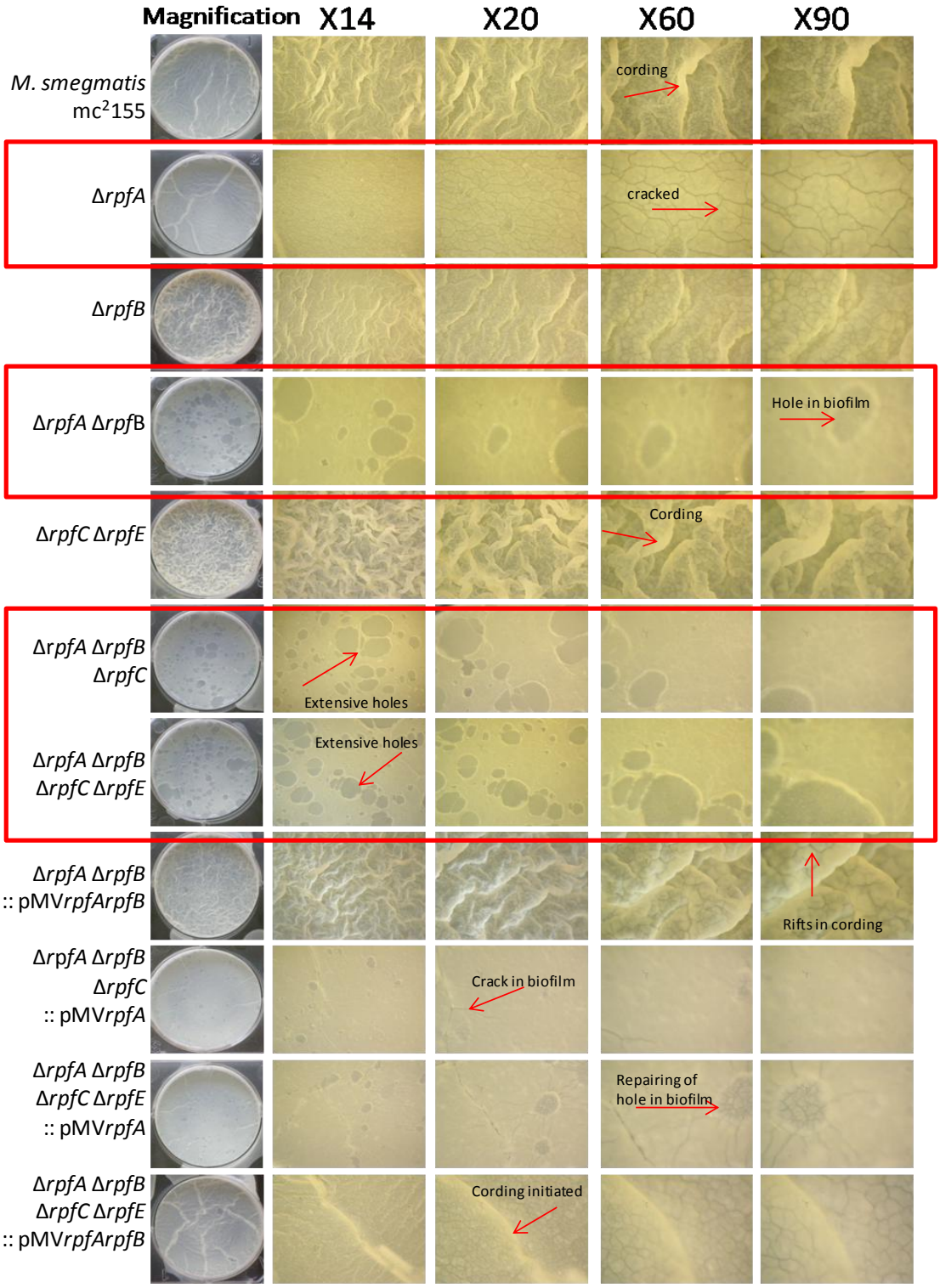

Figure 3.19: Photographs of biofilms grown on Sauton's media comparing different Mycobacterial strains. Images in the first column were taken with digital camera, the rest of the images were taken with a stereomicroscope. This adds an extra level magnification. Some *rpf* deficient mutants are not proficient at biofilm formation; these are shown with red squares. Arrows point at the biofilms characteristics that are different to the wrinkled phenotype of wild type biofilms.

Table 3.2: Initial bacterial inocula for biofilm experiments

Biofilms CFU/ml	
Strain	**CFU/ml at inoculation**
wild type mc^2155	4.60E+07
Δ*rpfA*	3.20E+07
Δ*rpfB*	6.20E+07
Δ*rpfA* Δ*rpfB*	1.90E+07
Δ*rpfC* Δ*rpfE*	2.90E+07
Δ*rpfA* Δ*rpfB* Δ*rpfC*	4.40E+07
Δ*rpfA* Δ*rpfB* Δ*rpfC* Δ*rpfE*	4.10E+07
Δ*rpfA* Δ*rpfB*::pMV*rpfArpfB*	3.00E+07
Δ*rpfA* Δ*rpfB* Δ*rpfC*::pMV*rpfA*	2.40E+07
Δ*rpfA* Δ*rpfB* Δ*rpfC* Δ*rpfE*::pMV*rpfA*	7.60E+07
Δ*rpfA* Δ*rpfB* Δ*rpfC* Δ*rpfE*::pMV*rpfArpfB*	6.00E+07

3.4.8. Sliding Motility of *rpf* mutants

The sliding motility assay was first described in mycobacteria by Kolter et al. in 2000 (Kolter et al., 2000). It was reported that mycobacteria have the ability to slide from an original colony on soft, solidified 7H9 media. To assess this ability to slide in *rpf* deficient strains, sliding experiments were performed on 7H9-solidified media, Figure 3.20. Our results indicate that there is an increase in the amount of sliding for *rpf* deficient strains. A very interesting observation is the fact that the complemented strain, containing the *M. tuberculosis rpf* genes, shows an increase in sliding capacity. This might be due to the fact that the expression of the complemented genes was not entirely similar to the expression of the *M. smegmatis rpfA* and *rpfB* homologues in the wild type strain. This would have to be tested with expression analysis in the complemented strains.

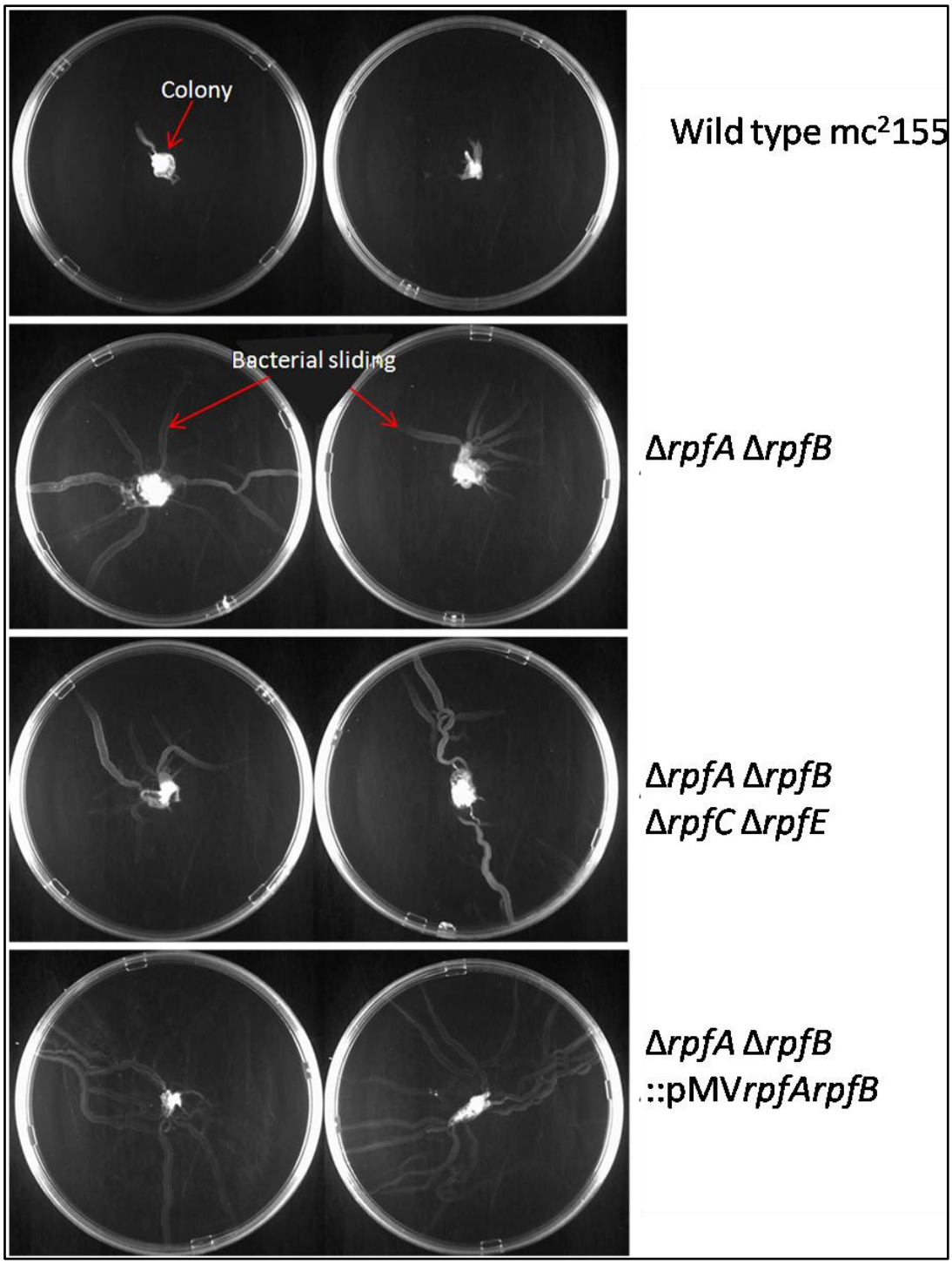

Figure 3.20: Sliding motility of *rpf* deficient strains. Middlebrook 7H9 media was solidified with 0.03% agarose to determine the sliding ability of the following strains: wild type *M. smegmatis* mc^{2}155, Δ*rpfA* Δ*rpfB*, Δ*rpfA* Δ*rpfB* Δ*rpfC* Δ*rpfE* and Δ*rpfA* Δ*rpfB*::pMV*rpfA rpfB*. A colony is placed in the centre of the plate and then monitored visually for sliding. Bacteria slide from the colony over the soft agar. There is a significant increase in the sliding of the *rpf* deficient mutants, when compared to wild type.

3.4.9. TLC analysis of glycopeptidolipids

Sliding motility has been attributed, in part, to glycopeptidolipids - GLPs (Recht and Kolter, 2001) and in this context, we reasoned that there may be a difference in the presence of these lipids in *rpf* mutant strains that were altered for sliding motility. We tested GLP production in some of these strains by TLC and found no significant differences with the single or double mutants, Figure 3.21.

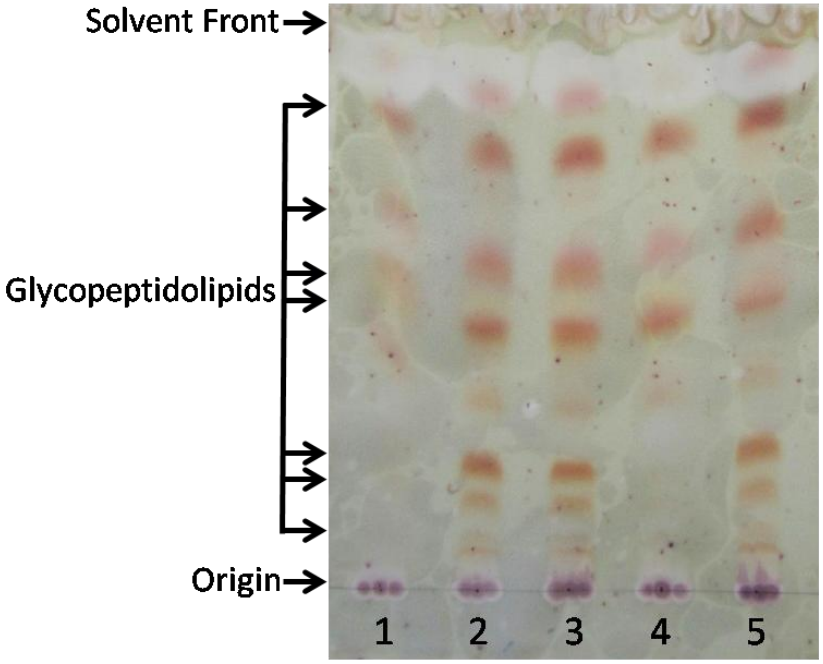

Figure 3.21: Thin Layer Chromatography of Glycopeptidolipids extracted from Mycobacterial strains. Lane 1: wild type, Lane 2: Δ*rpf*A Lane 3: Δ*rpf*B, Lane 4: Δ*rpf*A Δ*rpf*B and Lane 5: Δ*rpf*A Δ*rpf*B::pMV*rpf*A*rpf*B.

3.4.10. Confocal microscopy to assess cell morphology

Laser scanning confocal microscopy was carried out to determine if progressive *rpf* gene loss lead to changes in cell morphology. The cell wall stain, Cellmask, allowed for visualization of the cell membrane and facilitated the determination of cell length of *rpf* deficient mutant as well as any other defects that might occur. DAPI was used to stain the cytoplasm of bacteria. To assess the growth of the bacterial PG layer, fluorescently tagged vancomycin was used. Vancomycin binds new PG subunits in the PG, thereby disrupting cell wall synthesis by inhibiting cross-linking of the stem peptides. Addition of vancomycin, at low concentrations, allows for visualization of the location of newly synthesized PG subunits, that are not cross-linked, by the accumulation fluorescent light at a specific site. This can be seen in Figure 3.22, as indicated by the arrows.

From these experiments, a notable reduction in size of the Δ*rpfA* Δ*rpfB*, Δ*rpfA* Δ*rpfB* Δ*rpfC* and Δ*rpfA* Δ*rpfB* Δ*rpfC* Δ*rpfE*, can be seen with no difference in the amount of vancomycin staining or an increase in the localization thereof. The vancomycin did assist in the identification of cells that were in the process of dividing as indicated by an increase of fluorescence in the middle of cells, pointing to the formation of new septa. In the double mutant Δ*rpfA* Δ*rpfB*, Figure 3.22 (D) and triple mutant, Δ*rpfA* Δ*rpfB* Δ*rpfC* (F), cells appear significantly shorter with an average of length of 3.9 (+/- 0.4) µm and 3.8 (+/- 0.2) µm, respectively, compared to the 4.8 (+/- 0.4) µm in wild type (A). The quadruple mutant, Δ*rpfA* Δ*rpfB* Δ*rpfC* Δ*rpfE* (G), displayed the same phenotype with an average length of 3.5 (+/- 0.1) µm.

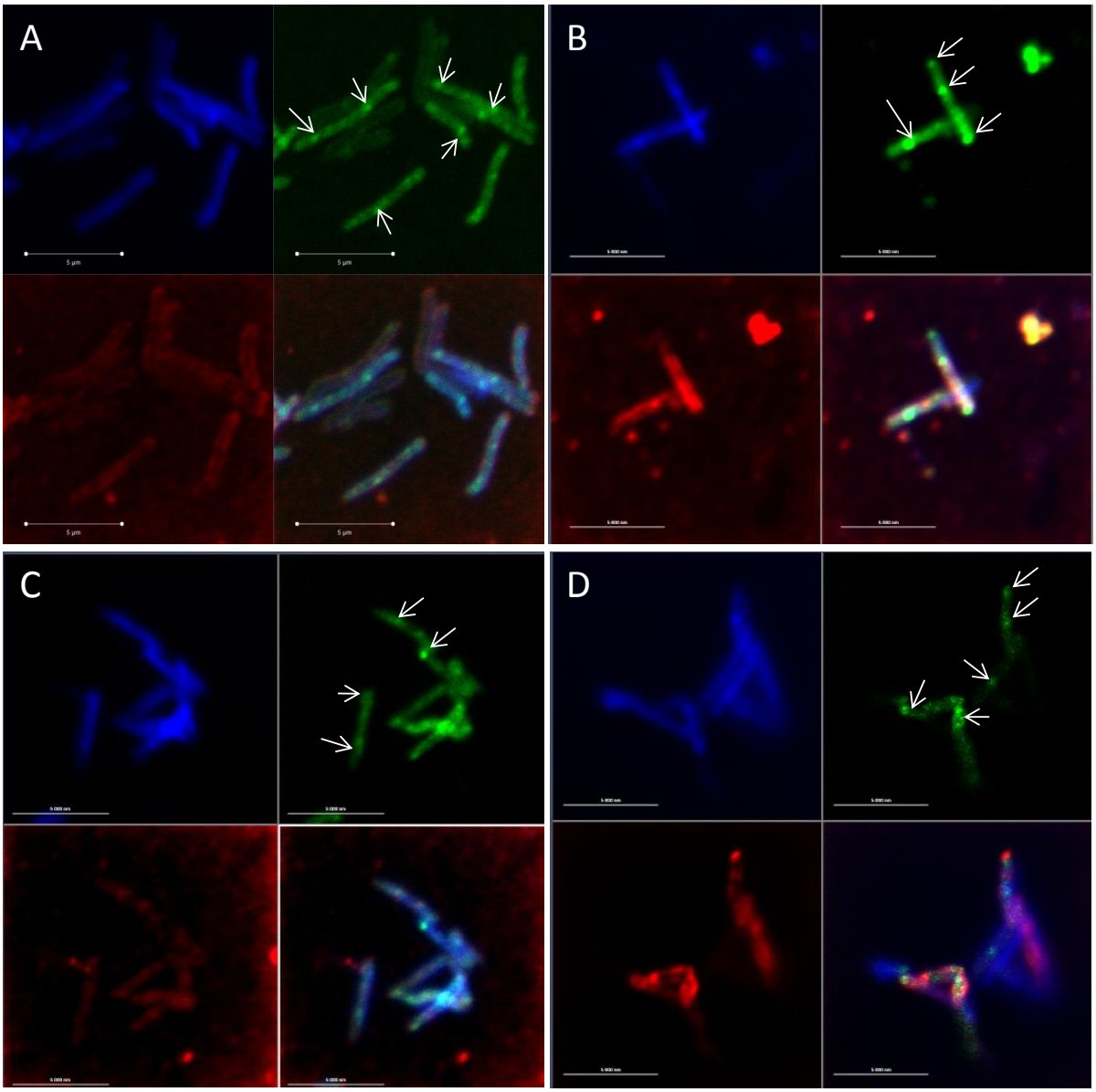
A
B
C
D

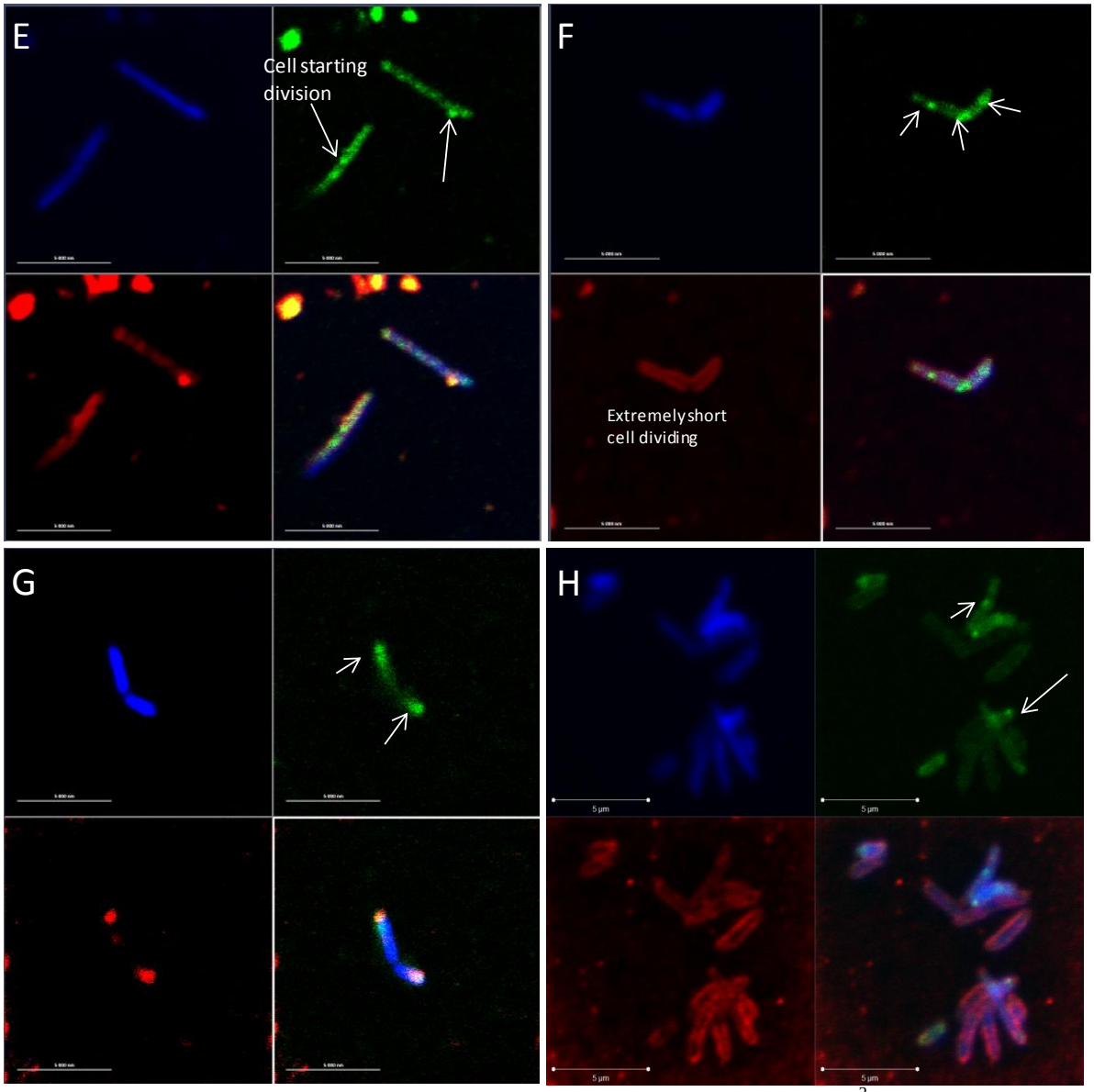

Figure 3.22: Confocal microscopy of mycobacterial strains. A: *M. smegmatis* mc^{2}155; B: Δ*rpfA*; C: Δ*rpfB*; D: Δ*rpfA* Δ*rpfB*. E: Δ*rpfC* Δ*rpfE*; F: Δ*rpfA* Δ*rpfB* Δ*rpfC*; G: Δ*rpfA* Δ*rpfB* Δ*rpfC* Δ*rpfE*; H: Δ*rpfA* Δ*rpfB*::pMV*rpfArpfB*. Blue: DAPI staining, Red: Cellmask Orange, Green Fluorescent vancomycin. Fourth quadrant: merged image of the three strains used. These images show the difference in size as well as incorporation of fluorescent vancomycin into nascent peptidoglycan. White arrows indicate strong signal from fluorescent vancomycin and where it has localized, scale bar is 5 µm.

3.4.11. High Resolution Scanning Electron Microscopy (HRSEM)

To assess the surface structure of *rpf* deficient mutants, HRSEM was performed. The cell wall inhibitor, imipenem, which is able to halt cell division, by inhibition of the cross-linking in the PG, was used to assess the effect of *rpf* gene loss.

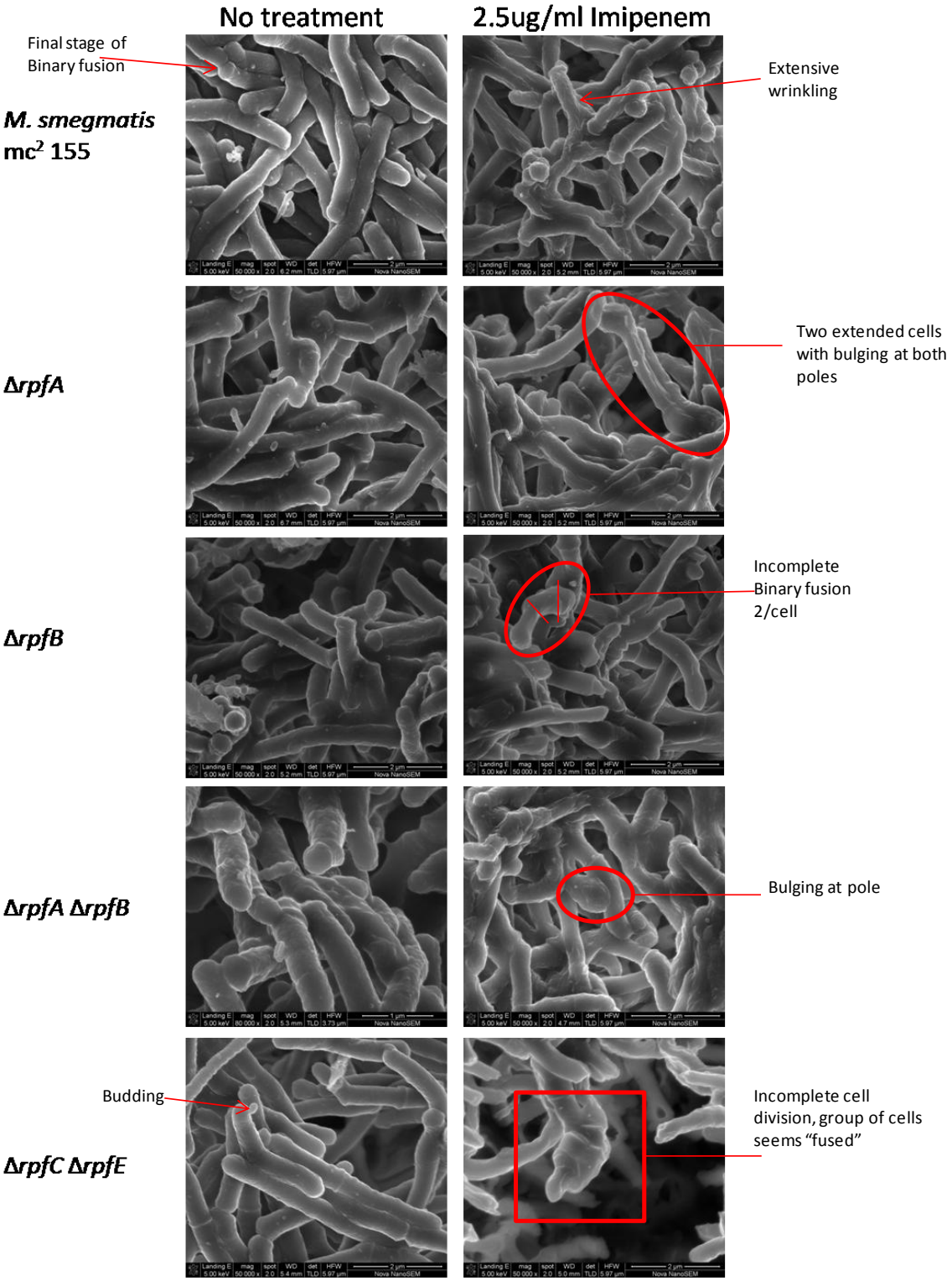

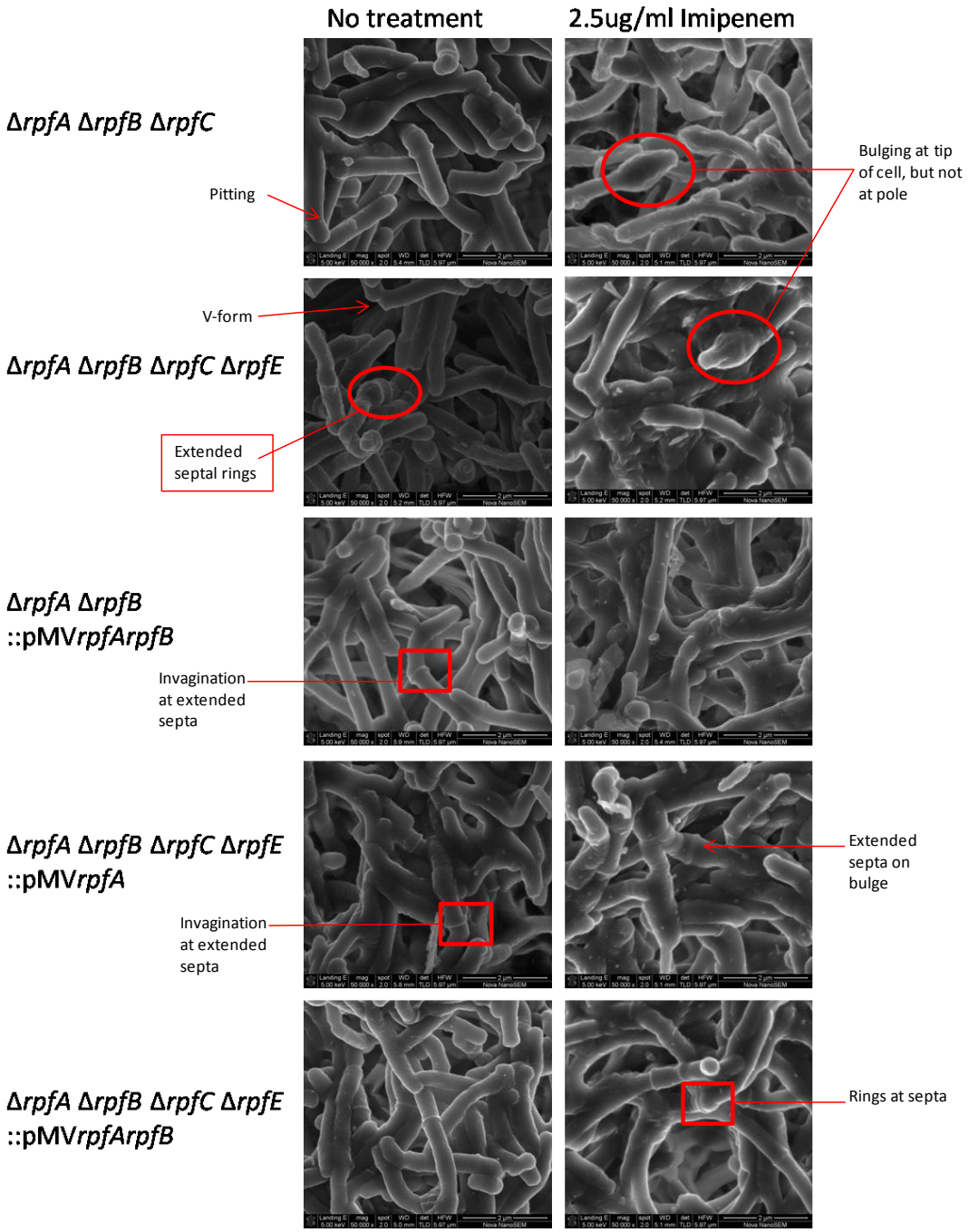

Figure 3.23: HRSEM micrographs of mycobacterial strains. These images show the difference between *rpf* deficient strains as well as the effects of imipenem treatment. Red arrows point out specific characteristics of the mycobacterial strains. Circle and blocks are drawn around extreme phenotypes that were noted in numerous sections. SEM was done three independent times.

Cell division has been described in *M. tuberculosis* using electron microscopy (Dahl, 2004) which revealed distinct characteristics in mycobacterial division. Mycobacteria divide by binary fusion, in a process called “snapping”, which results in the visual V-form. The septal

ring is visible from the outside of the cell, through formation of a ridge on the surface of the bacteria. Mycobacteria divide in an apolar fashion and form projections from the cell. Some of these projections, redundent, are referred to as buds, and are prominent in the micrographs shown in Figure 3.23. Another type of apolar division is the Y-form, where the cells start to branch, this is not seen very often and did not emerge in any in our micrographs. Some differences in *rpf* mutants can be noted, the extensive bulging of the poles with the double, triple and quadruple mutants is the most prominent difference. To further assess this, statistical analyses to determine the frequency of these phenomena were carried out as discussed in the Materials and Methods section 2.14, using the Bray-Curtis similarity test and data were plotted in a Dendrogram, Figure 3.24. Cell lengths were excluded from this analysis, and only cell wall visual characteristics were used. Four distinct groups clustered together from the analysis, with all strains showing a similarity of more than 65%. The triple and quadruple mutants clustered together and showed the biggest difference in morphology when compared to the rest of the strains. The double mutant Δ*rpfC* Δ*rpfE*, grouped with the majority of the complemented strains. Another interesting observation is that all the *rpfB* mutants and variations thereof grouped together, with a 75% similarity to the wild type.
The lengths of the bacteria were also measured and the data analyzed as discussed in the materials and methods, section 2.14. The data followed a non-normal distribution, as tested by the Kolmogorov Smirnov test, and was tested for significant differences using the Mann-Whitney U test. The Δ*rpfB* deficient mutant was the only strain that showed a significant difference, when compared to wild type, Mann-Whitney $U = 15.50$, $Z = 2.61$, $p<0.01$. The other *rpf* deficient strains did show a difference but data was not statistically significant, this was due to the variation in the lengths measured from the wild type. When data are plotted to show occurrence of specific lengths, qualitative differences between strains are evident, Figure 3.25.

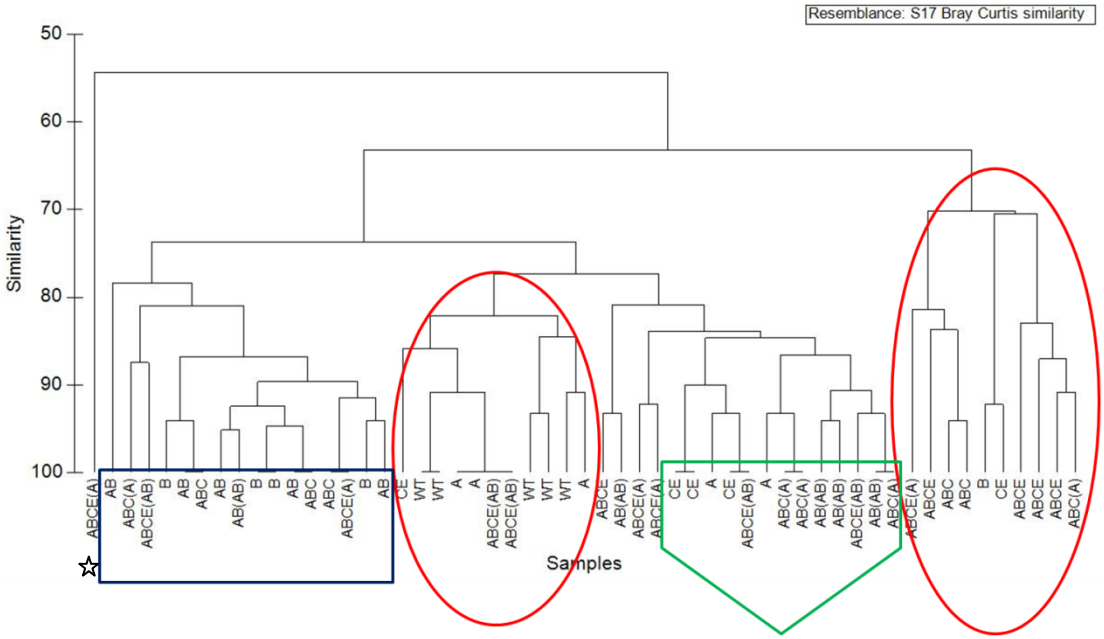

Figure 3.24: Dendrogram showing similarity between *rpf* deficient strains. All strains are compared together and show an overall similarity of >65%, with the exception of one strain (*). The red circles show the grouping of the triple and quadruple *rpf* mutants in comparison to wild type, with the lowest similarity. The green pentagon indicates the grouping of most of the complemented strains along with the double Δ*rpfC* Δ*rpfE* mutant, which is 80% similar to the wild type strain. The blue block is a group of *rpf* deficient mutants that are all deficient in Δ*rpfB* and cluster away from wild type in this analysis. Note: strain names are in shorthand, letters indicate which *rpf* genes have been deleted, brackets indicate genes that have been complemented, example: Δ*rpfA* Δ*rpfB* Δ*rpfC* Δ*rpfE* ::pMV*rpfArpfB* would be depicted as ABCE(AB).

The *rpf* deficient mutants clearly show a shift in average cell length when compared to the wild type. One can see that the Δ*rpfA* mutant still shows the same distribution as wild type but the resolution is notably different in the Δ*rpfA* Δ*rpfB* strain, the phenotype reverts to some degree when the *rpfA* and *rpfB* genes are added back into the mutant background. A significant shift can be seen for Δ*rpfB* mutant, triple Δ*rpfA* Δ*rpfB* Δ*rpfC* and the quadruple Δ*rpfA* Δ*rpfB* Δ*rpfC* Δ*rpfE* mutants. Moreover there seems to be a reduction in the heterogeneity of cell length in the quadruple *rpf* mutant.

3.4.12. Colony microscopy and SEM

During growth curves, we noted that the colony morphology of some *rpf* deficient mutants were different when compared to the wild type. To further assess this phenotype, stereomicroscopy was done on colonies grown on plates, Figure 3.26. There is a clear

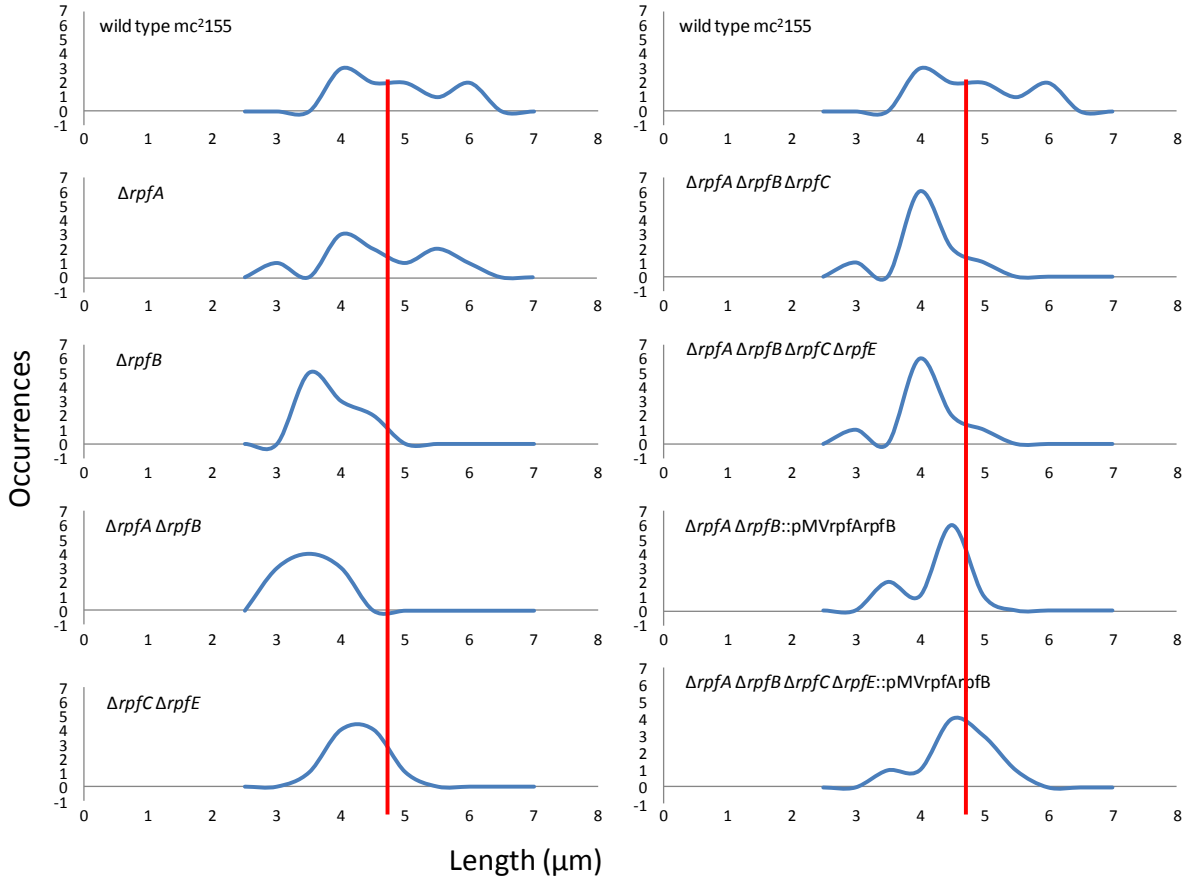

Figure 3.25: Comparative distribution of lengths in *rpf* deficient mycobacterial strains. Graphs of the occurrence of different lengths of the *rpf* deficient mutants compared to wild type. Average length of 4.8 µm for wild type was determined and indicated with a red line as reference for other strains. *Rpf* deficient mutants show a shift in size, as well as change in distribution.

difference between the *rpf* deficient mutants; the double Δ*rpfA* Δ*rpfB*, triple Δ*rpfA* Δ*rpfB* Δ*rpfC* and the quadruple Δ*rpfA* Δ*rpfB* Δ*rpfC* Δ*rpfE* mutants, form a very smooth colony when plated. When the *rpf* genes are added back by genetic complementation, Δ*rpfA* Δ*rpfB*::pMV*rpfArpfB*, the phenotype is restored, as indicated by the arrow in Figure 3.26. The wild type strain forms ruffled colonies with surface cording that is characteristic of mycobacteria. These *rpf* deficient mutants loose this ability and colonies have no cords but rather small, bulging protrusions, shown by the red circles in Figure 3.26. The protrusions on the surface of flat colonies gives the impression that the bacteria initiated the cording process but are unable to proceed to form complete cords. In the complemented strains, the phenotype reverts back to that seen in the wild type, confirming that it is due to loss of *rpf* genes.

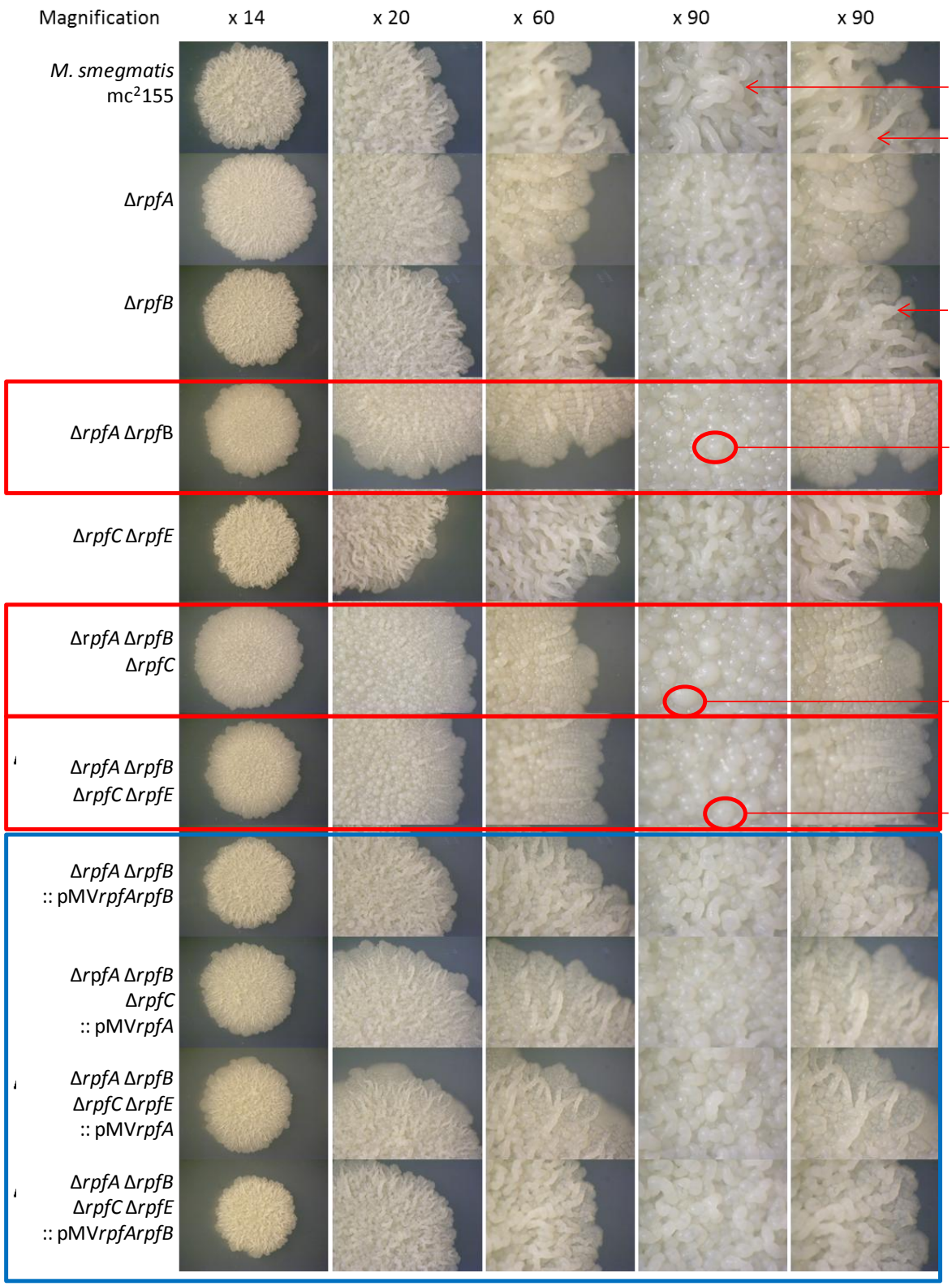

Figure 3.26: Colony morphology of different *rpf* deficient mycobacterial strains. Bacteria were grown on solid media. Shown are images taken with a stereomicroscope at different magnifications. A reduction in cording is one of the main observations. Red Arrows indicate cording, and red circles indicate bulging, protrusions. Red blocks are drawn around strains with a significant change in morphology. In the complemented strains, blue block, cording is restored.

Colony SEM

To further assess changes in colony morphology, SEM micrographs were taken of all strains, Figure 3.27, at different magnifications. From the SEM images, there is a clear difference in packing of individual cells in the colony in some of the *rpf* deficient mutants. There is a distinct criss-cross packing of cells in the wild type, which seems to disappear in some of the *rpf* deficient mutants. The *rpfB* mutant shows a very tightly packed structure even on the top of the colony. Colonies from the double, triple and quadruple mutants all look like the individual cells are smaller and packed tightly together. This might be due to differences in internal signaling between the bacteria and would account for the extreme phenotypes of the strains. The complementation of the double mutant Δ*rpfA* Δ*rpfB* ::pMV*rpfArpfB* strain results in reversion of the phenotype to wild type levels. Collectively, these data confirm that the *rpf* genes play an important role in bacterial growth and colony formation.

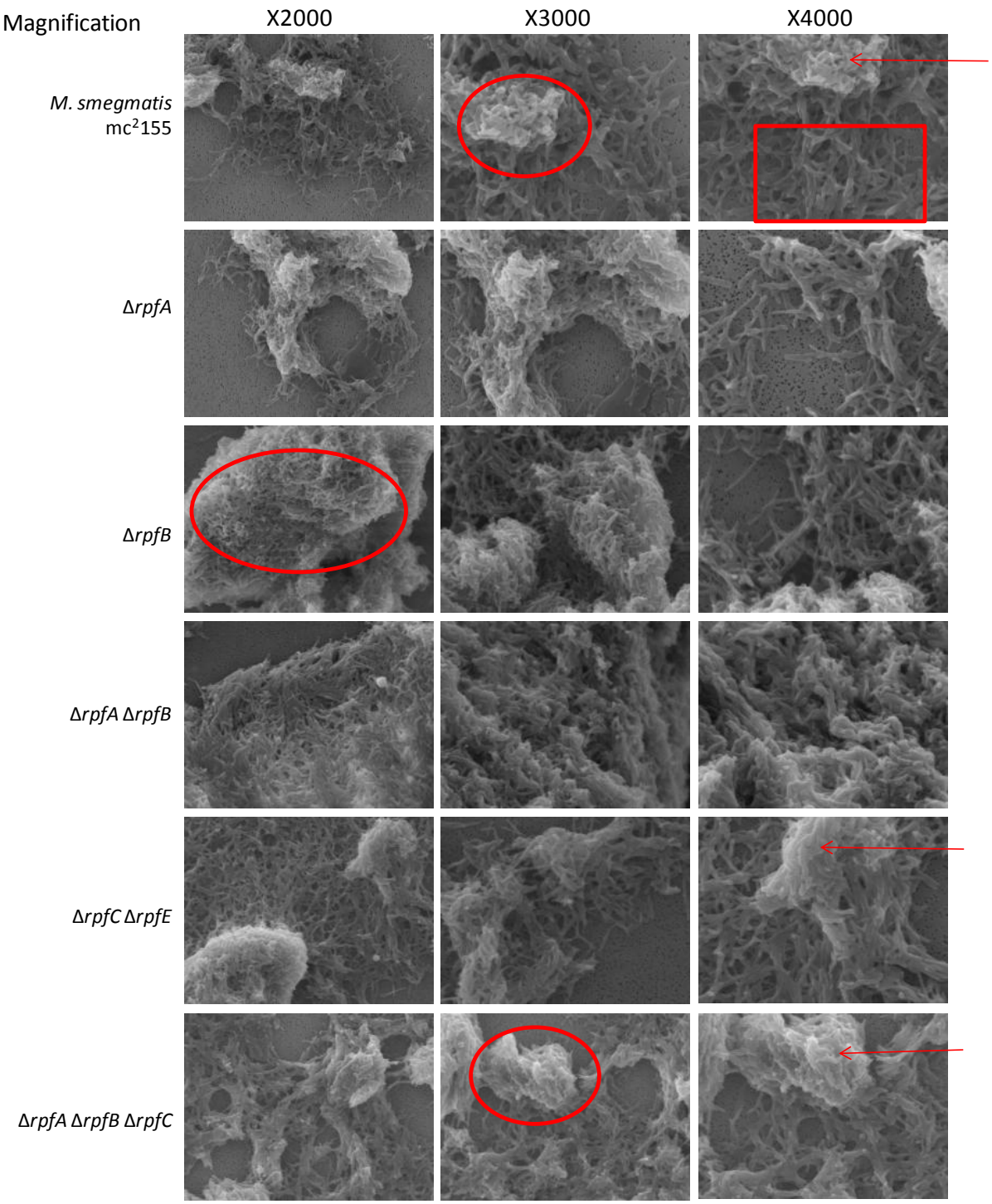
Magnification
X2000
X3000
X4000
M. smegmatis mc²155
ΔrpfA
ΔrpfB
ΔrpfA ΔrpfB
ΔrpfC ΔrpfE
ΔrpfA ΔrpfB ΔrpfC

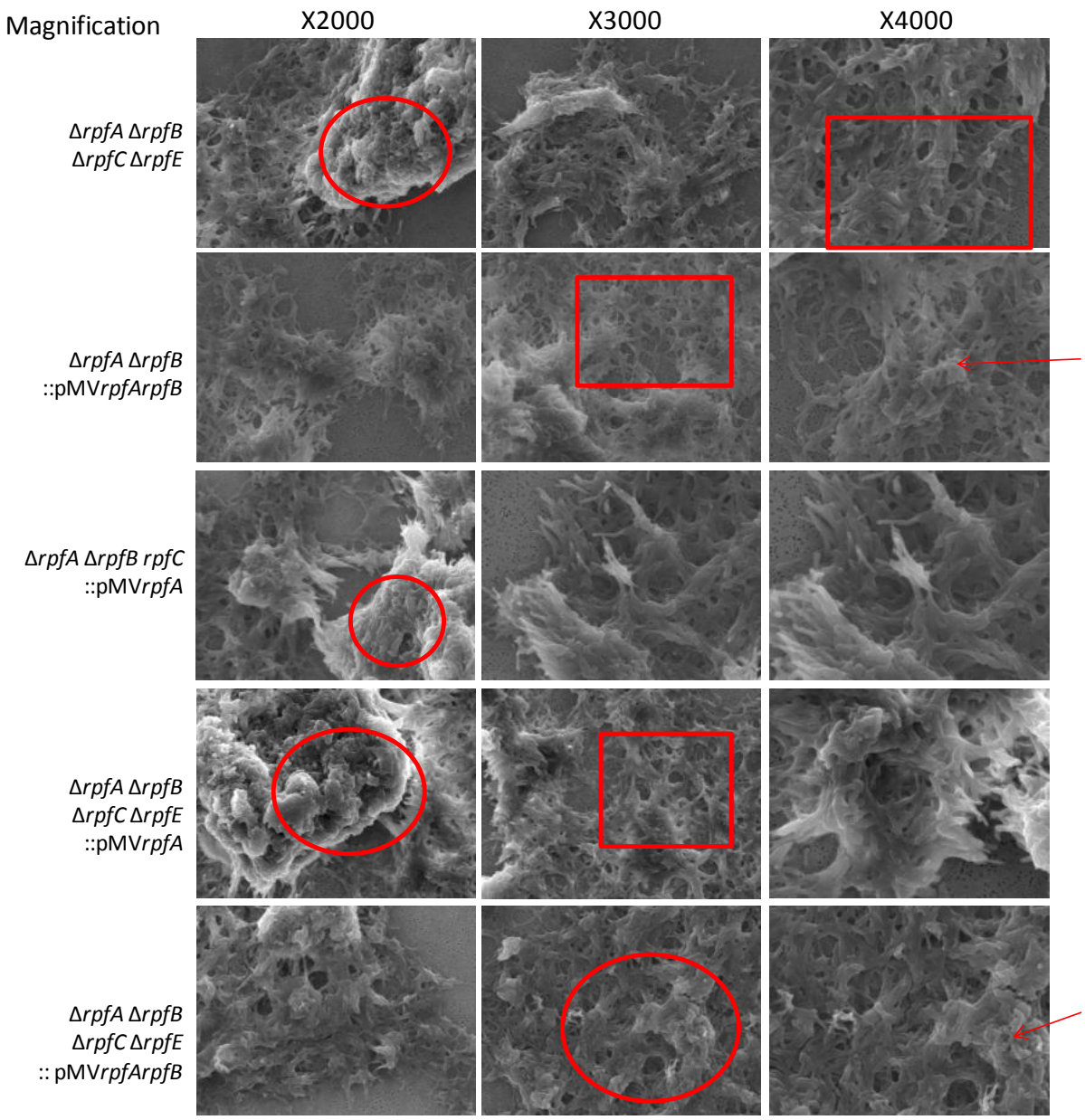

Figure 3.27: Electron micrographs showing colony morphology of different *rpf* deficient strains. Comparison is made of the different strains at different magnifications. Circles around areas show to the packing of bacteria in close proximity. Arrows point to top of colony cording to show the packing. Blocks highlight an area at the bottom of the colony and illustrate how bacteria are spreading away from the colony.

3.5. Deficiencies in dormancy for *rpf* deletion mutants

The dormancy model for *M. smegmatis* was first published by Shleeva et al in 2004. In this model, the authors were able to create a "non-culturable" state in *M. smegmatis* that is amenable to spontaneous resuscitation through the addition of culture filtrate, which contains Rpfs. We attempted to reproduce this model to create a system to test spontaneous resuscitation with our *rpf* deficient mutants and achieved some level of success in this regard. In the study that reports this *in vitro* model, wild type *M. smegmatis* achieved a state of non-culturability after 72 hours; in our experiments we achieved non-culturability for the wild type after 8 days of culture in nutrient limited media, Figure C8. For this model, bacteria are streaked from a growing culture, onto solidified nutrient rich media (NBE). Plates are incubated for four days before a single colony is picked and transferred to liquid nutrient rich media. Cultures are grown for exactly 30 hours before an aliquot is transferred to nutrient limited media (mHdeB). Culturability is monitored daily by plating bacteria to determine CFU/ml on solidified nutrient rich media (NBE). Initially, we reasoned that the growth time of the various strains differed, compared to that seen in the published model mentioned above. This is due to the fact that the transfer from the nutrient rich media to the nutrient poor media has to occur at exactly 30 hours post inoculation, irrespective of the optical density of the culture. To assess this, wild type was grown and transferred to mHdeB's media at 28, 30, 32 hours post growth in rich media to try and determine the optimal point of transfer into the dormancy model. Irrespective of time of growth - the wild type still entered a "non-culturable" state after 8 days, Figure 3.28. After contacting the authors who published the original dormancy model, we made some adjustments to our model. The nutrient poor media was altered, the trace element mixture was separated into two individual solutions and Bovine Serum Albumin (BSA) was included in the media.

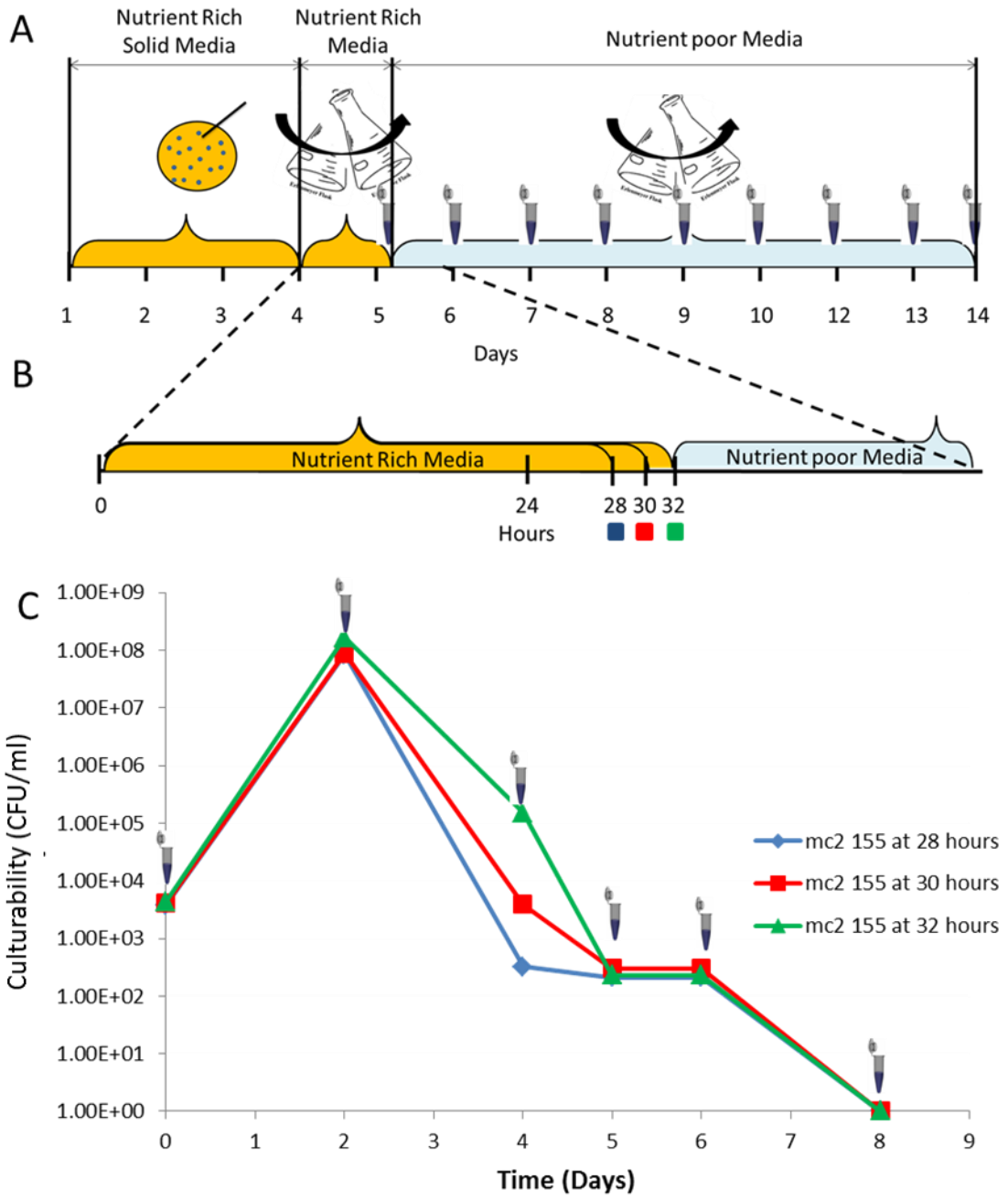

Figure 3.28: Establishment of the dormant state in *M. smegmatis*. Culturability (CFU/ml) versus the Time (days) of culturing for wild type in the dormancy model is shown. A: Diagram indicating the three phase in the dormancy model as well as where cultures are transferred from the rich media to nutrient limited media. Eppendorf tubes indicate where aliquots were taken to determine CFU/ml. B: Diagram is enlarged to indicate the transfer from nutrient rich media to nutrient poor media, at different time points: 28, 30, 32 hours. C: Graph depicting the culturability of the wild type strain over time, for the three different time points of transfer from nutrient rich media to nutrient poor media.

This new protocol resulted in entry into the "non-culturable" state after 72 hours with the wild type strain, which replicated the published findings, Figure 3. 29 (Shleeva et al., 2004).

Of particular interest in this case was the observation that the double Δ*rpfA* Δ*rpfB* mutant did

not enter into dormancy, however the complemented Δ*rpfA* Δ*rpfB*::pMV*rpfArpfB* restored this phenotype. Other mutants such as the triple Δ*rpfA* Δ*rpfB* Δ*rpfC*, quadruple Δ*rpfA* Δ*rpfB* Δ*rpfC* Δ*rpfE* as well as the quadruple complemented strains Δ*rpfA* Δ*rpfB* Δ*rpfC* Δ*rpfE*::pMV*rpfA*, Δ*rpfA* Δ*rpfB* Δ*rpfC* Δ*rpfE*::pMV*rpfArpfB* strains did not enter into a non-culturable dormant state. A representative experiment is shown in Figure 3.29 but these observations shown were consistently noted in 7 independent experiments, with minor differences in the time to reduction of culturability with some strains. This was an unexpected result and indicates that in addition to resuscitation from dormancy, the Rpfs play a critical role in entry into the dormant state. It is particularly encouraging to note that with the double Δ*rpfA* Δ*rpfB* mutant the complemented strain used in this experiment entered the dormant state confirming that the inability to enter dormancy was indeed due to *rpf* gene loss.

As shown in Figure 3.28 and 3.29, in this model, dormancy or the non-culturable state is measured by the reduction in CFU/ml over time until no CFUs are recovered. The underlying hypothesis for this experiment would be that the bacteria are in non-culturable but viable state. In the case where we confirmed the loss of culturability after 72 hours as evidenced by no CFUs being recovered, we then sought to confirm viability of these cells using FACS analysis to measure viable organisms. The flow cytometry was done with the LIVE/DEAD kit as discussed in the materials and methods section. As shown in Figure 3.29C, after 72 hours, 65-85% of all non-culturable cells remained viable suggesting that at this point in the experiment, these cells truly reflected the viable but non-culturable state. However, viability of these cells dropped further over time. The variability in viability may be a result of differential survival of strains in this model.

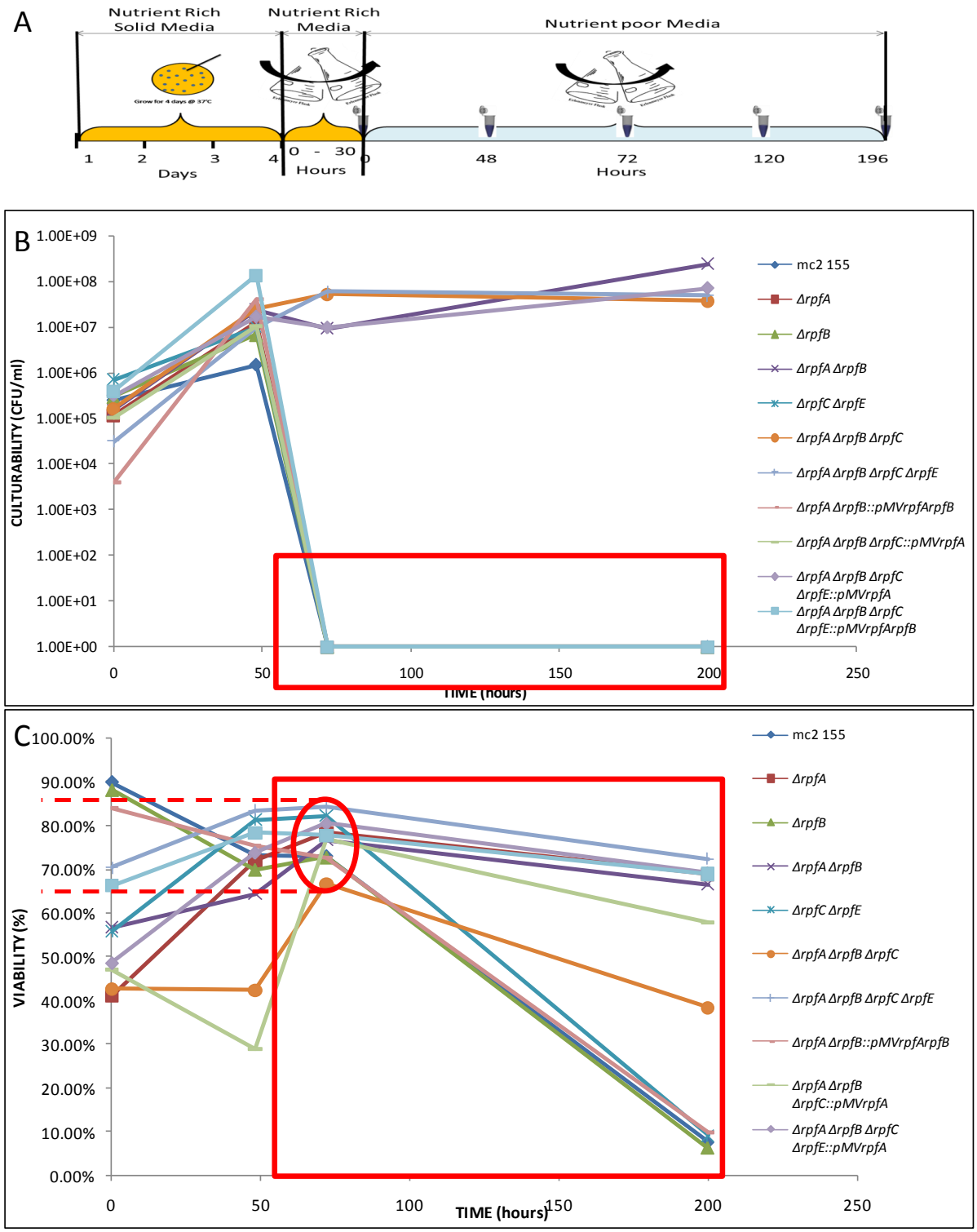

Figure 3.29: Establishment of dormancy and measurements of viability in *M. smegmatis*. A: Diagram of the dormancy model, Eppendorf tubes indicate when aliquots were taken for determining culturability and viability. B: Loss of culturability in the dormancy model. Culturability was determined by streaking CFU/ml onto nutrient rich agar plates. C: Viability of non-culturable cells. Viability was determined by flow cytometry. Red block indicate the stage were cells have enter a non-culturable stage, cells are still viable with between 85% and 65%, red circle, viability at 72 hours after transfer to mHdeB's media.

In those cells that remained viable but non-culturable after 72 hours, we attempted resuscitation experiments, shown in Figure 3.30. It's important to note that these experiments were done only at the 72 hour time point. Resuscitation was measured with most probable number (MPN) assays, which are carried out by diluting dormant cultures, in a ten-fold dilution series, before being transferred to 48 well plates. To obtain Rpf-containing and Rpf – deficient supernatant wild type (+Rpf) and the quadruple *rpf* deficient mutant (-Rpf) were grown in Sauton's media for 30 hours to an OD_{600nm} of 0.5. Culture filtrate from both Rpf + and Rpf – cultures were extracted and 0.025% yeast extract was added. For MPN assays, dormant cells were split into three groups: +Rpf, -Rpf and media only. This experiment was performed numerous times, but resuscitation, as measured by visible growth pellets in the wells of the MPN assays, was never seen, Figure 3.30. No difference was noted in any of the wells.

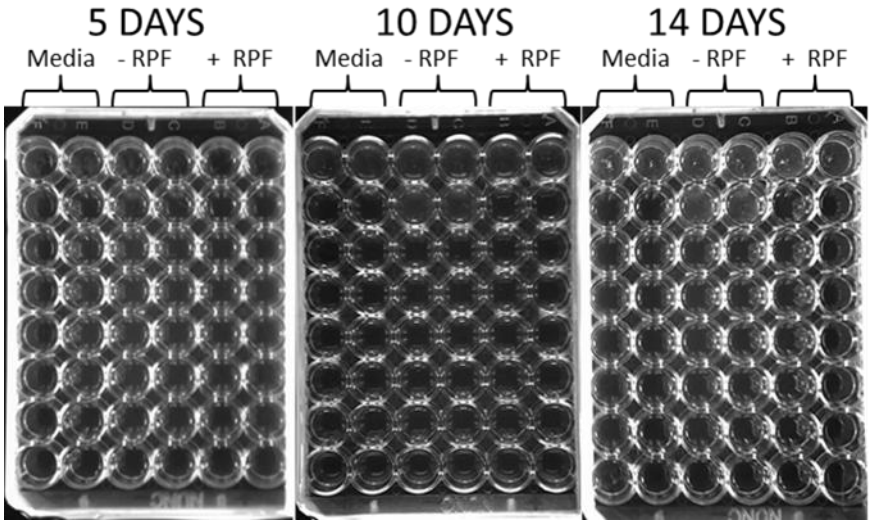

Figure 3.30: Resuscitation of dormancy cultures. Culture filtrate is diluted 1:1 with fresh media and used as growth media for the resuscitation experiments. Dormant cells are serially diluted and then added to media containing either culture filtrate from wild type (+RPF) or *rpf* quadruple mutant (-RPF). Media only is used to determine spontaneous resuscitation,

To analyze any changes in cell morphology in our dormancy model, TEM was carried out at different time points only on a subset of strains from the dormancy model. It has been reported that the bacteria change from rod shape to a spherical shape when entering dormancy (Salina et al., 2010). Whilst some ovoid and bulbous forms were observed in our model, most of the cells remained rod-like, Figure 3.31.

TEM microscopy on strains recovered from the dormancy model indicated that some of the *rpf* deficient mutants accumulated inclusion bodies, Figure 3.31, with the phenotype being more profound for the double Δ*rpfA* Δ*rpfB*, triple Δ*rpfA* Δ*rpfB* Δ*rpfC* and quadruple Δ*rpfA* Δ*rpfB* Δ*rpfC* Δ*rpfE* mutant strains, Figure 3.31. The number of inclusion bodies increased with progressive *rpf* gene loss and also increased the longer the strains remained in the model where wild type entered dormancy. The wild type had lost all inclusion bodies after 96 hours. We speculated that these inclusion bodies might be lipid storage bodies. To test this, we stained cells from all strains used in this model with Nile red, a lipid stain, Figure 3.32. The results were conclusive and pointed to the fact that these inclusion bodies were indeed lipids. Lipid storage is expected during dormancy (Salina et al., 2010) but the sheer number of lipid bodies in this case was unexpected and may explain why some *rpf* deficient strains are not able to enter dormancy.

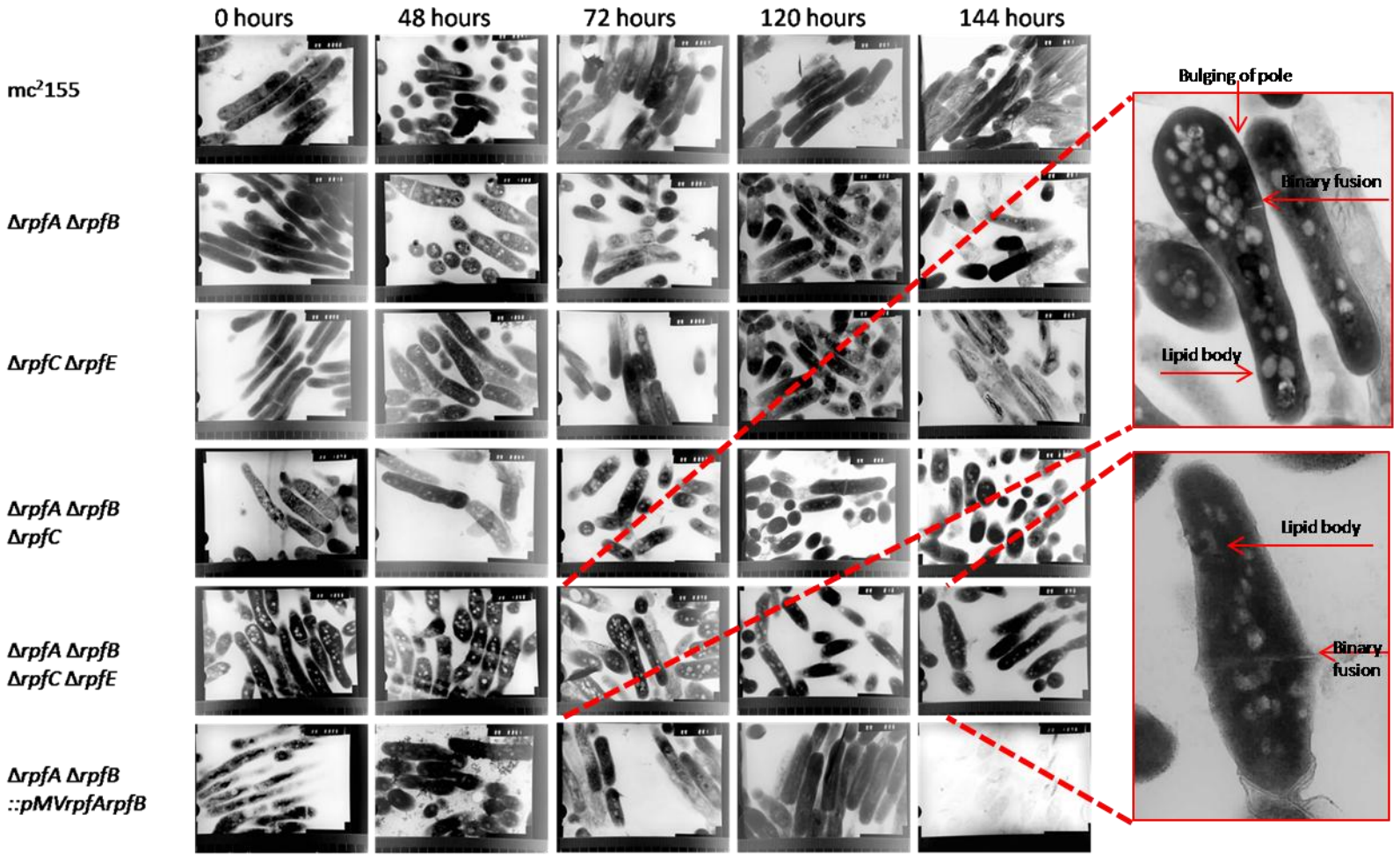

Figure 3.31: Transmission Electron Microscopy of all Strains at different times during dormancy model. Right: enlarged images to clearly indicate the accumulation of lipid bodies. Not all strains are shown.

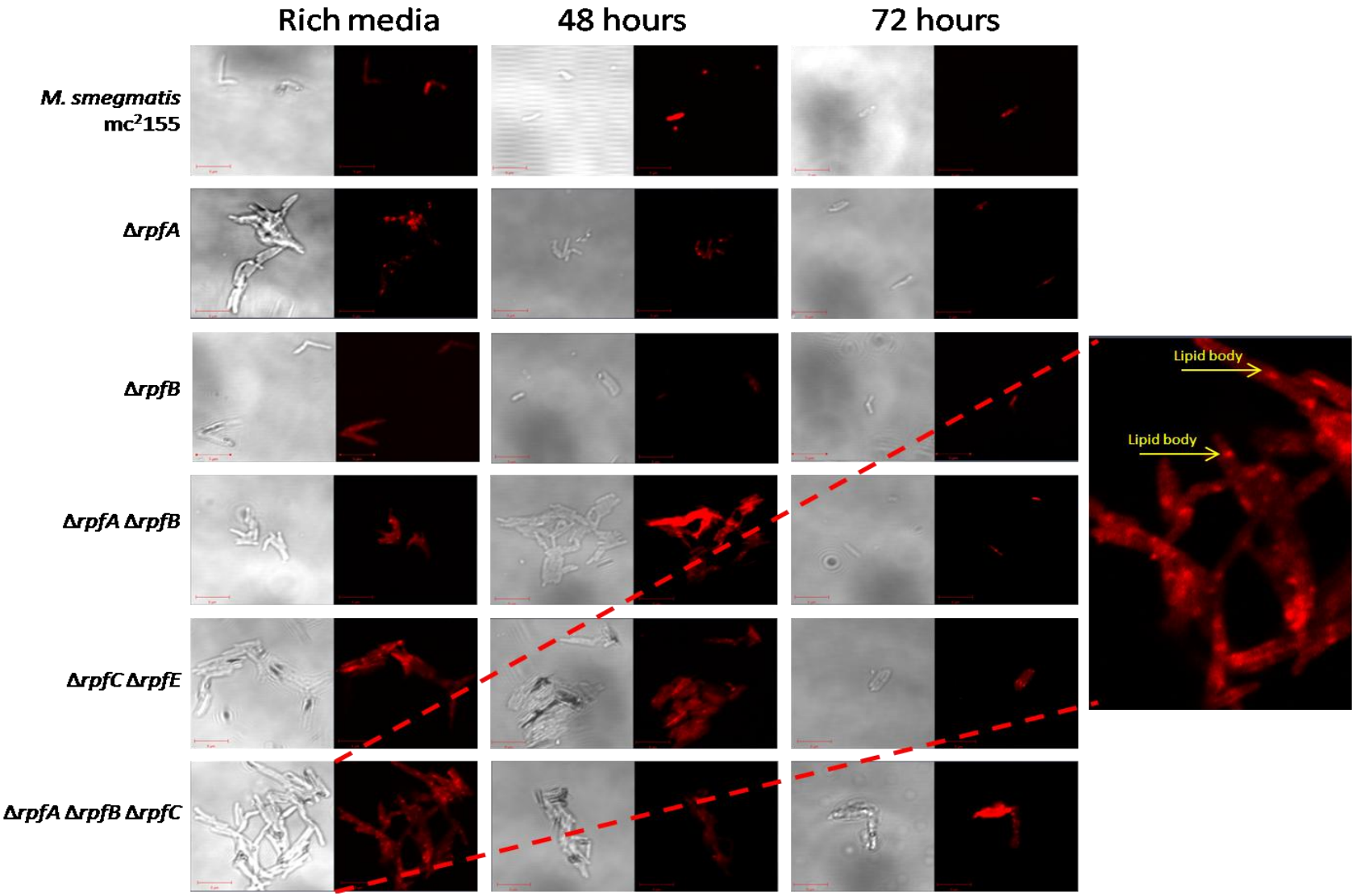
Rich media
48 hours
72 hours
M. smegmatis mc²155
ΔrpfA
ΔrpfB
ΔrpfA ΔrpfB
ΔrpfC ΔrpfE
ΔrpfA ΔrpfB ΔrpfC
Lipid body
Lipid body

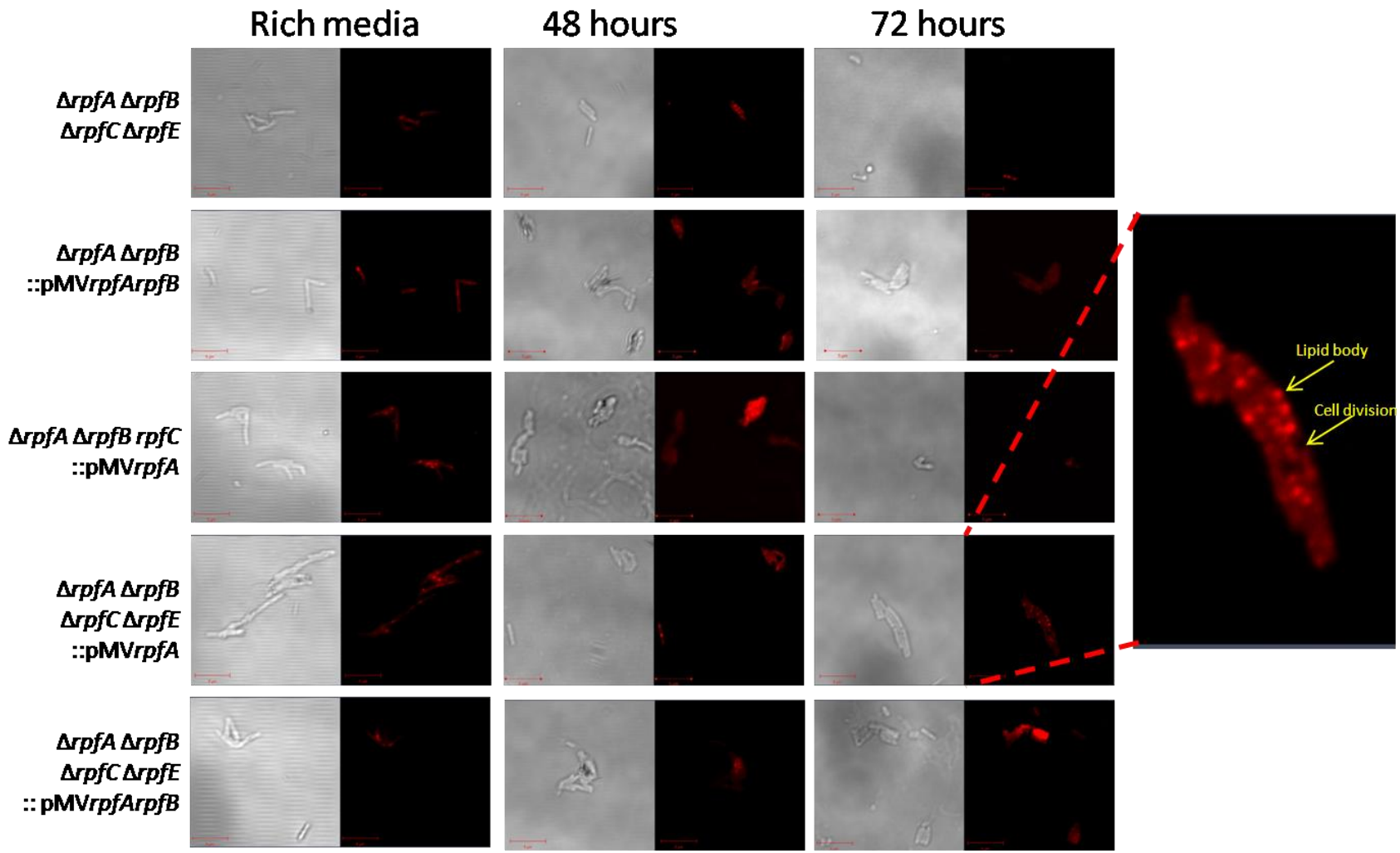

Figure 3.32: Confocal micrographs of cells stained with Nile red. Data represent four time point in the dormancy model where aliquots were taken and treated with Nile red, to visualize lipid bodies in bacterial strains as they enter dormancy. Right: enlarged images to clearly indicate the accumulation of lipid bodies.

4. Discussion

TB continues to be responsible for a massive loss of human life in the developing world. This is partly due to the emergence of drug resistant strains of *M. tuberculosis* and the ability of tubercle bacilli to adopt non-replicating states. To successfully fight this pandemic a better understanding of the bacterial growth states found during TB infection. The association of Rpf's with regulation of growth in *M. tuberculosis*, especially the reactivation of dormant *M. tuberculosis* cells, has sparked significant research into this area. The five *rpf*-like genes in *M. tuberculosis* have been extensively studied and their role in pathogenesis has been established from numerous studies (Downing et al., 2004, Downing et al., 2005, Kana et al., 2008, Kana et al., 2010, Tufariello et al., 2004, Tufariello et al., 2006). To facilitate further research into the role of Rpfs in growth as well their contribution to dormancy, the four *rpf*-like genes in *M. smegmatis* have been deleted in this study.

Conservation of rpf genes in M. tuberculosis and other species

M. tuberculosis encodes 5 *rpf*-like genes (Cole et al., 1998). This combined with the fact that numerous pathogenic mycobacteria, including *Mycobacterium leprae*, encode a multiplicity of *rpf*-like genes (Kana and Mizrahi, 2010) suggests that this expanded repertoire is required for the pathogenic process. The presence of three *rpf*-like genes in *M. leprae* (Kana and Mizrahi, 2010) is notable since this organism has undergone massive genome-wide reductive evolution to retain the minimal gene set required for pathogenesis (Cole et al., 2001). In this context, the retention of three *rpf* genes in this organism is significant. Our analysis of the genome of *M. smegmatis* mc^2155 and *M. tuberculosis* H37Rv, revealed that unlike the latter, *M. smegmatis* encodes four *rpf* homologues. In *M. smegmatis* mc^2155 *rpfA* and *rpfB* seems to be most highly conserved when compared to their *M. tuberculosis* counterparts, with respect

to similarity as well as genomic organization. The *rpfE* homologue in *M. smegmatis* also retains a significant level of similarity with the *M. tuberculosis* counterpart, with one exception, there is an additional *rpf*-like gene at the same locus. BLAST searches reveal that this additional gene from the *rpfE* locus in *M. smegmatis* mc^2155 is more similar to *rpfC*. ACT analysis revealed that *M. smegmatis* does not have a direct homologue of the *rpfC* gene from *M. tuberculosis*. Moreover, *M. smegmatis* does not encode a *rpfD* homologue, the region encoding *rpfE* is conserved between *M. smegmatis* and *M. tuberculosis* but the reading frame encoding *rpfD* has been lost. It is currently unclear how these differences in *rpf* gene complement between *M. smegmatis* and *M. tuberculosis* affect Rpf biology in these organisms but may in part explain the differences in phenotypes observed for mutants reported in this study and those reported for *M. tuberculosis* (Kana et al., 2008, Downing et al., 2004, Downing et al., 2005, Kana et al., 2010).

Collective dispensability of rpf-like genes in mycobacteria

The expanded repertoire of *rpf*-like genes in mycobacteria and other actinomycetes presents an interesting evolutionary enigma. The genetic expansion of this gene family in numerous bacterial species and firmicutes (Ravagnani et al., 2005a) when compared to the single gene in *Mi. lutues* suggests some level of functional divergence. A previous study demonstrated that the five *rpf*-like genes in *M. tuberculosis* are dispensable for growth *in vitro* (Kana et al., 2008). This is congruent with another similar finding that indicated the two *rpf*-like genes in *Corynebacterium glutamicum* ATCC 13032 (Hartmann et al., 2004) are dispensable for growth *in vitro*, in this case there were defects in recovery from stationary phase. In our study, we show that the four *rpf*-like genes in *M. smegmatis* are collectively dispensable for growth in vitro. These data contrast with the demonstration that the single *rpf* gene in *Micrococcus luteus* is essential (Mukamolova et al., 2002a). Currently, there is no clear

reason for this observation other that the notion that the different lifestyles of the above mentioned bacterial organisms, combined with the presence or absence of other PG degrading accessory proteins may be a major driving force in the evolutionary expansion of *rpf*-like genes in some bacteria. Apart from a delay in colony formation with a quadruple mutant and the quintuple *rpf* deletion mutant, sequential deletion of *rpf* genes in *M. tuberculosis* did not result in notable phenotypes *in vitro*. Moreover there were no defects in the manifestation of cording on the surface of colonies (Kana et al., 2008). There are some notable differences in this regard from our study. The double Δ*rpfA* Δ*rpfB,* triple Δ*rpfA* Δ*rpfB* Δ*rpfC,* and quadruple Δ*rpfA* Δ*rpfB* Δ*rpfC* Δ*rpfE* deletion mutant derived from *M. smegmatis* mc^2155 displayed notable differences in colony morphology and surface cording. These difference in phenotypes observed with *rpf* gene deletion in *M. smegmatis* and *M. tuberculosis* suggest that the *rpf*s may have some species specific function or may operate in conjunction with other proteins that are not present in both organisms.

Growth curve analysis further confirmed the *rpf*-like genes in *M. smegmatis* are collectively dispensable for growth *in vitro*. Rpfs retains the potential to stimulate the growth when added at very low concentrations to cultures of extensively washed organisms (Mukamolova et al., 1998). Extensive washing in this case would remove all extracellular/surface bound molecules that may retain some ability to stimulate growth. We reasoned that deletion of the *rpf* genes in *M. smegmatis* would affect the ability of the organism to recover from stationary phase and this would manifest in an extended lag phase in axenic culture. We tested this by conducting growth curves with extensively washed organisms but did not find any defects in exit from lag phase. Moreover, the number of organisms used for inoculation was diluted ten and one hundred fold to further assess the exit from lag phase with a low number of initial bacteria. Surprisingly, we found no defects in growth even at the lowest initial concentration

of extensively washed organisms. However, we noted consistent clumping in culture with certain *rpf* deficient strains, namely the double Δ*rpfA* Δ*rpfB* and quadruple Δ*rpfA* Δ*rpfB* Δ*rpfC* Δ*rpfE* mutants when the bacteria were cultured in the presence of glucose and salt but not in richer media supplemented with Middlebrook OADC enrichment. This suggested some level of growth stress. We sought to exacerbate this phenotype by culturing the *rpf*-decifient mutants in Sauton's minimal media but found no differential growth effects. Hence, the clumping observed during growth in Middlebrook 7H9 media may be due to some change in overall charge or hydrophobicity of the cell wall. This would need to be tested further by extraction and HPLC analysis of the PG from *rpf* deficient mutants.

Genetic redundancy versus functional divergence

Transcriptional profiling of *rpf* deletion mutants in *M. tuberculosis* using microarrays to assess global gene expression profiles, strongly suggested that there is partial redundancy in the function of the five *rpf*-like genes as evidenced by compensatory increases in gene expression of the remaining *rpf* genes in *rpf*-deficient mutants (Downing et al., 2004). Interestingly, a subsequent study demonstrated that the remaining *rpf* gene in quadruple *rpf* deletion mutants of *M. tuberculosis* was down-regulated, rather than the compensatory up-regulation seen in single, double and triple mutants (Kana et al., 2008). This suggested some level of regulatory cross-talk between the multiple *rpf* homologues present in this organism. Similar compensatory changes in gene expression in *M. smegmatis rpf* deficient mutants was not tested in this study but may provide useful information on the functional overlap, if any, between these genes. Further evidence for differentiation of gene function comes from *in vivo* studies with *rpf* deletion mutants of *M. tuberculosis*. The deletion of *rpfB* in *M. tuberculo*sis resulted in a delay in reactivation from chronic infection in mice (Tufariello et al., 2006). Further work demonstrated that a double *rpfA rpfB* deficient mutant displays an exacerbated

defect in reactivation from chronic disease in mice with a concomitant different modulation the innate immune response when compared to wild type (Russell-Goldman et al., 2008). Furthermore, it has been demonstrated that only RpfB and RpfE, is able to bind RipA (Hett et al., 2007) suggesting some functional hierarchy in gene function. Numerous mutants in our panel Δ*rpfA*, Δ*rpfB*, Δ*rpfC*, Δ*rpfE*, Δ*rpfC*Δ*rpfE*, did not display any notable defects in growth and/or colony formation suggesting that remaining *rpf*-like genes in these organisms may be compensating for function. However further gene expression studies and protein interaction work is required to assess individual versus collective *rpf* gene function in *M. smegmatis*.

Cell wall permeability in rpf deficient mutants

Previous data from our lab confirmed that the triple and quadruple *rpf* mutant strains in *M. tuberculosis* H37Rv displayed reduced growth in the presence of malachite green, contained in Middlebrook 7H11 solid media. This was further studied by assessing susceptibility to antibiotics and detergent stress, these data will be discussed later on, however, it has been hypothesized that these phenotypic effects seen with *M. tuberculosis rpf* deletion mutants was due to a change in permeability of the cell wall (Kana et al., 2008). Similar effects were observed with the *mar2* deficient mutant of *M. tuberculosis*, which displayed a very glossy phenotype when strains were grown on solid media containing tween, furthermore this mutant was able to absorb high concentrations of the Congo Red stain from solid media. These phenotypes were attributed to a distinct change in the permeability of the cell wall (Nguyen et al., 2010). To further test the permeability of the *rpf* deficient strains generated in this study, we attempted similar studies. All the *rpf* deficient strains tested showed no differential increase in permeability when compared to the wild type. Unpublished data from the CBTBR suggest that when *rpf* deficient strains of *M. tuberculosis* are stained with Neutral Red, quadruple and quintuple mutants did not take up the Neutral Red stain, consistent with

their reduced virulence (Kana et al., 2008, Soto et al., 2002). In this study, staining with Neutral Red did not give any notable uptake of the dye in the wild type strain hence no conclusion can be made regarding the lack of staining observed for the *M. smegmatis rpf* deficient mutants. It has been demonstrated that the *rpf* deficient strains of *M. tuberculosis,* have a reduced ability to grow in the presence of SDS, in particular it was found that the triple and quadruple mutants were sensitive to SDS with a reduction in growth on solid media (Kana et al., 2008). Data from this study are consistent with this report, we found that, the double Δ*rpfA* Δ*rpfB* and quadruple *rpf* deletion mutants of *M. smegmatis* show a reduction in growth on solid media containing 0.005% SDS. This phenotype was restored in the Δ*rpfA* Δ*rpfB*::pMV*rpfArpfB* mutant when the corresponding *M. tuberculosis* genes were used for genetic complementation. This confirmed that the observed defects were due to *rpf*-gene loss and confirmed the functionality of the *M. tuberculosis rpf* genes in *M. smegmatis*, despite the differences in *rpf* gene complement noted above between these organisms. To further assess these changes in cell wall stability, antibiotics were used as a probe for gene function where MIC analyses were done on the *rpf* deficient strains. Previous antibiotic susceptibility analysis in *M. tuberculosis* with the *rpf* deficient strains identified an increase in susceptibility to erythromycin and vancomycin with the quintuple *rpf* deletion mutant (Kana et al., 2010). In our study we found a 10 fold increase in susceptibility to both these antibiotics for the triple Δ*rpfA* Δ*rpfB* Δ*rpfC*, and quadruple Δ*rpfA* Δ*rpfB* Δ*rpfC* Δ*rpfE* mutants. Vancomycin inhibits new PG cross-linking by binding the pentapeptide at the terminal D- alanine, and thereby inhibiting the translocation to the periplasm and crosslinking (Hett and Rubin, 2008). The sensitization of the *rpf* deficient strains to vancomycin further implicates Rpfs in PG remodeling and suggests some change in PG structure in the mutant strains.

M. tuberculosis is inherently resistant to the penicillin class of antibiotics due to the presence of very active Class A β-lactamase, encoded by the *blaC* gene (Hugonnet et al., 2009). *M. smegmatis* also displays inherent resistance to β-lactam antibiotics as evidence by the lack of notable susceptibility to carbenicillin. However, unlike what has been observed in *M. tuberculosis* (Hugonnet et al., 2009), we have shown that addition of the β-lactamase inhibitor clavulanate has no effect on susceptibility to β-lactam antibiotics. This might be due to the increased β-lactamase activity in *M. smegmatis*, but this remains to be confirmed. In this context it is noteworthy that we also found that *rpf* deficient mutants have some degree of resistance towards ampicillin. Our antibiotic susceptibility analyses reveal an increase in susceptibility in the *rpf* deficient mutants to the cephalosporins used in this study. This is consistent with previous findings that indicate the *rpf* deficient mutant strains in *M. tuberculosis* are more susceptible to cephalosporins (Wivagg and Hung, 2012) and in this case it was shown that resistance is due to altered diffusion across the cell wall. We also observed increased susceptibility to imipenem in our study. Except for erythromycin, which also gave increased susceptibility with *rpf* mutants, all these antibiotics affect cell wall synthesis and the differential susceptibility, observed to varying degrees with some *rpf* deficient strains, point to some change in cell wall permeability. Erythromycin is a macrolide and the increased susceptibility to this antibiotic is most likely due to increased permeability of this drug across the cell wall. Similar effects have been reported in *M. tuberculosis*, where deletion of genes that are associated with cell wall metabolism, resulted in increased susceptibility to erythromycin (Vandal et al., 2009). Collectively, our data are suggestive that certain *rpf* deficient mutants in *M. smegmatis* have an altered PG structure which results in differential permeability to drug or changes the inherent susceptibility to these antibiotics.

Biofilm formation

Biofilms form when bacteria are stressed due to changes in environmental conditions such as oxygen depletion, nutrient starvation etc. Bacteria are able to switch from planktonic growth to biofilms, but in many cases this requires some stimulus or some form of bacterial communication to form higher order structures. In some organisms, molecules used for communication, termed bacterial "pheromones", can stimulate sporulation, virulence, bioluminescence and cell division (Voloshin and Kaprelyants, 2004). Furthermore, this pheromone-based effect has been attributed to a group of signaling molecules, *N*-acyl homoserine lactones, in gram negative bacteria (Fuqua and Greenberg, 1998) and peptides in gram positive organisms (Ohnishi et al., 1999). In *Mi. luteus*, Rpf has been implicated in communication between bacteria (Voloshin and Kaprelyants, 2004). For biofilm formation in particular, correct expression of the *fur* gene (iron-responsive repressor) is important since it has been shown that reduced expression, suppresses biofilm formation (Banin et al., 2005). Interestingly, in this study we found a similar effect where reduction of iron in the media, led to an inhibition of biofilm formation in the wild type (data not shown). When the *rpf* deficient mutants were grown in Sauton's media, in a biofilm assay, there was a clear reduction in the ability of the double Δ*rpfA* Δ*rpfB*, triple Δ*rpfA* Δ*rpfB* Δ*rpfC*, and quadruple Δ*rpfA* Δ*rpfB* Δ*rpfC* Δ*rpfE*, mutants to form biofilms. The progressive loss of *rpf*s resulted in the formation of flat, very fragile biofilms. The surface wrinkling of biofilms that is characteristic with wild type *M. smegmatis* (Ojha et al., 2005) is lost in biofilms of the mutant strains where holes can be seen in the biofilms. Genetic complementation in the case of the Δ*rpfA rpfB*::pMV*rpfA rpfB* strain resulted in reversion of the phenotype back to that seen in wild type, confirming that the biofilm defects were due to *rpf* gene loss in the Δ*rpfA* Δ*rpfB* double mutant. A similar effect was not seen with strains that were not genetically complemented back to the wild type genotype – presumably this is due to the fact that the remaining deletion alleles still

confer a significant defect in biofilm formation. It has been shown that the acetylation of glycopeptidolipids (GPL) affects the formation of biofilms and sliding motility in *M. smegmatis* (Recht and Kolter, 2001). We conducted TLC analysis on our strains to further analyze the sliding phenotypes (described further below) but did not find any defects in GPL production. Given the demonstrated role of Rpfs in PG degradation (Mukamolova et al., 2006), we hypothesize that these defects in biofilm formation may be due to a reduced ability in the *rpf* deletion mutant to produce muropeptides. Muropeptides have been shown to be important for signaling and reactivation from dormancy in *B. subtilis* (Shah et al., 2008) and may also be important for the signaling processes that are required during biofilm formation or for the switch from planktonic to biofilm growth.

Sliding motility

As mentioned previously, the absence of GPLs reduces the ability of mycobacterial strains to slide across the surface of agar plates (Recht and Kolter, 2001). The sliding effect was postulated to be due to the electrostatic interactions between the mycobacterial capsule and the abiotic surface of the sliding motility plates. GPLs contribute significantly to the hydrophobic surface of the mycobacterial cell and are thus a key element of the sliding effect on the hydrophilic surface of the agar plate. The lack of the GPLs in the certain mutant strains resulted in a more hydrophilic cell surface which lead to a reduction in sliding (Recht and Kolter, 2001). Considering this, the ability of the *rpf* deficient mutants to slide to a greater extent than wild type on sliding motility plates, could be due to the fact that the strains have become more hydrophobic. Even though the GPL content of these strains has not changed, we noticed a similar phenomenon before with regards to extensive clumping of the *rpf* deficient mutants when grown in liquid media. This clumping phenotype was only reduced when the OADC enrichment was used. It stands to reason that since the Rpfs catalyse

hydrolysis of the PG, their activity, or lack thereof in the mutants, could result in changes within other components of the cell wall such as GPLs, which could explain the sliding phenotypes seen with these strains. Due to the complete lack of complementation, it cannot be concluded that this phenotype is a consequence of *rpf* loss.

Colony formation

There is a growing body of evidence that suggests in a genetically homogeneous population of bacteria, there are phenotypically distinct subpopulations and the extent to which these proliferate will depend on the environmental conditions surrounding the population such as oxygen, nutrients and chemicals which create a variety of microhabitats for bacterial colonization (Stewart and Franklin, 2008). The formation of bacterial colonies in plates is an intriguing phenomenon and apart from the cording effect in mycobacteria not much further is known about the genetic factors that contribute to colony formation in this genus. In our electron micrographs wild type *M. smegmatis* displays a differential degree of cellular packing and changes in cell morphology in different locations of the colony. The cells at the bottom of the colony, on the ridges are much longer and broader compared to the cells on top of the colonies. The cells on top of the colonies are much shorter, which might be due to the lack of nutrient, as well as the pressure from being exposed to the environment. The cells at the bottom of the colony would have direct contact with nutrients derived from the agar plates.

Visual assessment of the colonies formed by some of the *rpf* deficient mutants when plated on solid media, revealed that the colonies seem to have a smoother surface morphology compared to the wild type. The double Δ*rpfA* Δ*rpfB*, triple Δ*rpfA* Δ*rpfB* Δ*rpfC*, and quadruples Δ*rpfA* Δ*rpfB* Δ*rpfC* Δ*rpfE* mutants lack the ability to form surface cording, which

can be observed in the wild type colonies. When the *M. tuberculosis rpfA* and *rpfB* genes were used in genetic complementation of the Δ*rpfA* Δ*rpfB* mutant (Δ*rpfA* Δ*rpfB*::pMV*rpfArpfB*) mutant, the phenotype was restored to that seen in wild type, implicating the *rpf* genes in this phenotype. The scanning electron microscopy micrographs show that there are subtle differences in the colonies formed by *rpf* mutant strains. Firstly, there is a reduction in cell size with some of the mutants. In wild type, there is a pronounced criss-cross pattern in the packing of bacteria moving away from the colony on the agar. This is very different in the *rpf* deficient mutants, which seems to lack this phenotype and in contrast the bacteria are tightly packed. This phenotype might also be due to changes in the electrostatic charge of the cell wall. These changes in colony packing suggest that the co-ordination of the individual bacteria during the colony formation process in these strains is altered.

Cell morphology

To assess the cellular morphology and growth of the *rpf* deficient mutants, confocal microscopy was performed with fluorescent dyes. The use of fluorescently tagged vancomycin allowed for localization of new PG crosslinking in these strains as well as the site of septum formation during cell division. In our study, vancomycin staining was found at the poles of wild type cells as well as at the septa. In many cases, the septa do not seem to be in the middle of the cell which is consistent with previous findings demonstrating that cell division of mycobacteria is asymmetric (Joyce et al., 2012, Aldridge et al., 2011). Wag31, a cell division protein which is localized at the septa and poles is phosphorylated indirectly by PknA through PknB and found to form a complex with CrgA and CrwA, and is also localized to the poles during growth and cell division (Kang et al., 2008). The depletion of this gene product causes polar swelling, very similar to that noted in our *rpf* deficient mutants,

especially in the presence of imipenem treatment (Kang et al., 2008). Furthermore, there is a distribution of vancomycin along the lateral axis of the cell wall in the double Δ*rpfA* Δ*rpfB,* triple Δ*rpfA* Δ*rpfB* Δ*rpfC* and quadruple Δ*rpfA* Δ*rpfB* Δ*rpfC* Δ*rpfE* mutants, implying that PG synthesis is occurring throughout the lateral axis of cell, this effect may be due to more extensive cell wall remodeling. Cells from the *rpf* deficient mutants; Δ*rpfA* Δ*rpfB,* Δ*rpfA* Δ*rpfB* Δ*rpfC*, Δ*rpfA* Δ*rpfB* Δ*rpfC* Δ*rpfE* were much shorter in size when compared to the wild type. Moreover, the successive loss of *rpf* seems to result in a more dramatic shortening of the cell suggesting that Rpfs play a role in determining cell size and shape.

HRSEM analysis confirmed some of these defects and also assisted in determining the mechanism of cell division for these strains. The *rpf* deficient mutants, show a very similar modality of cell division (V-snapping), compared to the wild type and normal characteristics were observed for these mycobacterial strains (Dahl, 2004). The *rpf* deficient mutants; Δ*rpfA* Δ*rpfB,* Δ*rpfA* Δ*rpfB* Δ*rpfC*, Δ*rpfA* Δ*rpfB* Δ*rpfC* Δ*rpfE* did however, show an increase in bulging at the poles. The triple Δ*rpfA* Δ*rpfB* Δ*rpfC* and quadruple Δ*rpfA* Δ*rpfB* Δ*rpfC* Δ*rpfE* mutants displayed bulging in the middle of dividing cells. The triple and quadruple mutants also showed more than one noticeable septa in dividing cells, suggesting that these cells are unable to complete cell division and seemingly initiate the formation of a new septum even though the first septum has not resolved. With regards to the phenotypic changes seen in the strains treated with imipenem, there is an increase in wrinkling of the cell surface in all strains, most likely due to the inhibition of new PG synthesis by the antibiotic. The wild type along with the single Δ*rpfA* and Δ*rpfB* mutants display bulging of the poles which is the site of new PG synthesis. This phenotype seems to shift away from the end of the pole in the triple Δ*rpfA* Δ*rpfB* Δ*rpfC* and quadruple Δ*rpfA* Δ*rpfB* Δ*rpfC* Δ*rpfE* mutants, where the bulges occur along the lateral axis of the cell.

Statistical analysis of the micrographs allowed for a more quantitative assessment of these changes since the inherent morphological heterogeneity in mycobacterial culture makes phenotypic assessment of cell size and shape difficult. Since we were observing cell division processes, we only analyzed micrographs where greater than 50% of the cells were dividing. The Bray-Curtis test for similarity proved valuable to group the *rpf* deficient strains, with the lowest degree of similarity at 65%. The analysis revealed that the triple Δ*rpfA* Δ*rpfB* Δ*rpfC* and quadruple Δ*rpfA* Δ*rpfB* Δ*rpfC* Δ*rpfE* mutants are most similar to each other and that the complemented strains are similar in some cases to the wild type, as expected. There is a clear difference in the occurrence of the different lengths in some *rpf* deficient mutant but due to the varying lengths of the wild type comparator, no definite conclusions can be made.

Dormancy

It has been reported that both *M. smegmatis* and *M. tuberculosis* have the ability to enter dormancy in certain *in vitro* models, (Mukamolova et al., 1998, Shleeva et al., 2004, Mukamolova et al., 2002a). In our study, we attempted to reproduce the published model of dormancy and resuscitation (Shleeva et al., 2004) and we were able to produce non-culturable cells but were not able to resuscitate these cells. To determine if the viability of the strains were affected in this model, the TEM micrographs as well the flow-cytometry data were used. Non-culturable cells undergo a morphological change when entering dormancy (Anuchin et al., 2009), we did notice some morphological changes but did not see a significant switch to ovoid type cells in the majority of our bacteria. The data from our TEM micrographs also reveal that the wild type strain accumulates lipid bodies accompanied by shortening of the cells. Of particular importance, we were able to show that 85 % of these cells are still viable when entering the non-culturable state, confirming that they truly represent the viable but non-culturable (VBNC) state. In this context, the inability to

resuscitate these cells is difficult to explain and indicates that further revision of the model and resuscitation parameters is required. The most significant observation from our analysis on dormancy relates to the inability of certain *rpf* deletion mutants, namely the Δ*rpfA* Δ*rpfB*, Δ*rpfA* Δ*rpfB* Δ*rpfC*, Δ*rpfA* Δ*rpfB* Δ*rpfC* Δ*rpfE* strains to enter into a non-culturable state. These results were reproducibly obtained over seven independent experiments and in the case of the double Δ*rpfA* Δ*rpfB* mutant, genetic complementation reversed this defect. These observations point to a new role for Rpfs in the establishment of the dormant state in mycobacteria.

TEM micrographs reveal that the Δ*rpfA* Δ*rpfB*, Δ*rpfA* Δ*rpfB* Δ*rpfC*, Δ*rpfA* Δ*rpfB* Δ*rpfC* Δ*rpfE* mutants to have an increase in inclusion bodies. Some of these inclusion bodies were so numerous that they seemed to distort the normal morphology of the cell. Staining with Nile red revealed that these inclusion bodies were in fact lipid bodies. The accumulation of lipid bodies has been seen in dormant or non-replicating *M. tuberculosis* before (Garton et al., 2008). However, in our study the number of these inclusion bodies increased with progressive loss of *rpf* genes and this effect phenotype was reversed with genetic complemention in the Δ*rpfA* Δ*rpfB*::pMV*rpfArpfB* strain. This accumulation of lipid might point to the important role for Rpfs in signalling the switch between active growth and dormancy. Interestingly, those strains that displayed high amounts of lipid storage bodies never entered the dormant state suggesting that these phenotypes are correlated. The fact that the *rpf* quintuple deficient mutant in *M. tuberculosis* is still able to enter into dormancy (Kana et al., 2008, Downing et al., 2005) and our quadruple deletion mutant cannot, confirms that different species may enter dormancy by different mechanisms. It also demonstrates that the Rpfs may have different function in different species.

Conclusion

This study provides the first demonstration that the four *rpf*-like genes are dispensable for growth of *M. smegmatis*. Our data demonstrate that in *M. smegmatis* the Rpfs are not required for growth from very low bacterial numbers but are important for colony formation on solid media. This is evidenced by the fact that *rpf* deficient mutants are unable to complete the cording process. High resolution analysis of colony structure suggested that bacterial signalling and cell surface structure is altered in double, triple and quadruple *rpf* deletion mutants. Consistent with this, these mutants display defects in biofilm formation presumably due to the inability to communicate effectively within the bacterial population. Antibiotic susceptibility analysis confirmed that multiple *rpf* deficient mutants have increased susceptibility to cell wall targeting antibiotics. This combined with the changes in sliding motility suggest that the PG structure is altered in these mutants. An unexpected finding from our study was the observation that multiple *rpf* deletion mutants were unable to enter into the VBNC state, strongly implicating Rpfs in the establishment of dormancy. Future work will involve further analysis of the Rpf function in bacterial signalling. The hydrophobicity of the cell wall in *rpf* deficient mutants will be tested further by extraction and HPLC analysis of the PG. Further work with regards to Rpf localization will also be done to determine where all the Rpfs are localized, which will allow some inference of function. The role of Rpfs in the establishment of dormancy will be studied by assessing gene transcriptional changes during entry into dormancy. These and other studies will provide unique insight into this fascinating group of proteins.

Appendix A:

Solutions and media
All media was made up in one litre de-ionized water and except otherwise stated and sterilized by autoclaving (121°C for 20 minutes)

General Media (per litre)

Luria-Bertani Broth (LB)
5 g yeast, 10 g tryptone, 10 g sodium chloride

Luria-Bertani Agar (LA)
5 g yeast, 10 g tryptone, 10 g sodium chloride, 15 g agar

2× TY
5 g sodium chloride, 10 g yeast extract, 16 g tryptone

Middlebrook 7H9
2 ml glycerol, 4.7 g Difco™ Middlebrook 7H9 broth

Middlebrook 7H10
5 ml glycerol, 19 g Difco™ Middlebrook 7H10 agar

Motility Plates
2 ml glycerol, 4.7 g Difco™ Middlebrook 7H9 broth solidified with 0.3% agar and left to dry overnight

Dormancy and Resuscitation Media (per litre)

Sauton's minimal media (pH 7.2)
4 g asparagine, 0.5 g magnesium sulphate, 2 g citric acid, 0.5 g potassium dihydrogen orthophosphate, 0.05 g ammonium ferric citrate, 60 ml glycerol.

NBE media
5 g $NaCl_2$, 1.5 g yeast extract, 3 g Beef extract, 7.5 g peptone

NBE Agar
5 g $NaCl_2$, 1.5 g yeast extract, 3 g Beef extract, 7.5 g peptone, 15 g Agar

mHdeB's media
17.9 g Na_2HPO_4, 1.2 g citric acid, 5 g $(NH_4)_2SO_4$, 30 ml of Glycerol, adjusted to pH 7 with citric acid, and autoclaved then the following added. 5 ml trace element solution 1, 5 ml trace element solution 2, 5ml Tween 80 and 0.025% bovine serum albumin (BSA).

Trace element solution 1
0.15 g Ethylenediaminetetraacetic acid (EDTA), 3 g $MgCl_2$, 0.03 g $CaCl_2$, 0.15 g $FeSO_4$ in 150 ml of water, filtered

Trace element solution 2

0.15 g EDTA, 0.012 g $CoCl_2$, 0.037 g $MnCl_2$, 0.006 g Na_2MoO_4, 0.006 g $ZnSO_4$, $CuSO_4$ in 150 ml of water, filtered

Spent media
Culture filtrate, diluted with an equal volume Sauton's media, containing 0.6% Glycerol and 0.025% yeast extract

Genomic Preparation Solutions

TAE buffer
1mM EDTA, 40 mM Tris-acetic acid pH 8.5

TE buffer
10 mM Tris-HCl pH 8.0, and 1mM EDTA

DNA extraction solutions

Solution1
50 mM glucose, 25 mM Tris-Cl pH 8.0, 10 mM EDTA

Solution 2
1% SDS, 0.2 M NaOH

Solution 3
3 M Potassium acetate, pH5.5

Southern Blotting Solutions

20× SSC
8.82% sodium citrate, 17.53% NaCl; pH to 7.0 with HCl

Solution I
2× SSC, 0.1% SDS

Solution II
0.5 × SSC, 0.1% SDS

Microscopy solutions

Ruthenium Red Fixative solution
0.1M HEPES, 2.5% Glutaldehyde, 2% Formaldehyde, 0.005% Ruthenium Red

Resin
5.62 g of Araldite, 7.75 g Epon 812 and 15 g DDSA

Lead citrate
1% aqueous solution, 4% NaOH (25:1)

Uranyl acetate

Saturated solution in 100% methanol,

Fixative solution
Glutaldehyde (2.5%) in PBS (0.1%)

Staining solution (non-microscopy)

Neutral red
0.002% Neutral red in Barbital buffer (1% sodium barbital, 5% $NaCl_2$, pH9.8)

TLC

Running Buffer
Chloroform : methanol solution (100:7)

Staining spray
Orcinol (0.1%) and sulphuric acid (40%)

Appendix B

Lambda DNA molecular weight markers.

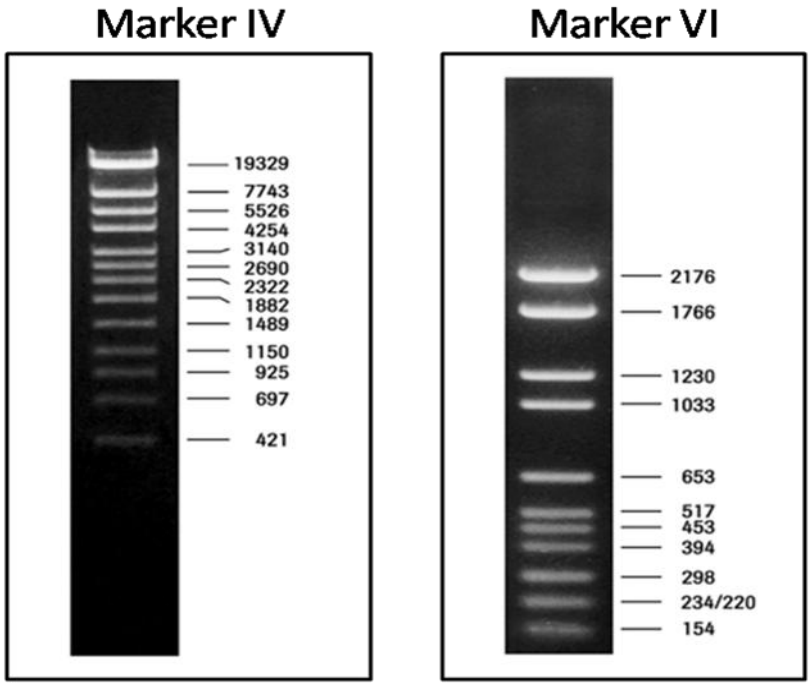

The above DNA molecular weight markers IV and VI used in this study were supplied by Roche Applied Science

Appendix C

Excluded Results

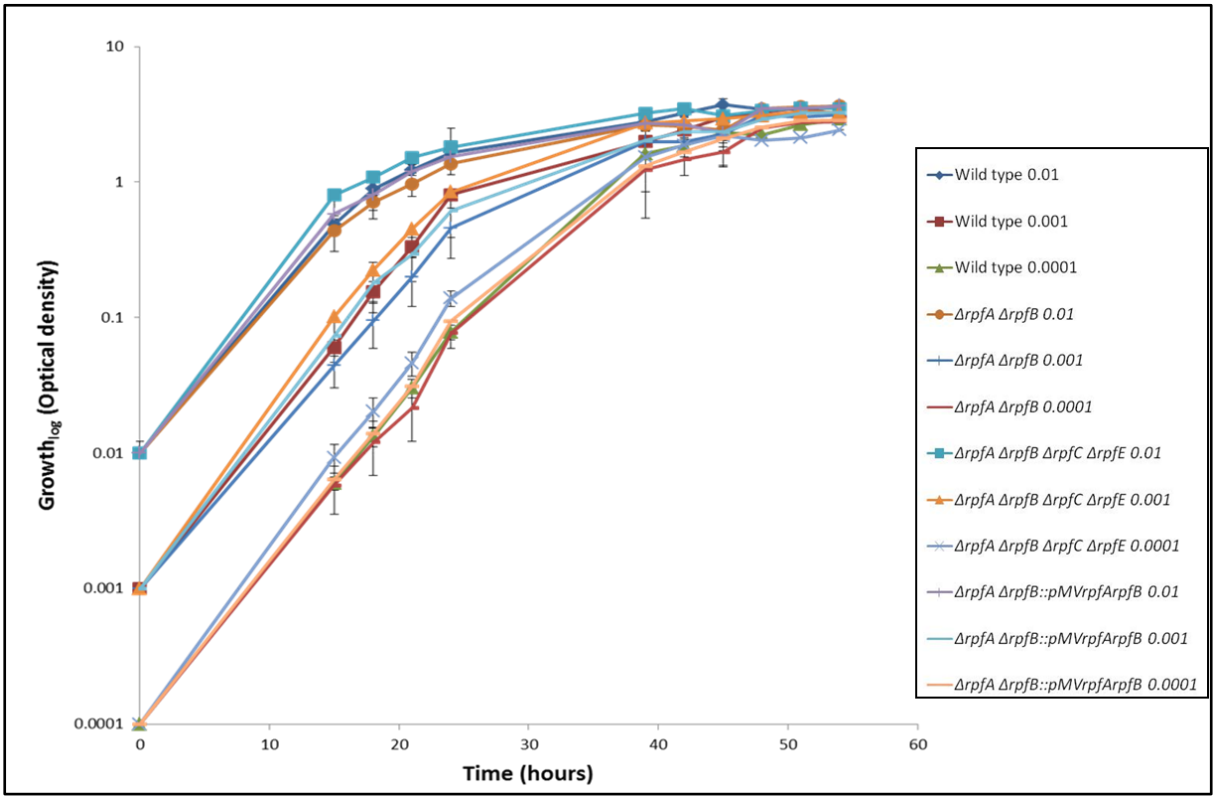

Figure C1: Growth curve analysis with Glucose salt enrichment using 0.002 % Tyloxypol. Growth curve showing optical density versus time for 7H9 media, supplemented with glucose, salt, and 0.002 % Tyloxypol. Strains were grown with different starting bacterial concentrations and monitored 3 hourly to determine growth. Strains used in this experiment were wild type, Δ*rpfA* Δ*rpfB*, Δ*rpfA* Δ*rpfB* Δ*rpfC* Δ*rpfE* and Δ*rpfA* Δ*rpfB*::pMV*rpfArpfB*. This graph is an average of two experiments.

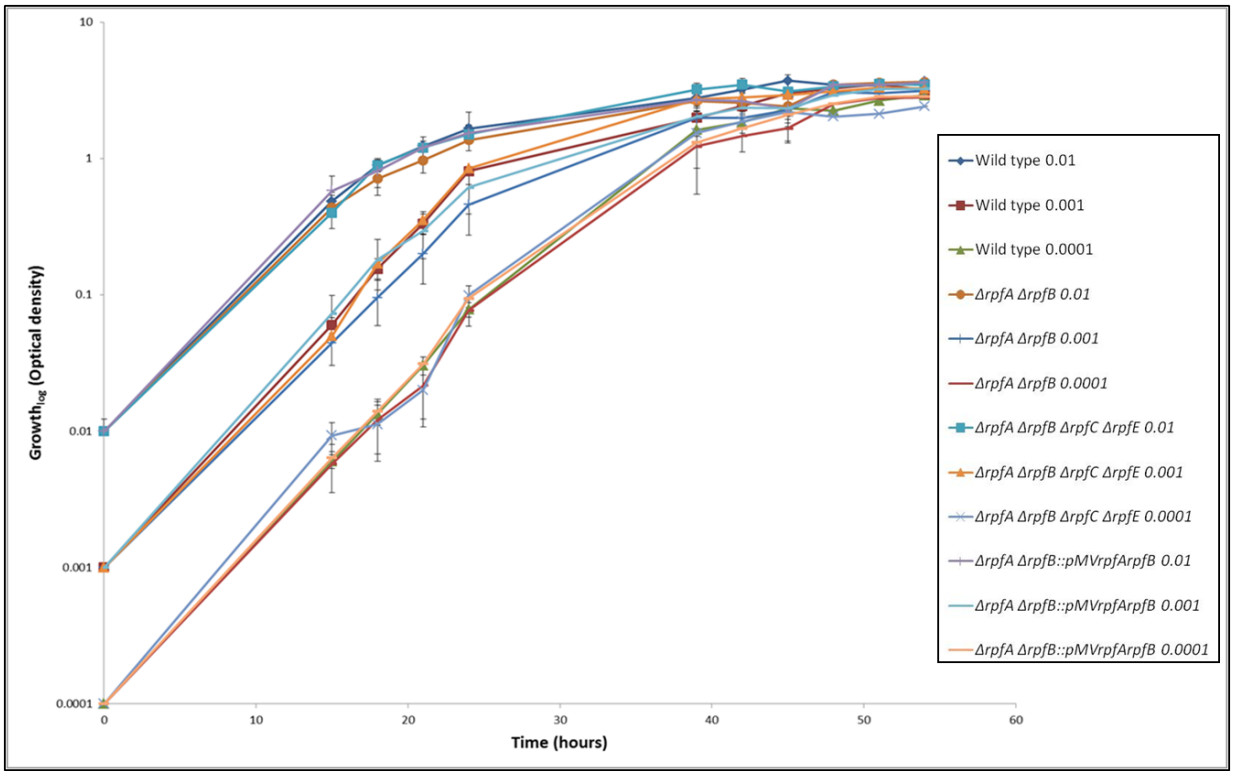

Figure C2: Growth curve analysis with Glucose salt enrichment using 0.003% Tyloxypol. Growth curve showing optical density versus time for 7H9 media, supplemented with glucose, salt, and 0.003 % Tyloxypol. Strains were grown with different starting bacterial concentrations and monitored 3 hourly to determine growth. Strains used in this experiment were wild type, Δ*rpfA* Δ*rpfB*, Δ*rpfA* Δ*rpfB* Δ*rpfC* Δ*rpfE* and Δ*rpfA* Δ*rpfB*::pMV*rpfArpfB*. This graph is an average of two experiments.

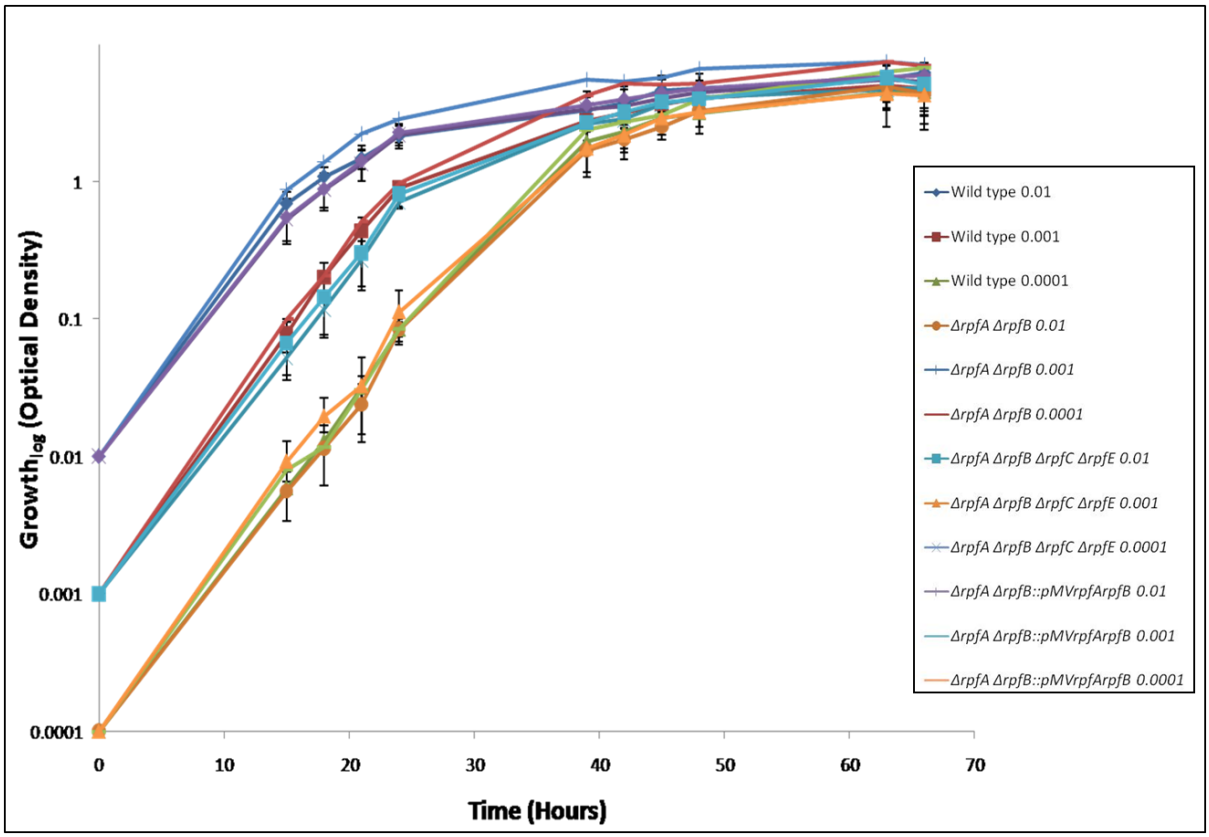

Figure C3: Growth curve analysis with OADC enrichment and 0.002 % Tyloxypol. Growth curve showing optical density versus time for 7H9 media, supplemented with OADC and 0.002 % Tyloxypol. Strains were grown with different starting bacvterial concentrations and monitored 3 hourly to determine growth. Strains used in this experiment were wild type, Δ*rpfA* Δ*rpfB*, Δ*rpfA* Δ*rpfB* Δ*rpfC* Δ*rpfE* and Δ*rpfA* Δ*rpfB*::pMV*rpfArpfB*. This graph is an average of three experiments.

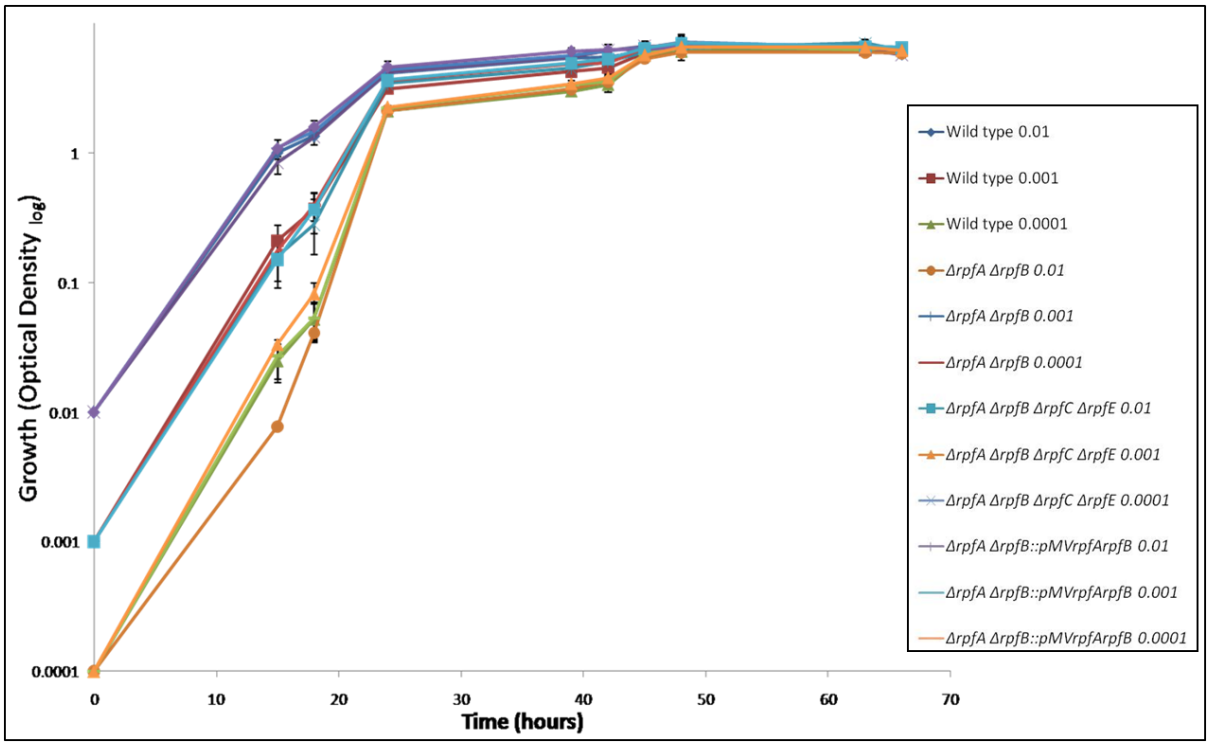

Figure C4: Growth curve analysis with OADC enrichment and 0.003% Tyloxypol. Growth curve showing optical density versus time for 7H9 media, supplemented with OADC and 0.003% Tyloxypol. Strains were grown uwith different starting bacterial concentrations and monitored 3 hourly to determine growth. Strains used in this experiment were wild type, Δ*rpf*A Δ*rpf*B, Δ*rpfA* Δ*rpfB* Δ*rpfC* Δ*rpfE* and Δ*rpfA* Δ*rpfB*::pMV*rpfArpfB*. This graph is an average of three experiments.

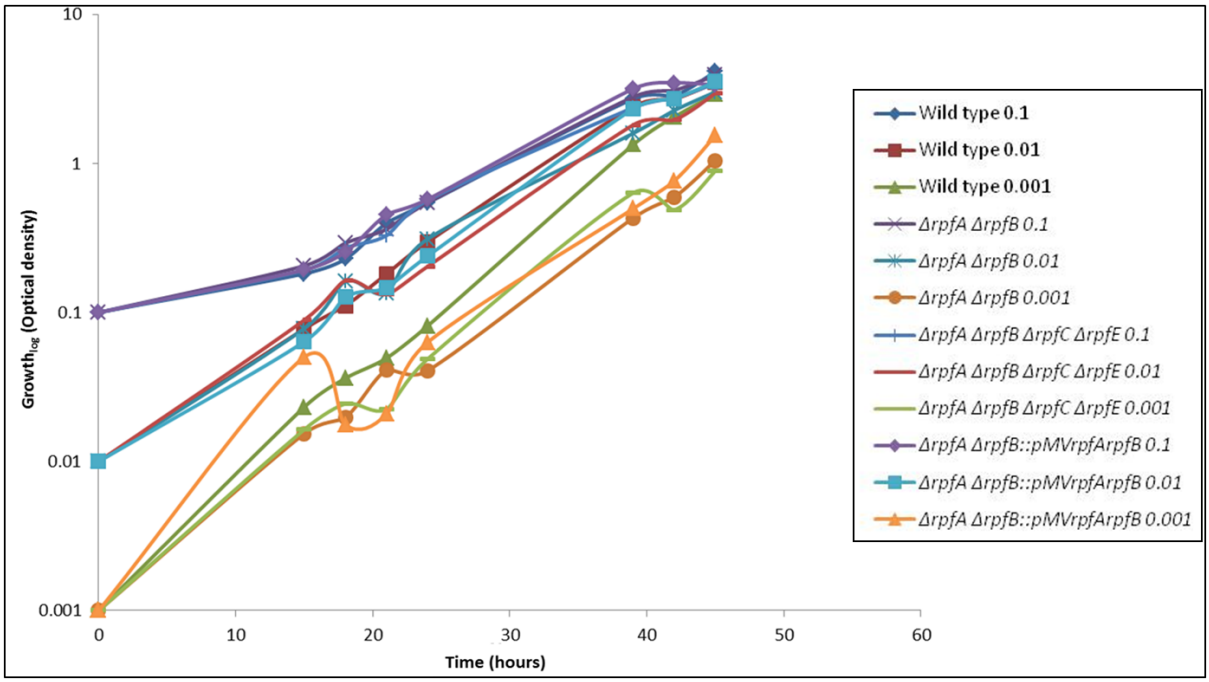

Figure C5: Growth curve analysis in Sauton's Media. Growth curve showing optical density versus time for Sauton's media, containing 0.002% Tyloxypol. Strains were grown under normal conditions, with different starting concentrations and monitored 3 hourly to determine growth. Strains used in this experiment were wild type, Δ*rpfA* Δ*rpfB*, Δ*rpfA* Δ*rpfB* Δ*rpfC* Δ*rpfE* and Δ*rpfA* Δ*rpfB*::pMV*rpfArpfB*.

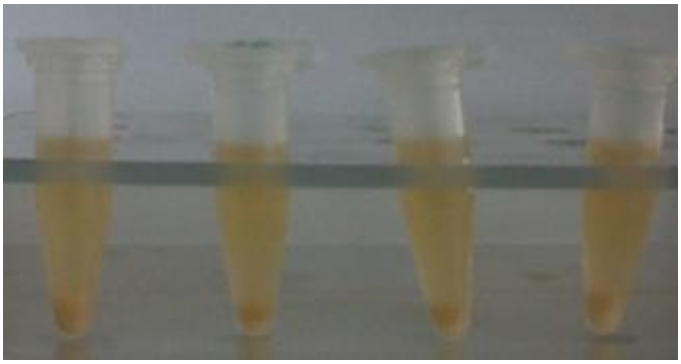

Figure C6: Photographs of mycobacterial strains stained with Neutral red. No difference was observed since the cultures did not stain at all. Eppendorf tubes contain the following from left; wild type, Δ*rpfA* Δ*rpfB*, Δ*rpfA* Δ*rpfB* Δ*rpfC* Δ*rpfE* and Δ*rpfA* Δ*rpfB*::pMV*rpfArpfB*.

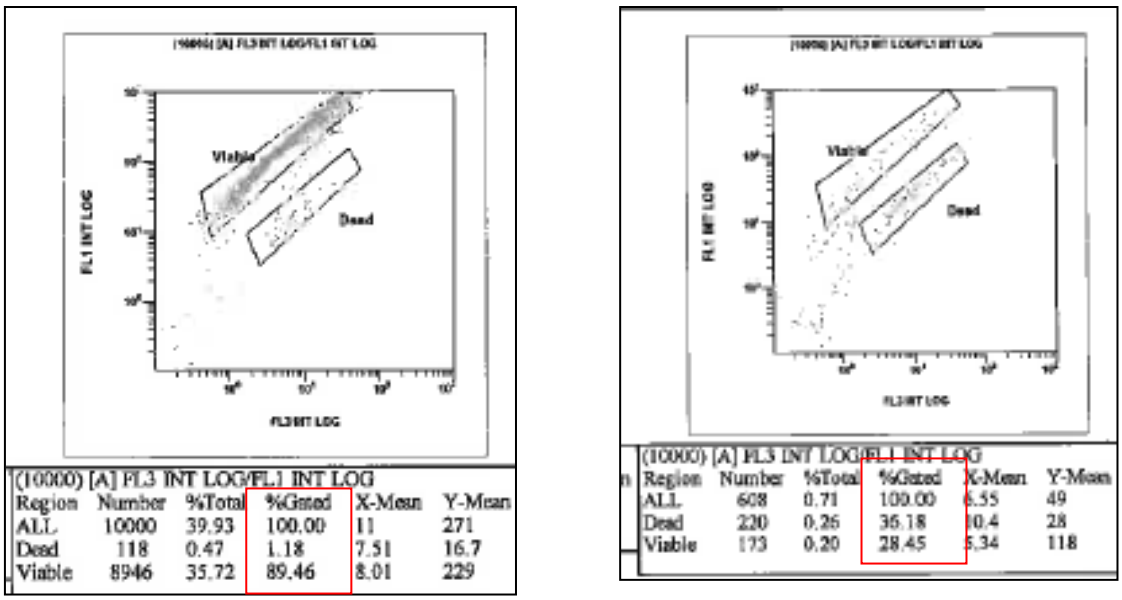

Figure C7: Difference between a life cell culture and a dead cell culture. Screenshot of Flow Cytometry Results when using the LIVE/DEAD staining kit. Left: viable cell culture; Right: dead cell culture.

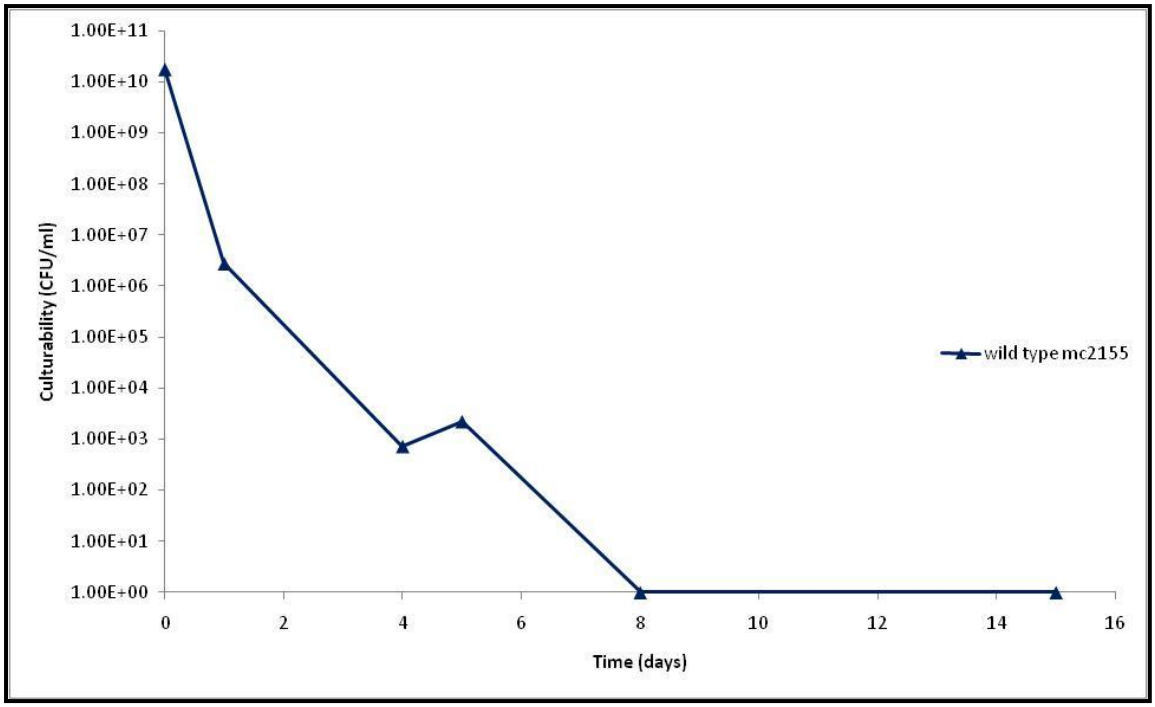

Figure C8: Establishment of the dormant state in *M. smegmatis*. Culturability (CFU/ml) versus the Time (days) of culturing for wild type in the dormancy model is shown. Graph depicting the culturability of the wild type strain over time, after transfer from nutrient rich media to nutrient poor media, used to establish dormancy.

References:

ADAMS, D. W. & ERRINGTON, J. (2009) Bacterial cell division: assembly, maintenance and disassembly of the Z ring. *Nat Rev Microbiol,* 7**,** 642-53.

ALDRIDGE, B. B., FERNANDEZ-SUAREZ, M., HELLER, D., AMBRAVANESWARAN, V., IRIMIA, D., TONER, M. & FORTUNE, S. M. (2011) Asymmetry and aging of mycobacterial cells lead to variable growth and antibiotic susceptibility. *Science,* 335**,** 100-4.

ANUCHIN, A. M., MULYUKIN, A. L., SUZINA, N. E., DUDA, V. I., EL-REGISTAN, G. I. & KAPRELYANTS, A. S. (2009) Dormant forms of *Mycobacterium smegmatis* with distinct morphology. *Microbiology,* 155**,** 1071-9.

BANIN, E., VASIL, M. L. & GREENBERG, E. P. (2005) Iron and *Pseudomonas aeruginosa* biofilm formation. *Proc Natl Acad Sci U S A,* 102**,** 11076-81.

BARRY, C. E., 3RD, BOSHOFF, H. I., DARTOIS, V., DICK, T., EHRT, S., FLYNN, J., SCHNAPPINGER, D., WILKINSON, R. J. & YOUNG, D. (2009) The spectrum of latent tuberculosis: rethinking the biology and intervention strategies. *Nat Rev Microbiol,* 7**,** 845-55.

BATEMAN, A., HOLDEN, M. T. & YEATS, C. (2005) The G5 domain: a potential N-acetylglucosamine recognition domain involved in biofilm formation. *Bioinformatics,* 21**,** 1301-3.

BIKETOV, S., MUKAMOLOVA, G. V., POTAPOV, V., GILENKOV, E., VOSTROKNUTOVA, G., KELL, D. B., YOUNG, M. & KAPRELYANTS, A. S. (2000) Culturability of *Mycobacterium tuberculosis* cells isolated from murine macrophages: a bacterial growth factor promotes recovery. *FEMS Immunol Med Microbiol,* 29**,** 233-40.

CARVER, T. J., RUTHERFORD, K. M., BERRIMAN, M., RAJANDREAM, M. A., BARRELL, B. G. & PARKHILL, J. (2005) ACT: the Artemis Comparison Tool. *Bioinformatics,* 21**,** 3422-3.

CHAO, M. C. & RUBIN, E. J. (2010) Letting sleeping *dos* lie: does dormancy play a role in tuberculosis? *Annu Rev Microbiol,* 64**,** 293-311.

CHAUHAN, A., LOFTON, H., MALONEY, E., MOORE, J., FOL, M., MADIRAJU, M. V. & RAJAGOPALAN, M. (2006) Interference of *Mycobacterium tuberculosis* cell division by Rv2719c, a cell wall hydrolase. *Mol Microbiol,* 62**,** 132-47.

CLARKE, K. R. & GORLEY, R. N. (2006) Primer6. *Primer V.6: User Manual Tutorial.* 6.1.5 ed. Plymouth.

CLEWLEY, J. P. (1995) Macintosh sequence analysis software. DNAStar's LaserGene. *Mol Biotechnol,* 3**,** 221-4.

COHEN-GONSAUD, M., BARTHE, P., BAGNERIS, C., HENDERSON, B., WARD, J., ROUMESTAND, C. & KEEP, N. H. (2005) The structure of a resuscitation-promoting factor domain from *Mycobacterium tuberculosis* shows homology to lysozymes. *Nat Struct Mol Biol,* 12**,** 270-3.

COHEN-GONSAUD, M., KEEP, N. H., DAVIES, A. P., WARD, J., HENDERSON, B. & LABESSE, G. (2004) Resuscitation-promoting factors possess a lysozyme-like domain. *Trends Biochem Sci,* 29**,** 7-10.

COLE, S. T., BROSCH, R., PARKHILL, J., GARNIER, T., CHURCHER, C., HARRIS, D., GORDON, S. V., EIGLMEIER, K., GAS, S., BARRY, C. E., 3RD, TEKAIA, F., BADCOCK, K., BASHAM, D., BROWN, D., CHILLINGWORTH, T., CONNOR, R., DAVIES, R., DEVLIN, K., FELTWELL, T., GENTLES, S., HAMLIN, N., HOLROYD, S., HORNSBY, T., JAGELS, K., KROGH, A., MCLEAN, J., MOULE, S., MURPHY, L., OLIVER, K., OSBORNE, J., QUAIL, M. A., RAJANDREAM, M.

A., ROGERS, J., RUTTER, S., SEEGER, K., SKELTON, J., SQUARES, R., SQUARES, S., SULSTON, J. E., TAYLOR, K., WHITEHEAD, S. & BARRELL, B. G. (1998) Deciphering the biology of *Mycobacterium tuberculosis* from the complete genome sequence. *Nature,* 393**,** 537-44.

COLE, S. T., EIGLMEIER, K., PARKHILL, J., JAMES, K. D., THOMSON, N. R., WHEELER, P. R., HONORE, N., GARNIER, T., CHURCHER, C., HARRIS, D., MUNGALL, K., BASHAM, D., BROWN, D., CHILLINGWORTH, T., CONNOR, R., DAVIES, R. M., DEVLIN, K., DUTHOY, S., FELTWELL, T., FRASER, A., HAMLIN, N., HOLROYD, S., HORNSBY, T., JAGELS, K., LACROIX, C., MACLEAN, J., MOULE, S., MURPHY, L., OLIVER, K., QUAIL, M. A., RAJANDREAM, M. A., RUTHERFORD, K. M., RUTTER, S., SEEGER, K., SIMON, S., SIMMONDS, M., SKELTON, J., SQUARES, R., SQUARES, S., STEVENS, K., TAYLOR, K., WHITEHEAD, S., WOODWARD, J. R. & BARRELL, B. G. (2001) Massive gene decay in the leprosy bacillus. *Nature,* 409**,** 1007-11.

DAHL, J. L. (2004) Electron microscopy analysis of *Mycobacterium tuberculosis* cell division. *FEMS Microbiol Lett,* 240**,** 15-20.

DATTA, P., DASGUPTA, A., BHAKTA, S. & BASU, J. (2002) Interaction between FtsZ and FtsW of *Mycobacterium tuberculosis*. *J Biol Chem,* 277**,** 24983-7.

DATTA, P., DASGUPTA, A., SINGH, A. K., MUKHERJEE, P., KUNDU, M. & BASU, J. (2006) Interaction between FtsW and penicillin-binding protein 3 (PBP3) directs PBP3 to mid-cell, controls cell septation and mediates the formation of a trimeric complex involving FtsZ, FtsW and PBP3 in mycobacteria. *Mol Microbiol,* 62**,** 1655-73.

DEMINA, G. R., MAKAROV, V. A., NIKITUSHKIN, V. D., RYABOVA, O. B., VOSTROKNUTOVA, G. N., SALINA, E. G., SHLEEVA, M. O., GONCHARENKO, A. V. & KAPRELYANTS, A. S. (2009) Finding of the low molecular weight inhibitors of resuscitation promoting factor enzymatic and resuscitation activity. *PLoS One,* 4**,** e8174.

DOMENECH, P., REED, M. B. & BARRY, C. E., 3RD (2005) Contribution of the Mycobacterium tuberculosis MmpL protein family to virulence and drug resistance. *Infect Immun,* 73**,** 3492-501.

DOWNING, K. J., BETTS, J. C., YOUNG, D. I., MCADAM, R. A., KELLY, F., YOUNG, M. & MIZRAHI, V. (2004) Global expression profiling of strains harbouring null mutations reveals that the five *rpf*-like genes of *Mycobacterium tuberculosis* show functional redundancy. *Tuberculosis (Edinb),* 84**,** 167-79.

DOWNING, K. J., MISCHENKO, V. V., SHLEEVA, M. O., YOUNG, D. I., YOUNG, M., KAPRELYANTS, A. S., APT, A. S. & MIZRAHI, V. (2005) Mutants of *Mycobacterium tuberculosis* lacking three of the five *rpf*-like genes are defective for growth in vivo and for resuscitation in vitro. *Infect Immun,* 73**,** 3038-43.

DZIADEK, J., MADIRAJU, M. V., RUTHERFORD, S. A., ATKINSON, M. A. & RAJAGOPALAN, M. (2002) Physiological consequences associated with overproduction of *Mycobacterium tuberculosis* FtsZ in mycobacterial hosts. *Microbiology,* 148**,** 961-71.

DZIEDZIC, R., KIRAN, M., PLOCINSKI, P., ZIOLKIEWICZ, M., BRZOSTEK, A., MOOMEY, M., VADREVU, I. S., DZIADEK, J., MADIRAJU, M. & RAJAGOPALAN, M. (2010) *Mycobacterium tuberculosis* ClpX interacts with FtsZ and interferes with FtsZ assembly. *PLoS One,* 5**,** e11058.

FERNANDEZ, P., SAINT-JOANIS, B., BARILONE, N., JACKSON, M., GICQUEL, B., COLE, S. T. & ALZARI, P. M. (2006) The Ser/Thr protein kinase PknB is essential for sustaining mycobacterial growth. *J Bacteriol,* 188**,** 7778-84.

FRIEDEN, T. R., STERLING, T. R., MUNSIFF, S. S., WATT, C. J. & DYE, C. (2003) Tuberculosis. *Lancet,* 362**,** 887-99.

FUQUA, C. & GREENBERG, E. P. (1998) Self perception in bacteria: quorum sensing with acylated homoserine lactones. *Curr Opin Microbiol,* 1**,** 183-9.

GARTON, N. J., WADDELL, S. J., SHERRATT, A. L., LEE, S. M., SMITH, R. J., SENNER, C., HINDS, J., RAJAKUMAR, K., ADEGBOLA, R. A., BESRA, G. S., BUTCHER, P. D. & BARER, M. R. (2008) Cytological and transcript analyses reveal fat and lazy persister-like bacilli in tuberculous sputum. *PLoS Med,* 5**,** e75.

GORDHAN, B. G. & PARISH, T. (Eds.) (2001) *Gene Replacement using Pretreated DNA,* Totowa, NJ, Humana Press Inc.,.

HARTMANN, M., BARSCH, A., NIEHAUS, K., PUHLER, A., TAUCH, A. & KALINOWSKI, J. (2004) The glycosylated cell surface protein Rpf2, containing a resuscitation-promoting factor motif, is involved in intercellular communication of *Corynebacterium glutamicum*. *Arch Microbiol,* 182**,** 299-312.

HETT, E. C., CHAO, M. C. & RUBIN, E. J. (2010) Interaction and modulation of two antagonistic cell wall enzymes of mycobacteria. *PLoS Pathog,* 6**,** e1001020.

HETT, E. C., CHAO, M. C., STEYN, A. J., FORTUNE, S. M., DENG, L. L. & RUBIN, E. J. (2007) A partner for the resuscitation-promoting factors of *Mycobacterium tuberculosis*. *Mol Microbiol,* 66**,** 658-68.

HETT, E. C. & RUBIN, E. J. (2008) Bacterial growth and cell division: a mycobacterial perspective. *Microbiol Mol Biol Rev,* 72**,** 126-56, table of contents.

HU, Y. M., BUTCHER, P. D., SOLE, K., MITCHISON, D. A. & COATES, A. R. (1998) Protein synthesis is shutdown in dormant *Mycobacterium tuberculosis* and is reversed by oxygen or heat shock. *FEMS Microbiol Lett,* 158**,** 139-45.

HUGONNET, J. E., TREMBLAY, L. W., BOSHOFF, H. I., BARRY, C. E., 3RD & BLANCHARD, J. S. (2009) Meropenem-clavulanate is effective against extensively drug-resistant *Mycobacterium tuberculosis*. *Science,* 323**,** 1215-8.

JAIN, A. & DIXIT, P. (2008) Multidrug-resistant to extensively drug resistant tuberculosis: what is next? *J Biosci,* 33**,** 605-16.

JOYCE, G., WILLIAMS, K. J., ROBB, M., NOENS, E., TIZZANO, B., SHAHREZAEI, V. & ROBERTSON, B. D. (2012) Cell division site placement and asymmetric growth in mycobacteria. *PLoS One,* 7**,** e44582.

KANA, B. D., GORDHAN, B. G., DOWNING, K. J., SUNG, N., VOSTROKTUNOVA, G., MACHOWSKI, E. E., TSENOVA, L., YOUNG, M., KAPRELYANTS, A., KAPLAN, G. & MIZRAHI, V. (2008) The resuscitation-promoting factors of *Mycobacterium tuberculosis* are required for virulence and resuscitation from dormancy but are collectively dispensable for growth in vitro. *Mol Microbiol,* 67**,** 672-84.

KANA, B. D. & MIZRAHI, V. (2010) Resuscitation-promoting factors as lytic enzymes for bacterial growth and signaling. *FEMS Immunol Med Microbiol,* 58**,** 39-50.

KANA, B. D., MIZRAHI, V. & GORDHAN, B. G. (2010) Depletion of resuscitation-promoting factors has limited impact on the drug susceptibility of *Mycobacterium tuberculosis*. *J Antimicrob Chemother,* 65**,** 1583-5.

KANG, C. M., ABBOTT, D. W., PARK, S. T., DASCHER, C. C., CANTLEY, L. C. & HUSSON, R. N. (2005) The *Mycobacterium tuberculosis* serine/threonine kinases PknA and PknB: substrate identification and regulation of cell shape. *Genes Dev,* 19**,** 1692-704.

KANG, C. M., NYAYAPATHY, S., LEE, J. Y., SUH, J. W. & HUSSON, R. N. (2008) Wag31, a homologue of the cell division protein DivIVA, regulates growth, morphology and polar cell wall synthesis in mycobacteria. *Microbiology,* 154**,** 725-35.

KAPOPOULOU, A., LEW, J. M. & COLE, S. T. (2010) The MycoBrowser portal: a comprehensive and manually annotated resource for mycobacterial genomes. *Tuberculosis (Edinb),* 91**,** 8-13.

KAPRELYANTS, A. S. & KELL, D. B. (1993) Dormancy in Stationary-Phase Cultures of *Micrococcus luteus*: Flow Cytometric Analysis of Starvation and Resuscitation. *Appl Environ Microbiol,* 59**,** 3187-96.

KEEP, N. H., WARD, J. M., COHEN-GONSAUD, M. & HENDERSON, B. (2006) Wake up! Peptidoglycan lysis and bacterial non-growth states. *Trends Microbiol,* 14**,** 271-6.

KESAVAN, A. K., BROOKS, M., TUFARIELLO, J., CHAN, J. & MANABE, Y. C. (2009) Tuberculosis genes expressed during persistence and reactivation in the resistant rabbit model. *Tuberculosis (Edinb),* 89**,** 17-21.

KOLTER, R., RECHT, J., MARTINEZ, A., TORELLO, S. & KOLTER, R. (2000) Genetic analysis of sliding motility in *Mycobacterium smegmatis*. *J Bacteriol,* 182**,** 4348-51.

KRISTICH, C. J., WELLS, C. L. & DUNNY, G. M. (2007) A eukaryotic-type Ser/Thr kinase in *Enterococcus faecalis* mediates antimicrobial resistance and intestinal persistence. *Proc Natl Acad Sci U S A,* 104**,** 3508-13.

LEE, B. H., MURUGASU-OEI, B. & DICK, T. (1998) Upregulation of a histone-like protein in dormant *Mycobacterium smegmatis*. *Mol Gen Genet,* 260**,** 475-9.

LEW, J. M., KAPOPOULOU, A., JONES, L. M. & COLE, S. T. (2011) TubercuList--10 years after. *Tuberculosis (Edinb),* 91**,** 1-7.

LIM, A., ELEUTERIO, M., HUTTER, B., MURUGASU-OEI, B. & DICK, T. (1999) Oxygen depletion-induced dormancy in *Mycobacterium bovis BCG*. *J Bacteriol,* 181**,** 2252-6.

LIN, M. Y. & OTTENHOFF, T. H. (2008) Host-pathogen interactions in latent *Mycobacterium tuberculosis* infection: identification of new targets for tuberculosis intervention. *Endocr Metab Immune Disord Drug Targets,* 8**,** 15-29.

LODDENKEMPER, R. & HAUER, B. (2010) Drug-resistant tuberculosis: a worldwide epidemic poses a new challenge. *Dtsch Arztebl Int,* 107**,** 10-9.

LYNNON.CORP. (2007) DNAMAN. 7 ed. Canada, Lynnon Corporation.

MALMROS, H. (1948) The efficacy of B.C.G. vaccination. *Br Med J,* 1**,** 1129-32.

MCCUNE, R. M., FELDMANN, F. M., LAMBERT, H. P. & MCDERMOTT, W. (1966) Microbial persistence. I. The capacity of tubercle bacilli to survive sterilization in mouse tissues. *J Exp Med,* 123**,** 445-68.

MUKAMOLOVA, G. V., KAPRELYANTS, A. S., YOUNG, D. I., YOUNG, M. & KELL, D. B. (1998) A bacterial cytokine. *Proc Natl Acad Sci U S A,* 95**,** 8916-21.

MUKAMOLOVA, G. V., MURZIN, A. G., SALINA, E. G., DEMINA, G. R., KELL, D. B., KAPRELYANTS, A. S. & YOUNG, M. (2006) Muralytic activity of *Micrococcus luteus* Rpf and its relationship to physiological activity in promoting bacterial growth and resuscitation. *Mol Microbiol,* 59**,** 84-98.

MUKAMOLOVA, G. V., TURAPOV, O. A., KAZARIAN, K., TELKOV, M., KAPRELYANTS, A. S., KELL, D. B. & YOUNG, M. (2002a) The rpf gene of *Micrococcus luteus* encodes an essential secreted growth factor. *Mol Microbiol,* 46**,** 611-21.

MUKAMOLOVA, G. V., TURAPOV, O. A., YOUNG, D. I., KAPRELYANTS, A. S., KELL, D. B. & YOUNG, M. (2002b) A family of autocrine growth factors in *Mycobacterium tuberculosis*. *Mol Microbiol,* 46**,** 623-35.

NGUYEN, H. T., WOLFF, K. A., CARTABUKE, R. H., OGWANG, S. & NGUYEN, L. (2010) A lipoprotein modulates activity of the MtrAB two-component system to provide intrinsic multidrug resistance, cytokinetic control and cell wall homeostasis in Mycobacterium. *Mol Microbiol,* 76**,** 348-64.

OHNISHI, Y., KAMEYAMA, S., ONAKA, H. & HORINOUCHI, S. (1999) The A-factor regulatory cascade leading to streptomycin biosynthesis in *Streptomyces griseus* : identification of a target gene of the A-factor receptor. *Mol Microbiol,* 34**,** 102-11.

OJHA, A., ANAND, M., BHATT, A., KREMER, L., JACOBS, W. R., JR. & HATFULL, G. F. (2005) GroEL1: a dedicated chaperone involved in mycolic acid biosynthesis during biofilm formation in mycobacteria. *Cell,* 123**,** 861-73.

PELICIC, V., REYRAT, J. M. & GICQUEL, B. (1996) Expression of the *Bacillus subtilis* sacB gene confers sucrose sensitivity on mycobacteria. *J Bacteriol,* 178**,** 1197-9.

PILLAY, M. & STURM, A. W. (2007) Evolution of the extensively drug-resistant F15/LAM4/KZN strain of *Mycobacterium tuberculosis* in KwaZulu-Natal, South Africa. *Clin Infect Dis,* 45**,** 1409-14.

PLOCINSKI, P., ARORA, N., SARVA, K., BLASZCZYK, E., QIN, H., DAS, N., PLOCINSKA, R., ZIOLKIEWICZ, M., DZIADEK, J., KIRAN, M., GORLA, P., CROSS, T. A., MADIRAJU, M. & RAJAGOPALAN, M. (2012) *Mycobacterium tuberculosis* CwsA interacts with CrgA and Wag31, and the CrgA-CwsA complex is involved in peptidoglycan synthesis and cell shape determination. *J Bacteriol,* 194**,** 6398-409.

PLOCINSKI, P., ZIOLKIEWICZ, M., KIRAN, M., VADREVU, S. I., NGUYEN, H. B., HUGONNET, J., VECKERLE, C., ARTHUR, M., DZIADEK, J., CROSS, T. A., MADIRAJU, M. & RAJAGOPALAN, M. (2011) Characterization of CrgA, a new partner of the *Mycobacterium tuberculosis* peptidoglycan polymerization complexes. *J Bacteriol,* 193**,** 3246-56.

RACHMAN, H., STRONG, M., ULRICHS, T., GRODE, L., SCHUCHHARDT, J., MOLLENKOPF, H., KOSMIADI, G. A., EISENBERG, D. & KAUFMANN, S. H. (2006) Unique transcriptome signature of *Mycobacterium tuberculosis* in pulmonary tuberculosis. *Infect Immun,* 74**,** 1233-42.

RAVAGNANI, A., FINAN, C. L. & YOUNG, M. (2005a) A novel firmicute protein family related to the actinobacterial resuscitation-promoting factors by non-orthologous domain displacement. *BMC Genomics,* 6**,** 39.

RAVAGNANI, A., FINAN, C. L. & YOUNG, M. (2005b) A novel firmicute protein family related to the actinobacterial resuscitation-promoting factors by non-orthologous domain displacement. *BMC Genomics,* 6**,** 39.

RECHT, J. & KOLTER, R. (2001) Glycopeptidolipid acetylation affects sliding motility and biofilm formation in *Mycobacterium smegmatis*. *J Bacteriol,* 183**,** 5718-24.

RIANO, F., ARROYO, L., PARIS, S., ROJAS, M., FRIGGEN, A. H., VAN MEIJGAARDEN, K. E., FRANKEN, K. L., OTTENHOFF, T. H., GARCIA, L. F. & BARRERA, L. F. (2012) T cell responses to DosR and Rpf proteins in actively and latently infected individuals from Colombia. *Tuberculosis (Edinb),* 92**,** 148-59.

RUGGIERO, A., MARCHANT, J., SQUEGLIA, F., MAKAROV, V., DE SIMONE, A. & BERISIO, R. (2012) Molecular determinants of inactivation of the resuscitation promoting factor B from *Mycobacterium tuberculosis*. *J Biomol Struct Dyn,* 31**,** 195-205.

RUGGIERO, A., TIZZANO, B., PEDONE, E., PEDONE, C., WILMANNS, M. & BERISIO, R. (2009) Crystal structure of the resuscitation-promoting factor (DeltaDUF)RpfB from *M. tuberculosis*. *J Mol Biol,* 385**,** 153-62.

RUSSELL-GOLDMAN, E., XU, J., WANG, X., CHAN, J. & TUFARIELLO, J. M. (2008) A *Mycobacterium tuberculosis* Rpf double-knockout strain exhibits profound defects in reactivation from chronic tuberculosis and innate immunity phenotypes. *Infect Immun,* 76**,** 4269-81.

SAKULA, A. (1983) Robert koch: centenary of the discovery of the tubercle bacillus, 1882. *Can Vet J,* 24**,** 127-31.

SALINA, E. G., ZHOGINA, Y. A., SHLEEVA, M. O., SOROKOUMOVA, G. M., SELISHCHEVA, A. A. & KAPRELYANTS, A. S. (2010) Biochemical and morphological changes in dormant ("Nonculturable") *Mycobacterium smegmatis* cells. *Biochemistry (Mosc),* 75**,** 72-80.

SCHEURWATER, E., REID, C. W. & CLARKE, A. J. (2008) Lytic transglycosylases: bacterial space-making autolysins. *Int J Biochem Cell Biol,* 40**,** 586-91.

SHAH, I. M., LAABERKI, M. H., POPHAM, D. L. & DWORKIN, J. (2008) A eukaryotic-like Ser/Thr kinase signals bacteria to exit dormancy in response to peptidoglycan fragments. *Cell,* 135**,** 486-96.

SHLEEVA, M., MUKAMOLOVA, G. V., YOUNG, M., WILLIAMS, H. D. & KAPRELYANTS, A. S. (2004) Formation of 'non-culturable' cells of *Mycobacterium smegmatis* in stationary phase in response to growth under suboptimal conditions and their Rpf-mediated resuscitation. *Microbiology,* 150**,** 1687-97.

SHLEEVA, M. O., BAGRAMYAN, K., TELKOV, M. V., MUKAMOLOVA, G. V., YOUNG, M., KELL, D. B. & KAPRELYANTS, A. S. (2002) Formation and resuscitation of "non-culturable" cells of *Rhodococcus rhodochrous* and *Mycobacterium tuberculosis* in prolonged stationary phase. *Microbiology,* 148**,** 1581-91.

SOTO, C. Y., ANDREU, N., GIBERT, I. & LUQUIN, M. (2002) Simple and rapid differentiation of *Mycobacterium tuberculosis* H37Ra from *M. tuberculosis* clinical isolates through two cytochemical tests using neutral red and nile blue stains. *J Clin Microbiol,* 40**,** 3021-4.

STATSOFT.INC. (2004) Statistica, version 6.1. 6.1 ed.

STEWART, G. R., ROBERTSON, B. D. & YOUNG, D. B. (2003) Tuberculosis: a problem with persistence. *Nat Rev Microbiol,* 1**,** 97-105.

STEWART, P. S. & FRANKLIN, M. J. (2008) Physiological heterogeneity in biofilms. *Nat Rev Microbiol,* 6**,** 199-210.

SUREKA, K., HOSSAIN, T., MUKHERJEE, P., CHATTERJEE, P., DATTA, P., KUNDU, M. & BASU, J. (2010) Novel role of phosphorylation-dependent interaction between FtsZ and FipA in mycobacterial cell division. *PLoS One,* 5**,** e8590.

SVENSON, S., KALLENIUS, G., PAWLOWSKI, A. & HAMASUR, B. (2010) Towards new tuberculosis vaccines. *Hum Vaccin,* 6**,** 309-17.

THAKUR, M. & CHAKRABORTI, P. K. (2006) GTPase activity of mycobacterial FtsZ is impaired due to its transphosphorylation by the eukaryotic-type Ser/Thr kinase, PknA. *J Biol Chem,* 281**,** 40107-13.

TUBB, R. S. & LILJESTROEM, P. L. (1986) A colony-colour method which differentiates alpha-galactosidase-positive strains of yeast. *Journal of hte Institute of Brewing,* 92**,** 588-590.

TUFARIELLO, J. M., JACOBS, W. R., JR. & CHAN, J. (2004) Individual *Mycobacterium tuberculosis* resuscitation-promoting factor homologues are dispensable for growth *in vitro* and *in vivo*. *Infect Immun,* 72**,** 515-26.

TUFARIELLO, J. M., MI, K., XU, J., MANABE, Y. C., KESAVAN, A. K., DRUMM, J., TANAKA, K., JACOBS, W. R., JR. & CHAN, J. (2006) Deletion of the

Mycobacterium tuberculosis resuscitation-promoting factor *Rv1009* gene results in delayed reactivation from chronic tuberculosis. *Infect Immun,* 74**,** 2985-95.
VAN ZYL-SMIT, R. N., ZWERLING, A., DHEDA, K. & PAI, M. (2009) Within-subject variability of interferon-g assay results for tuberculosis and boosting effect of tuberculin skin testing: a systematic review. *PLoS One,* 4**,** e8517.
VANDAL, O. H., ROBERTS, J. A., ODAIRA, T., SCHNAPPINGER, D., NATHAN, C. F. & EHRT, S. (2009) Acid-susceptible mutants of *Mycobacterium tuberculosis* share hypersusceptibility to cell wall and oxidative stress and to the host environment. *J Bacteriol,* 191**,** 625-31.
VELAYATI, A. A., MASJEDI, M. R., FARNIA, P., TABARSI, P., GHANAVI, J., ZIAZARIFI, A. H. & HOFFNER, S. E. (2009) Emergence of new forms of totally drug-resistant tuberculosis bacilli: super extensively drug-resistant tuberculosis or totally drug-resistant strains in iran. *Chest,* 136**,** 420-5.
VOLOSHIN, S. A. & KAPRELYANTS, A. S. (2004) Cell-cell interactions in bacterial populations. *Biochemistry (Mosc),* 69**,** 1268-75.
WAYNE, L. G. & HAYES, L. G. (1996) An *in vitro* model for sequential study of shiftdown of *Mycobacterium tuberculosis* through two stages of nonreplicating persistence. *Infect Immun,* 64**,** 2062-9.
WHO (2009) Global Tuberculosis Control: A short update to the 2009 report. Geneva, World Health Organisation.
WHO (2012) Tuberculosis Fact Sheet
WHO (2013) South Africa Tuberculosis profile.
WIVAGG, C. N. & HUNG, D. T. (2012) Resuscitation-promoting factors are required for beta-lactam tolerance and the permeability barrier in *Mycobacterium tuberculosis*. *Antimicrob Agents Chemother,* 56**,** 1591-4.
YOUNG, D. B., GIDEON, H. P. & WILKINSON, R. J. (2009) Eliminating latent tuberculosis. *Trends Microbiol,* 17**,** 183-8.